DOUGLAS TASKS FOR AIRBORNE SOLAR ECLIPSE EXPEDITION OF MAY 30, 1965

AUGUST 1965

Prepared under contract No. NAS 2-2703
by Douglas Aircraft Company, Inc.
Missile and Space Systems Division
Santa Monica, California
for
NATIONAL AERONAUTICS AND SPACE ADMINISTRATION

DOUGLAS REPORT SM-48792

DOUGLAS TASKS FOR AIRBORNE SOLAR ECLIPSE EXPEDITION OF MAY 30, 1965

AUGUST 1965

by R.M. CAMERON

with contributions by

J.D. Clarke
T.H. Elkins
J.D. Gehris
S.N. Nathanson
Dr. P.C. Steffey
M.C. Young
J.L. Whittaker

Prepared under Contract No. NAS 2-2703
by Douglas Aircraft Company, Inc.
Missile and Space Systems Division
Santa Monica, California
for
NATIONAL AERONAUTICS AND SPACE ADMINISTRATION

ACKNOWLEDGMENT

The writer wishes to express his gratitude to the many persons whose enthusiasm and resourcefulness made the Douglas Aircraft Company's contribution to Project ASEE (Airborne Solar Eclipse Expedition) an unqualified success. The Company personnel associated with Project ASEE wish to express their appreciation to Dr. Michel Bader and his colleagues at NASA-Ames, and to the participants in the expedition, for their cooperation and support which made the association both pleasant and memorable.

The death of Dr. W. B. Klemperer in March was a tragic loss to all. Characteristically, Dr. Klemperer was involved in all Company tasks relating to ASEE. His wealth of experience and knowledge, his immense scientific curiosity, and his enthusiasm for the expedition powered the Douglas team through the difficult early stages. We are certain that "Klemp," as he preferred being called, would have been pleased with the results.

CONTENTS

FIGURES

TABLES

DOUGLAS TASKS FOR AIRBORNE SOLAR ECLIPSE FLIGHT EXPEDITION OF MAY 30, 1965

R. M. Cameron

Douglas Aircraft Company, Inc.

SUMMARY

This is the final report of the work accomplished by the Douglas Aircraft Company, Inc., under Contract NAS2-2703, for the 1965 Airborne Solar Eclipse Expedition (Project ASEE).

It describes the following four major responsibilities undertaken by Douglas:

(1) Procure, mount, and environmentally test optical viewing windows prior to installation in the NASA CV-990 aircraft

(2) Certify the tie-down of scientific equipment to Federal Aviation Agency (FAA) emergency load specifications and install aboard expedition aircraft

(3) Analyze navigational problems and prepare a plan for mid-Pacific interception of the solar eclipse path

(4) Fabricate a gyroscopically controlled heliostat system for Aerospace Research Laboratories, Wright-Patterson AFB, Ohio, and operate this instrument during the solar eclipse flight.

The success of Project ASEE, in terms of the accumulation of worthwhile scientific knowledge, is not wholly determinable at this time. It will be many months, or even years, before all data are reduced and analyzed. However, it can be stated without exaggeration that a most remarkable data-gathering opportunity was presented to the collection of scientists and instruments carried aboard the CV-990 on the hot-run flight of May 30, 1965. The expedition-aircraft intercepted the umbra path of the eclipse as planned and flew a carefully programmed path that produced a viewing time of 9 min and 42 sec, only 2 sec less than the theoretical maximum obtainable at the aircraft's speed of 520 knots. No serious mishap occurred to disrupt the expedition's plans. Without significant exception, the work of preparation produced the desired hot-run conditions. In terms of this interim result, the tasks carried out by Douglas and the other participants were successful.

INTRODUCTION

Douglas's assistance in the implementation of the NASA-sponsored Airborne Solar Eclipse Expedition (Project ASEE) stemmed from a meeting between Company and NASA-Ames personnel on Nov. 13, 1964 in Santa Monica, California. This meeting led to the submittal of a proposal (ref. 1) to NASA in December. Work was begun almost immediately in order to meet the eclipse schedule. In February 1965, Douglas was officially awarded a contract (NAS2-2703) to conduct the four-point program outlined in the following paragraphs.

Task I: Optical Viewing Ports

Ten selected plate-glass windows of optical quality were procured and, along with additional windows furnished by participants, subjected to pressure and environmental tests. They were subsequently installed on the port side of the NASA CV-990. These tests proved the integrity of the optical windows in an environment simulating that which would be encountered by the aircraft. Frames to contain the optical windows were also fabricated.

Task II: Certification of Participants' Equipment and Assistance in the Installation of the Equipment in the NASA Aircraft

Douglas personnel, using guidelines set forth by the Federal Aviation Agency and Convair Aircraft, were charged with certifying that all experimenters' equipment installed in the expedition aircraft could sustain emergency load factors. In addition, the Company agreed to furnish, through a sole-source vendor, the floor and sidewall seat-rail clamps and adapters required to secure equipment in the cabin of the aircraft. During the latter phases of the expedition (April-May), Douglas furnished a task force of structural engineers and technicians at Moffett Field, California to expedite the installation and substantiate safe tie-down of equipment into the NASA CV-990 aircraft.

Task III: Navigational Studies

Task III developed the navigational strategy and techniques for Project ASEE. This work included preparation of maps and flight plans for the hot run and two alternate flight plans for May 30 (a weather alternate and a second alternate); 13 practice flights, which utilized the sun and moon as simulated targets for the eclipsed sun; and one calibration flight, which was flown after the hot run. In addition, an error matrix was prepared for the aircraft at interception for the hot run and the weather alternate, and an elaborate and detailed analysis was performed to enable the aircraft navigators to correct their course for the effects of winds of variable magnitudes and direction. A sun compass, which subsequently proved to be invaluable as a navigational aid, was designed, fabricated, and installed on the NASA CV-990.

Task III is presented as a complete treatise. The author and his associates feel that the analyses and techniques developed for the navigation of the NASA CV-990 during Project ASEE can serve as the foundation for navigation of most future airborne astronomical programs and, therefore, a rather detailed presentation is warranted.

Task IV: Air Force Heliostatic System

Douglas delivered a gyroscopically controlled heliostat to Aerospace Research Laboratory of Wright-Patterson AFB, Ohio, through NASA-Ames. This heliostat was similar to that designed and developed for the Douglas-Mt. Wilson spectrograph experiment, and was required to maintain image stability within the predicted performance tolerance throughout the period of totality.

The following sections describe in detail the work accomplished under each of the four tasks. The bulk of calculations relating to Tasks I and II were submitted to NASA-Ames in separate reports issued prior to the departure of the expedition from Moffett Field. These are referenced in the appropriate sections of this report.

Task IV describes only the operation of the heliostat system built for ARL, which was a duplicate of that used on the Douglas-Mt. Wilson spectrograph experiment. A more detailed presentation of development of the latter heliostat system is given in ref. 2.

SYMBOLS

α	astronomical right ascension (geocentric)
a	semimajor axis of umbra ellipse
AZ	azimuth
β	aircraft bank angle
b	semi-minor axis of umbra ellipse
ζ	astronomical declination (geocentric)
D	great circle distance on a sphere
Δ	instantaneous measure of aircraft proximity to periphery of umbra ellipse
ϵ	elevation angle of celestial object
ϵ'	elevation angle seen from floor of pitched aircraft
g	local acceleration of gravity
GST	Greenwich sidereal time at 0 hours Universal Time
h	aircraft heading angle
H	astronomical hour angle (geocentric)
i	aircraft angle of attack, or pitch angle; current output
I_{GP}	gyro package moment of inertia
I_{OA}	outer axis moment of inertia
I_{IA}	inner axis moment of inertia
λ	longitude
m	1/Poisson's ratio
Ω	absolute value of aircraft angular velocity

$$\Omega \quad \pm \quad 2 \text{ ARCSIN} \left(\sqrt{\frac{x_A^2 + y_A^2}{2R}} \right) ; \text{ see definitions of } x_A, y_A, \text{ and R below}$$

$$\Omega_o = \text{ARCTAN} \left(\frac{\bar{x}}{\bar{y}} \right) ; \text{ see definition of } \bar{x}, \bar{y} \text{ below}$$

P	absolute pressure in $lb/in.^2$

ΔP = change in pressure

ω azimuth angle of umbra path at mid-intercept point measured in tangent plane.

ψ change in relative bearing of sun as seen from aircraft because of non-level aircraft attitude.

ϕ latitude (geocentric)

R_E equatorial radius of Earth

R_o scaled multiple of R_E

R flight-path radius of curvature in coordinated bank turn

S Laplace operator

St tensile strength in $lb/in.^2$

$\rho = R_E \cos \phi$

U. T. Universal Time

t time; also U. T. - U. T. (at mid-intercept)

tg thickness of glass

Δt correction of U. T. interval to corresponding sidereal time interval

T tangency point of gnomonic projection; also mid-intercept point

T_{tot} duration of total eclipse

T_f frictional torque

T_M motor torque

T_D disturbing torque

T_E error torque

θ instantaneous solar azimuth in gnomonic plane

θ_o angular displacement of gyro

$\theta_{Aircraft}$ angular displacement of the aircraft

$\dot{\theta}_{Aircraft}$ angular rate of the aircraft

$\ddot{\theta}_{\text{Aircraft}}$	angular acceleration of the aircraft
θ_M	angular displacement of the mirror
$\dot{\theta}_M$	angular rate of the mirror
$\ddot{\theta}_M$	angular acceleration of the mirror
$\Delta\dot{\theta}$	angular rate of the mirror with respect to the aircraft
V	aircraft ground speed; output voltage
(X_o, Y_o)	instantaneous coordinates of umbra ellipse along umbra path in gnomonic plane
$(\bar{\bar{x}}, \bar{\bar{y}})$	coordinates of center of curvature of aircraft's flight path for eclipse flight
(x_A, y_A)	instantaneous coordinates of aircraft in tangent plane
$(\bar{x}, \bar{y})$	left-handed rectangular coordinate system with origin at center of umbra ellipse
(X, Y, Z)	right-handed local horizon coordinate system
$(\bar{X}, \bar{Y}, \bar{Z})$	right-handed pitched aircraft coordinate system
ZT	local standard zone time
ζ	astronomical zenith distance or angle
Z	direction of local vertical; zenith direction

TASK I: OPTICAL VIEWING PORTS

To enable experimenters to view the 1965 solar eclipse, the Convair Aircraft Division of General Dynamics cut 13 openings in the portside fuselage of the NASA CV-990 at an elevation of 65^{o}. Special optical-quality windows were installed in these openings. Douglas procured from Sudden Service Glass Company, Los Angeles, 10 pieces of selected soda lime plate glass that had been reground and polished to an optical quality of four fringes overall with surfaces parallel to within 0.001 in.

Each glass was coated on both surfaces with a magnesium fluoride coating to reduce reflection effects.

Figure 1 shows the spectral transmission properties of one sample of glass as determined by a scanning spectrophotometer of Douglas's Electro-Optical Laboratory.

The required thickness of the glass was determined from calculations based on Roark's equation for flat rectangular plates (ref. 3) under uniform load on one side and simply supported around the edges of the panes.

$$St = \frac{0.75\, wb^2}{tg^2\,(1 + 1.61\alpha^3)} \qquad (1)$$

Stress and thickness determined from equation (1) are as follows:

$a = 12$ in.

$b = 14$ in.

$\alpha = \frac{a}{b} = \frac{12}{14} = 0.857$ in.

$St =$ tensile stress in psi

$w = \Delta P$

$W =$ total load $= \Delta P$ (area of glass)

$m = \frac{1}{\text{Poisson's ratio}} = 3.33$

$P = 12.72$ psi

$t_g =$ glass thickness

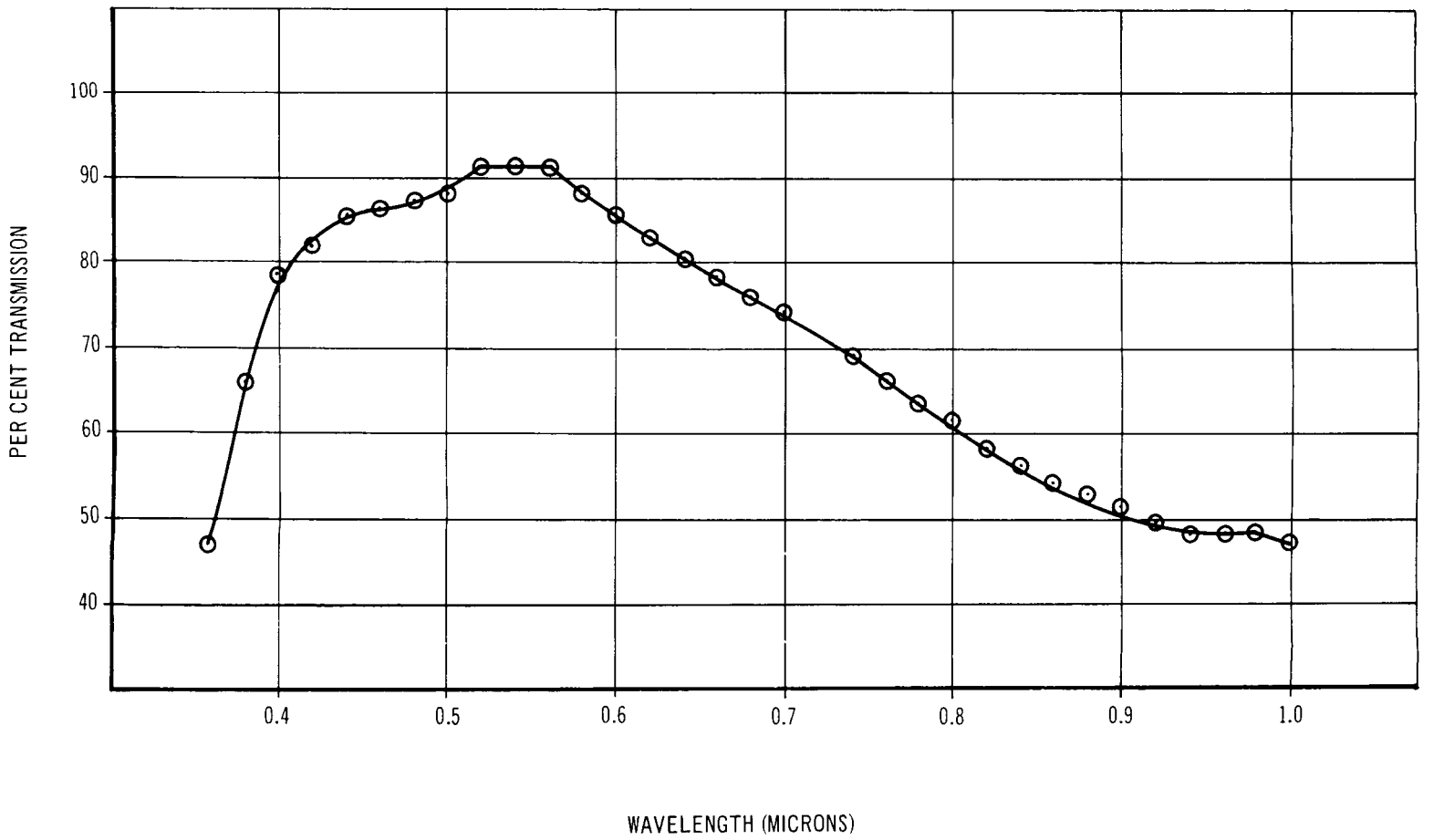

Figure 1. Spectral Transmission of a Sample Optical Window

Adapters

Frames for the 10 pieces of glass were fabricated according to Douglas Drawing No. ITO3441-1. Other optical windows were supplied by some of the experimenters and were mounted in special adapters.

The adapter built for Mr. Kissell of the USAF Aerospace Research Laboratory (ARL), was designed for a glass which was available at ARL. This adapter is detailed in Douglas Drawing No. ITO3478-1. The clear aperture of this frame is 12 in. by 12 in. with corner radii of 3.1 in. in the four corners.

Since this glass was 0.625-in. thick, the stress level was higher than the other windows, but still quite safe. The stress in the glass can be calculated from Roark's equation for a square plate (ref. 3)

$$\text{St max} = \frac{0.2208\ wa^2\ (m + 1)}{mtg^2} \tag{2}$$

The adapter for the Larmore-Ireland equipment of Douglas Aircraft, Douglas Drawing No. ITO3477-1, was fabricated from a solid plate of aluminum and contained a 7-in. diam by 1-in. thick piece of fused silica. The glass was mounted with the convex side on the inside to cancel out the errors that were caused by the aircraft pressure differential. This glass had previously been used on aircraft installations. The stress level is quite low and was derived by Roark in his equation for a round window (ref. 3):

$$\text{St max} = \frac{3W\ (3m + 1)}{8\pi\ mtg^2} \tag{3}$$

A special adapter, containing a 5 1/2-in. diam opening at one end and a rectangular opening at the other, was designed for NASA-Goddard. Two identical adapters were fabricated, one by Douglas and one by NASA-Goddard. One adapter contained an arsenic trisulfide window; the other adapter contained a calcium fluoride window. Maximum stress to be encountered (in flight) by the round glass elements of these assemblies was calculated from equation (3); stress encountered by the rectangular glass was calculated from equation (1).

The calculation is an approximation, since the rectangular opening in 5.750 in. by 11.175 in. with a 7/8-in. radius in two corners and a 2.675-in. radius in the remaining two corners. Douglas Drawing No. ITO3469-1 details the design of this adapter. The stress in this pane of the adapter is high compared to the tensile strength of the material; it was decided that the environmental test would represent sufficient qualification of this particular installation.

The adapter for Dr. Dunn of Sacramento Peak Observatory was essentially the same as the 10 special frames for NASA, except that the glass thickness

was 1.250 in. instead of 1.000 in. The material was better for temperature differentials. This plate glass and the whole assembly represented a more than adequate margin of safety.

The adapters for Smith-Torrey of NASA-Ames and Dossin-Macar of the University of Liège were made from solid aluminum plate with a 12-in. diam clear aperture. The glass was 13 in. in diam by 1 in. thick. This adapter is detailed in Douglas Drawing No. ITO3477-501.

The adapter for the Cameron-Deutsch spectrograph equipment of Douglas Aircraft was made from a solid aluminum plate with a 10-1/2-in. diam clear aperture and employing an 11-in. diam glass, 1 in. thick. Douglas Drawing No. ITO3411-69 details this adapter.

An adapter, detailed in Douglas Drawing No. ITO3481-1, with a valve for mounting a periscopic sextant was fabricated. When mounted, the valve would be level if the aircraft pitch angle was 1.8°.

Pressure Testing

To provide a measure of safety against window failure at altitude, the Company conducted pressure and environmental tests on each of the window assemblies. These tests were performed in the Environments Laboratory of the Engineering Laboratory and Services Department of Douglas between April 6 and May 3, 1965. The tests on each of the 19 window assemblies were witnessed and certified by Douglas Quality Control personnel.

Each assembly (fig. 2) was first mounted and sealed into a cabin simulator vessel detailed in Douglas Drawing No. ITO3453. The vessel was a welded aluminum box approximately 24 in. by 24 in. by 24 in., encased in an insulated plywood box (fig. 3). This assembly was then placed in a burst chamber, and the vessel was pressurized to 27 $\pm$ 1 psig for 5 min and then reduced to zero psig. Each assembly was subjected to this proof test three times.

The maximum pressure differentials for the proof test and the environmental tests were determined in the following manner: the maximum cabin pressure differential for the Convair 990 at attitude was estimated to be 9.27 psi, including the relief-valve tolerance of the cabin air system. To this value was added the maximum aerodynamic suction associated with the flight of the aircraft. This value was estimated to be 3.45 psi. The maximum pressure differential is the sum of the maximum cabin pressure differential plus the maximum aerodynamic suction, in this case 12.72 psi. The ultimate operating pressure differential was determined by postulating a safety factor of 1.5 times the pressure differential; the result is 19.08 psi. This pressure differential was used in the environmental tests. An arbitrary figure of 27 psi pressure differential on the windows was adopted for the proof tests. This pressure more than twice the operating pressure differential, was used to test the bond, and seal of the silicon rubber gaskets.

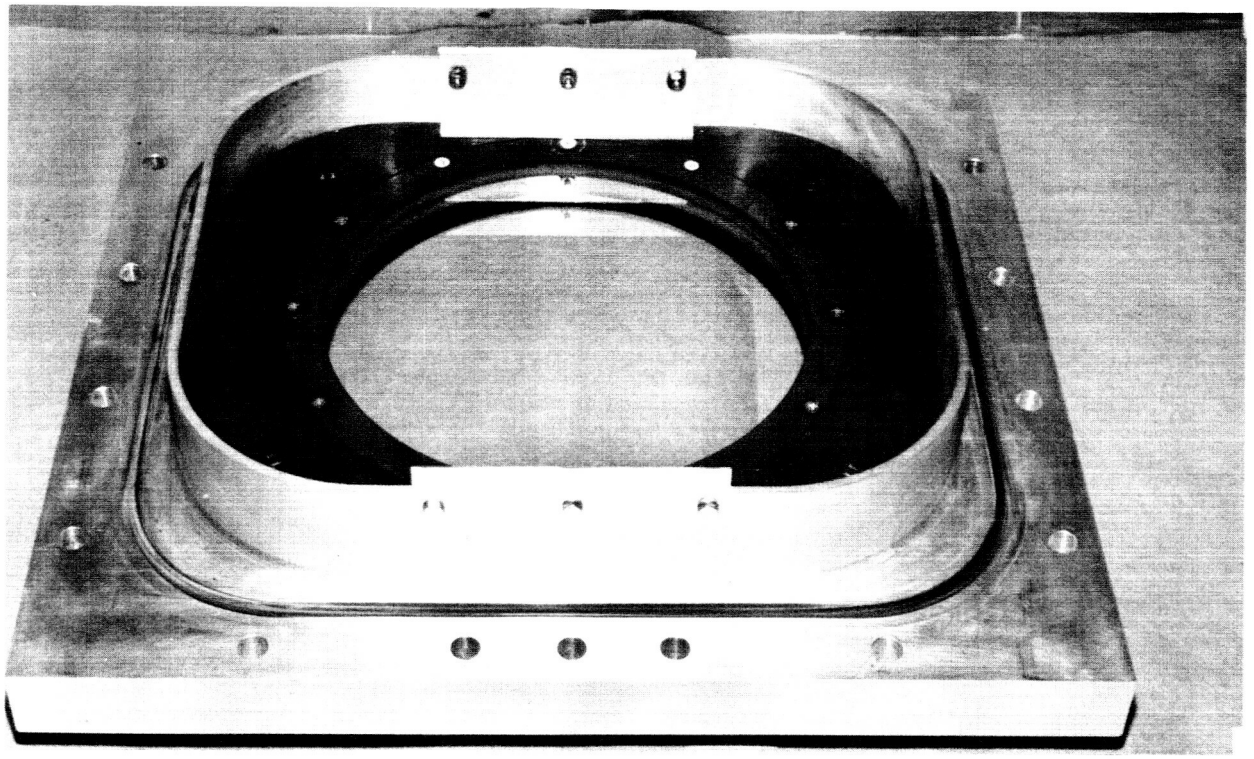

Figure 2. Window Adapter and Optical Glass

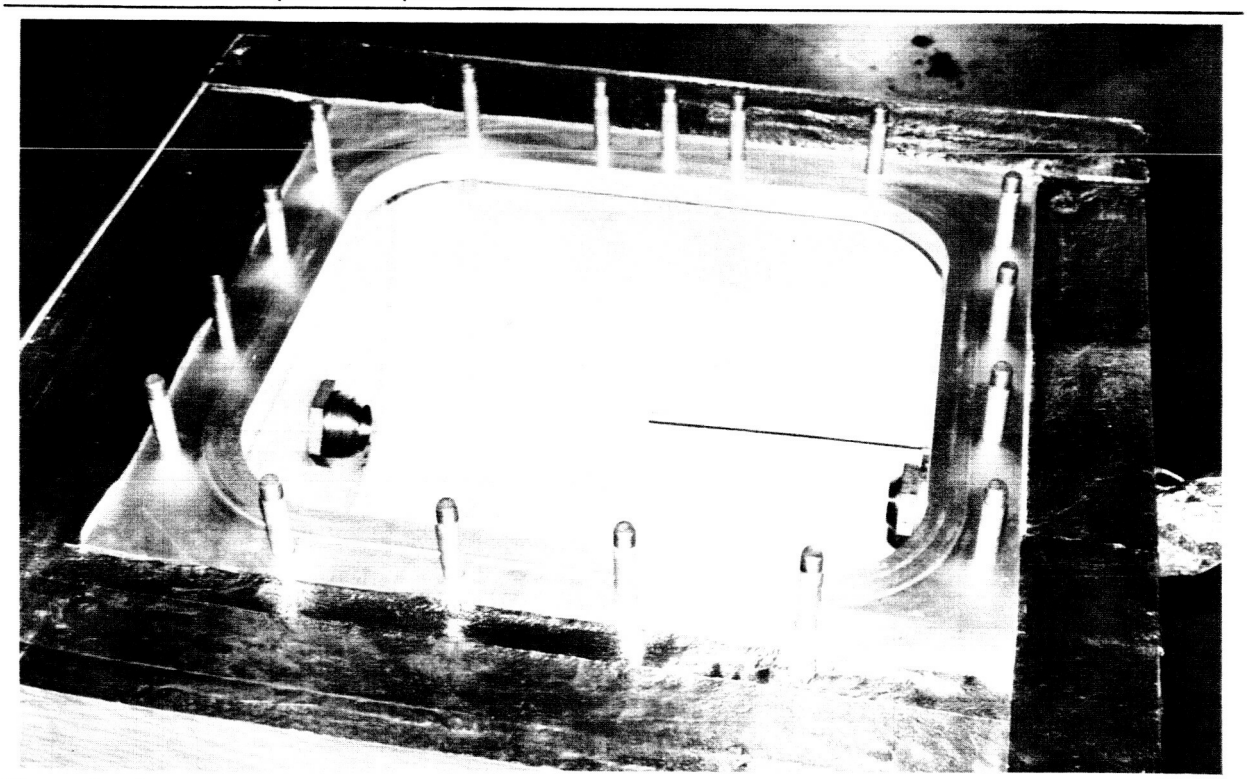

Figure 3. Cabin Simulator Vessel

Environmental Testing

Upon completion of the pressure and leak tests, the window assembly, mounted in the pressure vessel, was placed in an environmental chamber (fig. 4). The chamber and cabin simulator conditions were then adjusted to subject the optical window to a differential pressure of 19.1 psia and a differential temperature of approximately 200°F. The temperature differential on the window was determined by assuming that the ambient temperature at 40,000 ft would not be colder than -60°F and that the warm air purging the window would not be warmer than 140°F. These conditions were attained by circulating warm air (T = 140°F max) through the pressure vessel and onto the inside surface of the optical windows while simultaneously lowering the outer chamber temperature to -60°F. While the outer chamber temperature was being lowered, the pressure inside the vessel was maintained at approximately 8.9 in. Hg. As the differential temperature approached the desired 200°F, the outer environmental chamber pressure was changed to approximately 4 in. Hg, which corresponds roughly to an altitude of 47,000 ft. The pressure vessel was then pressurized to 21.2 psia to obtain the desired differential pressure of 19.1 psi on the window. These conditions were maintained for 20 min, then reduced to room ambient pressure and temperature in about 2 min.

Each of the window assemblies passed the pressure and environmental tests. The data obtained from the tests and the equipment used (fig. 5) are documented in Douglas Report No. TM-GEN-ME-R5073 (ref. 4).

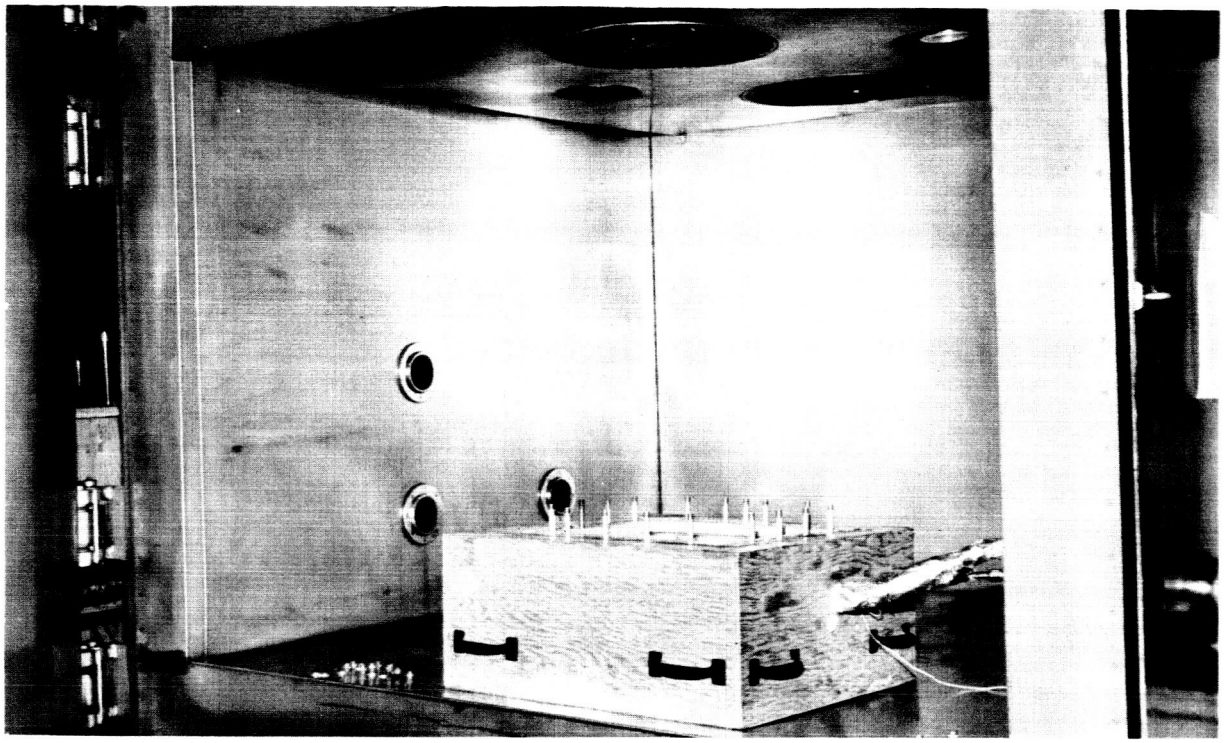

Figure 4. Cabin Simulator Installed in Environment Chamber

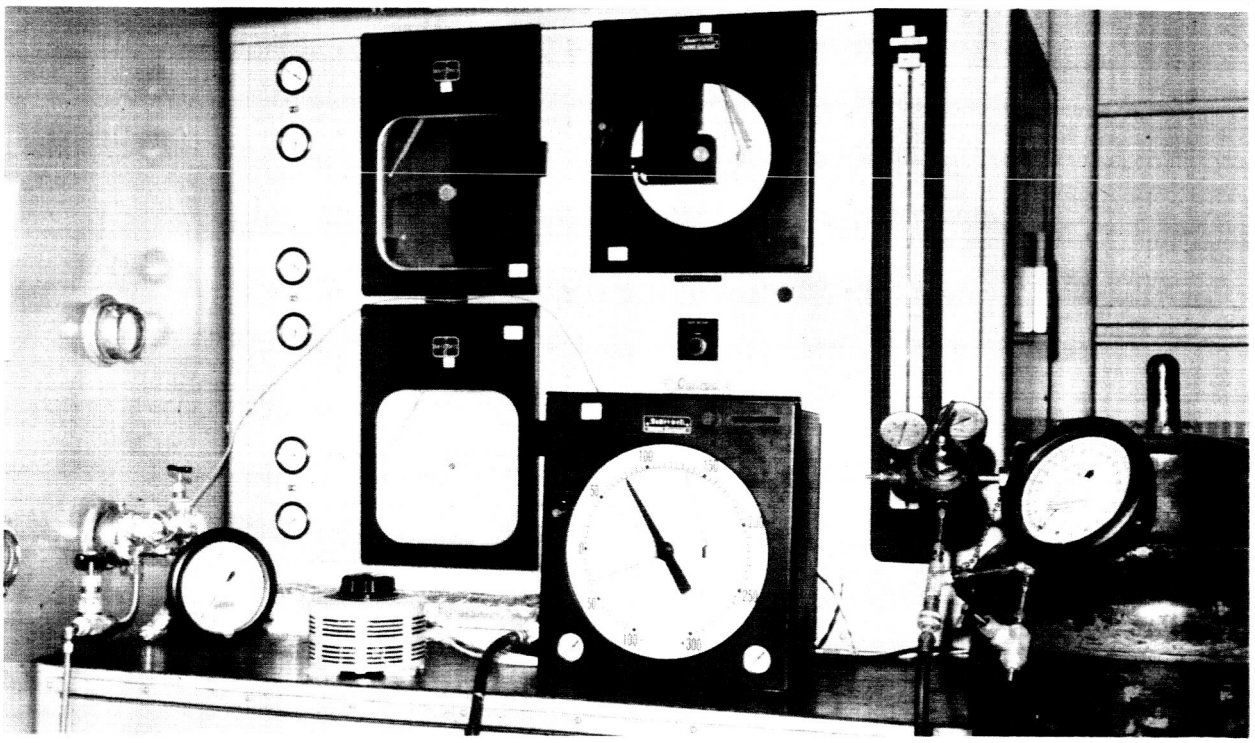

Figure 5. Environment Monitoring Equipment

TASK II. EQUIPMENT AND TIE-DOWN BRACKETRY

Douglas was responsible for certifying safe installation of participants' equipment in the NASA aircraft. Standard FAA requirements for securing material in commercial transport aircraft were adopted and rigorously enforced, although FAA certification was not required by NASA since this aircraft was registered "experimental". All installations were substantiated by Douglas Report SM 48330 (ref. 5). Each participant was responsible for the design, fabrication, and installation of his own equipment into the airplane. However, Douglas personnel conducted stress analyses on this equipment to ensure conformance with the safety requirements and emergency precautions. In some instances, Douglas structural engineers assisted participants with the design or redesign of their equipment mounts and tie-down techniques, and Douglas provided technicians to assist with part of the equipment installation.

The track configuration available for equipment mounting was the standard one side-wall track and one floor track provided for attaching passenger seats; the seats had been removed from the aircraft to permit equipment installation. Equipment loads on the floor and side-wall tracks were calculated and checked to make certain they were at a safe level.

Load Factors

All equipment installed in the NASA CV 990 aircraft was attached and re-enforced as required to meet the following design and crash load factors (refs. 6, 7, and 8):

9.0 g. forward
*7.0 g. down
*3.0 g. up
3.0 g. side
1.5 g. aft

*All scientific equipment was installed between stations 400 and 1,192 (Convair designation) and, therefore, would experience a max. 2.8 g. up and 6.9 g. down.

Load Ratings

The side-wall track-load ratings were the following:

1,785 lb forward and aft on 34-in. centers (min.)
1,759 lb vertically on 15 5/8-in. centers (min.), provided the adjacent loads are in opposite directions.
1,433 lb laterally on 34-in. centers (min.)

The left hand-side floor track-load ratings were the following:

2,195 lb forward and aft on 34-in. centers (min.)
3,165 lb vertically on 15 5/8-in. center (min.), provided the adjacent loads are in opposite directions.

The right hand-side floor track-load ratings were the following:

3,990 lb forward and aft on 34-in. centers (min.)
5,830 lb vertically on 15 5/8-in. center (min.), provided the adjacent loads are in opposite directions.

The right hand-side floor track was able to carry more load than the left hand-side track because it was designed to carry three seats, whereas the left hand-side track was designed to carry only two. The standard left- or right-side passenger seat installation on commercially operated CV 990 aircraft had two clamping attachments to a floor track and two clamping attachments to a side-wall track. To be conservative, the load ratings were used exactly as the seats apply the loads on the tracks. These ratings could have been used differently, such as by adding more shear to the floor track at closer spacing, provided the total shear at any point would not be more than the shear used for design of the floor beam. Two vertical loads might also have been spaced adjacent to each other, provided the net load would not have overloaded the track and the floor beam.

Installation Checks

The floor-track clamps used on the experimenter's equipment were checked for proper installation on the site. For example, if additional shear loads must be carried, a rear floor track fitting may be used on the forward end of a piece of equipment, but it must be turned 180° from the normal installation position to properly take the combined down loads and shear loads.

The forward floor-track clamps are normally located by a spacer from the rear clamp, which is indexed in the track by a pin. Since these spacers were not used, except for the equipment in station no. 4, all forward clamps were carefully checked for full engagement with the floor track.

Equipment Installation

The interior arrangement of the CV 990 aircraft is shown in fig. 6. Each piece of equipment was weighed and the location of the center of gravity was determined experimentally to enable calculation of stresses in the equipment and the consequent loads imposed on the tracks.

Station 1.--The Kissell-Byard equipment installed in experimenter's station no. 1 was too heavy for the length of floor track allocated. The weight was reduced by removing a power supply and several other components (fig. 7). These were mounted a short distance from the equipment on members connected to the left-hand side-wall seat track. Since a further reduction in weight was not possible, another member was added to make the equipment safe. This member tied the equipment into the floor track in the area of station no. 2 (figs. 7 and 8). This member took vertical loads as well as forward shear. Some of the Allen bolts in the fitting for the floor-track attachment were replaced by AN bolts in order to take the shear and tension loads (fig. 9). Some of the bolts in the diffraction grating housing were replaced by AN bolts with self-locking nuts. Other minor pieces of equipment were bolted down to adequately withstand the g. loads. Figure 8 shows the electronics for this equipment.

Station 2.--The Larmore-Ireland equipment in station no. 2 was installed as designed, since it was determined to be sufficiently strong to withstand the required loads. This installation is shown in fig. 10.

Station 3.--The equipment used in station no 3 (Stockhausen-Mangus) had a very high c.g. which caused an overload in the rear floor track fitting. To alleviate this, some of the components at the top of the console were moved to the bottom and the three nitrogen bottles standing upright were changed to one small bottle standing vertically, and one reserve bottle lying horizontally (figs. 11 and 12). The path of the load from the console to the floor track passed through shock mounts and 3/4-in. plywood. Since the plywood lacked sufficient bending strength, another floor track fitting was added to take the vertical reaction at the rear of the equipment (fig. 12). This fitting tied the console directly to the floor track. The floor track fitting under the console was replaced by a Douglas-manufactured fitting which took the shear load. Figure 11 shows this bracket which was added on the front of the equipment tying the interferometer directly to the floor track. This increased the natural frequency and strengthened the equipment. The major problem with this equipment was low-frequency vibration, which was especially noticeable on takeoff and landing. The causes of this shaking were the high c.g. location, the narrow base of the equipment, the complex structure involving shock mounts, and the flexible floor of the aircraft. Unfortunately, the left-hand floor beams of the aircraft were designed for two seats as compared to three seats for the right-hand side.

Station 4.--The top of Professor Waldmeier's stand installed in station no. 4 lacked sufficient strength for takeoff and landing with the camera installed (fig. 13). Therefore, the camera was stowed in a box during takeoff and landing as shown in fig. 14.

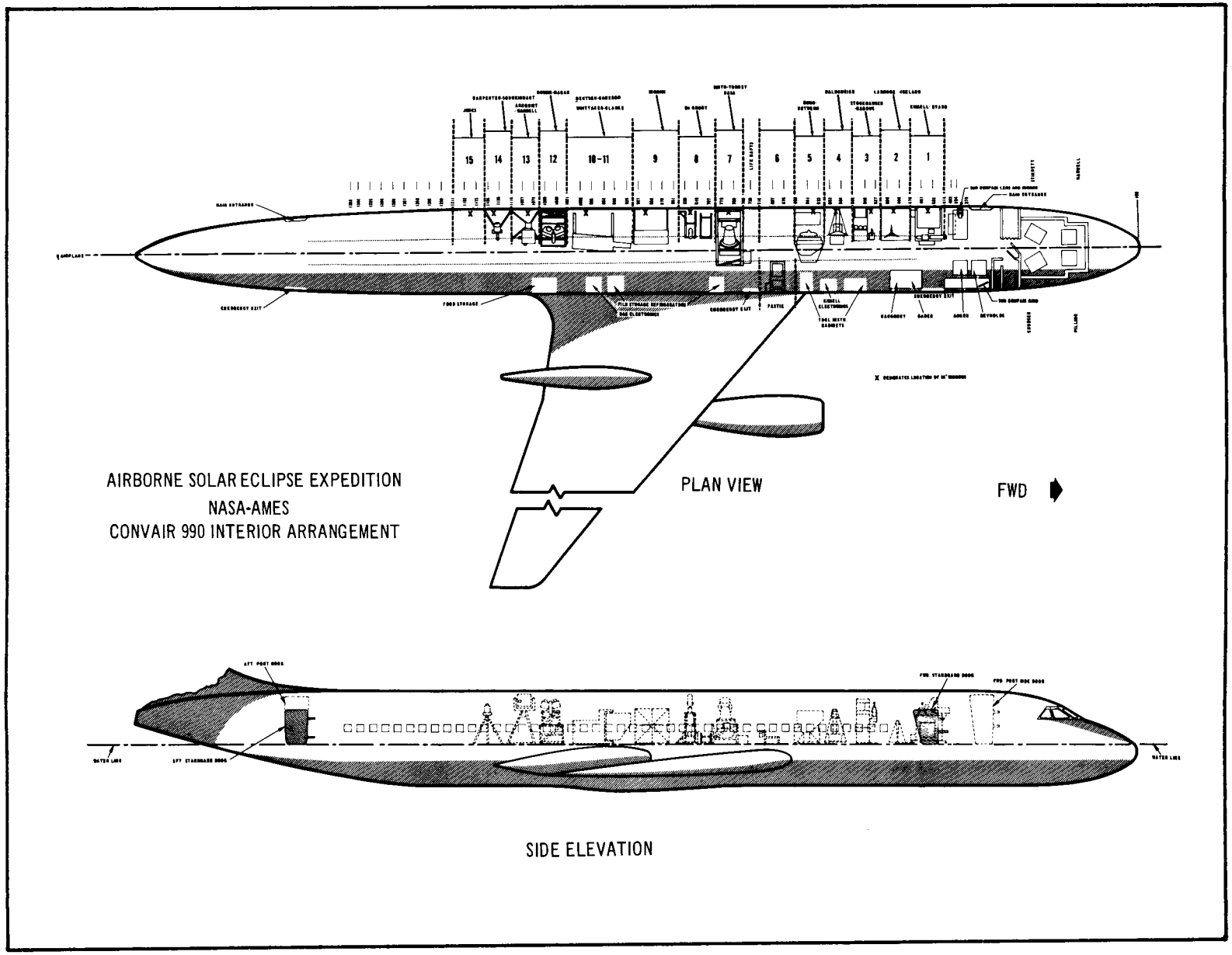

Figure 6. Interior Arrangement of NASA CV-990 Aircraft

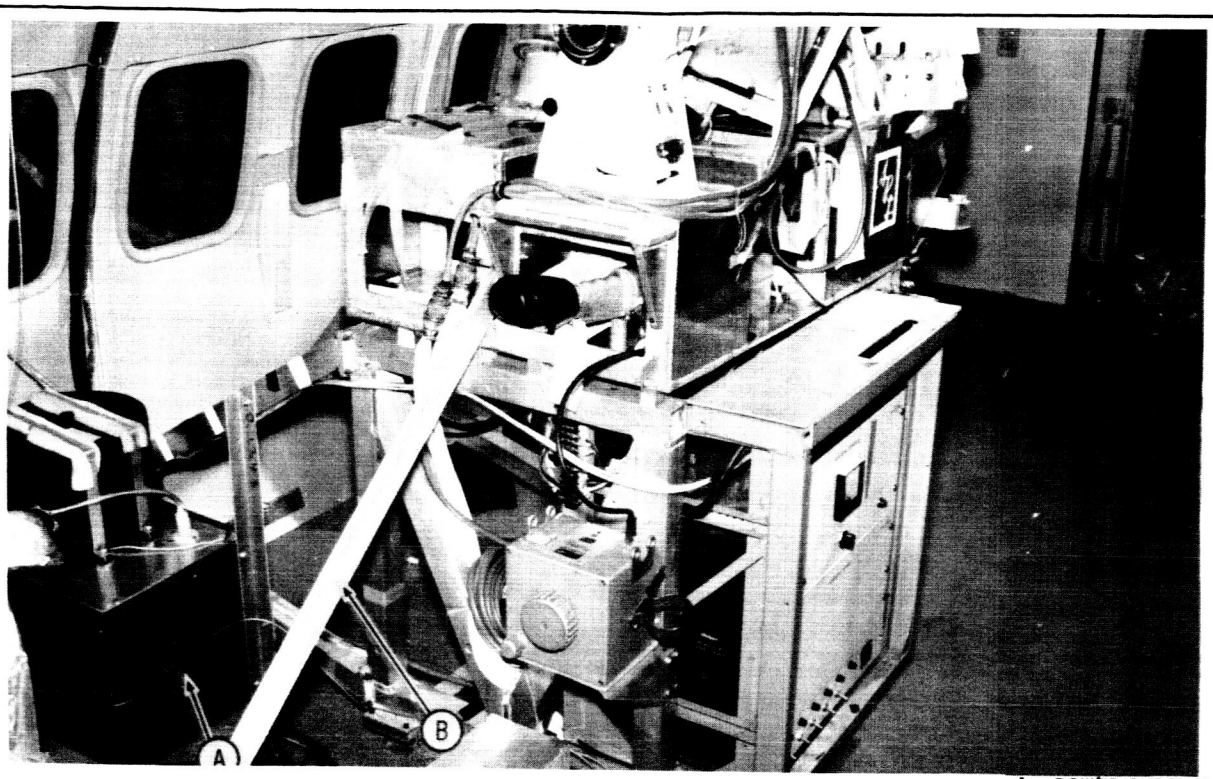

Figure 7. Aerospace Research Laboratory Spectrograph Installation

A = POWER SUPPLY
B = BRACE MEMBER

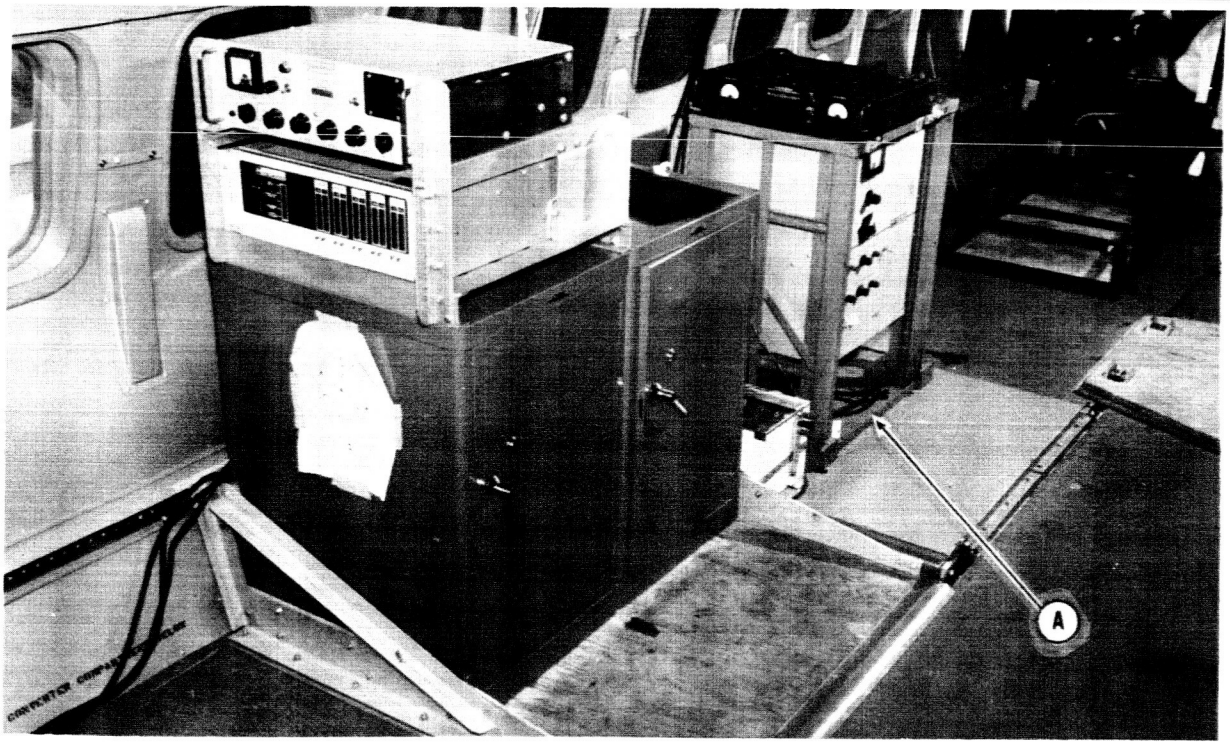

Figure 8. Aerospace Research Laboratory Electronics Installation

A = TIE-DOWN MEMBER

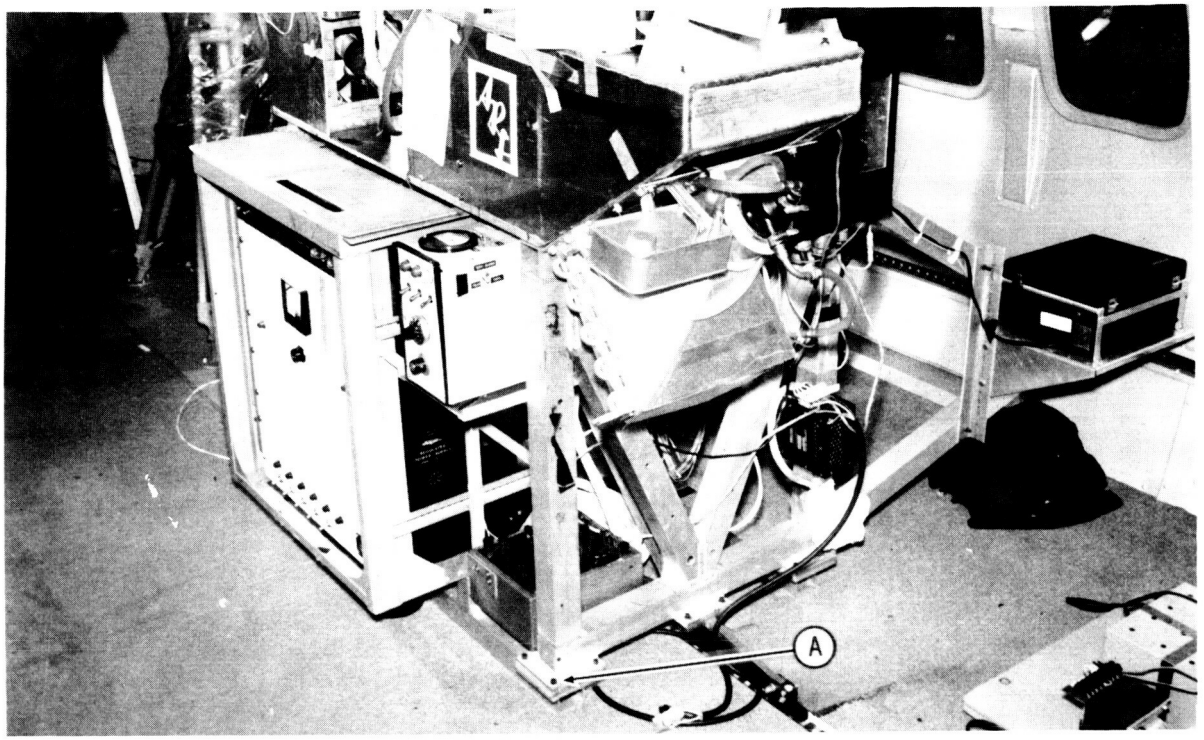

Figure 9. Aerospace Research Laboratory Floor-Track Attachment

A = CLAMPING MECHANISM

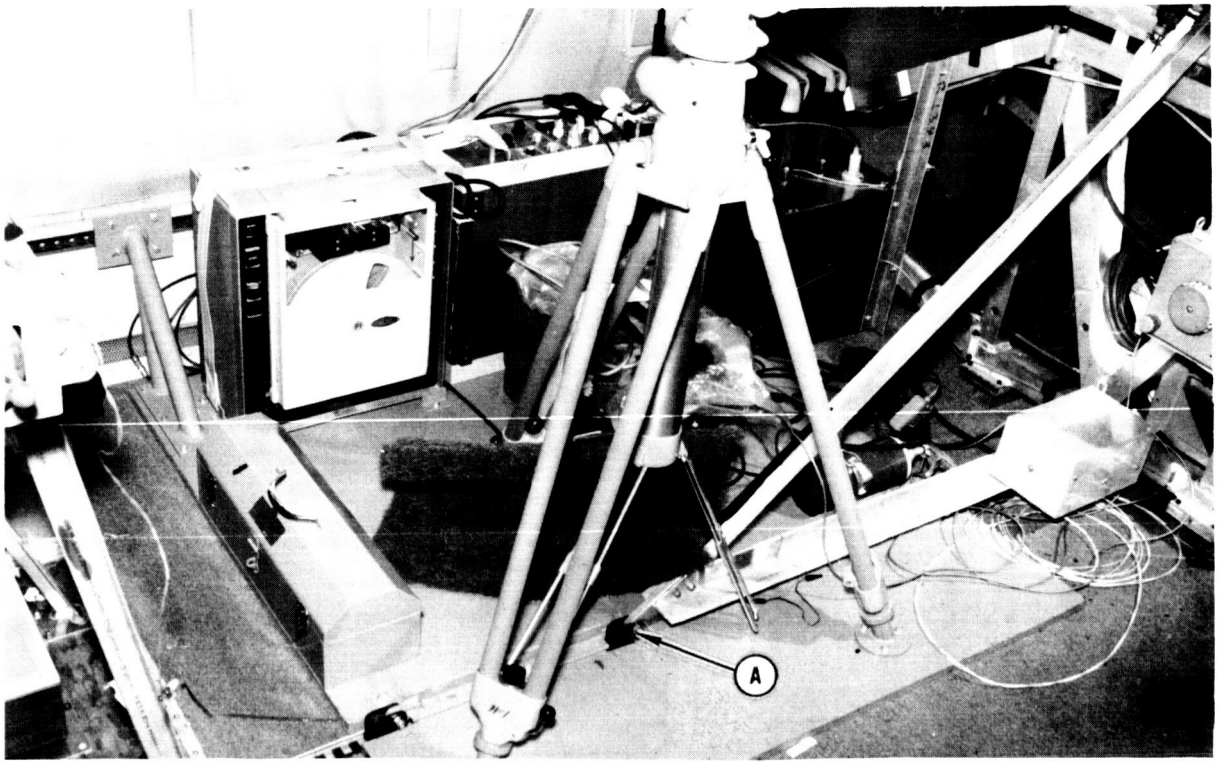

Figure 10. Douglas IR Flash-Spectrum Equipment

A = SEAT RAIL CLAMP

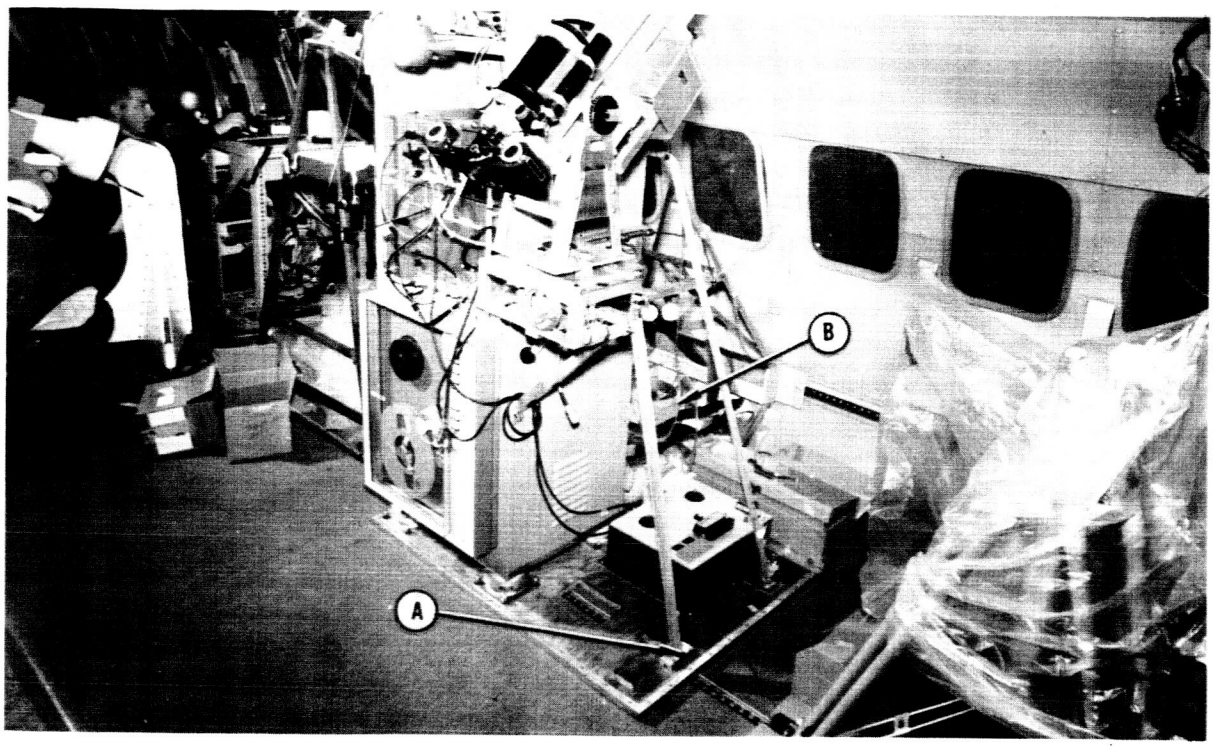

A = SEAT RAIL CLAMP B = NITROGEN BOTTLE

Figure 11. NASA – Goddard IR Corona Instrument (Forward View)

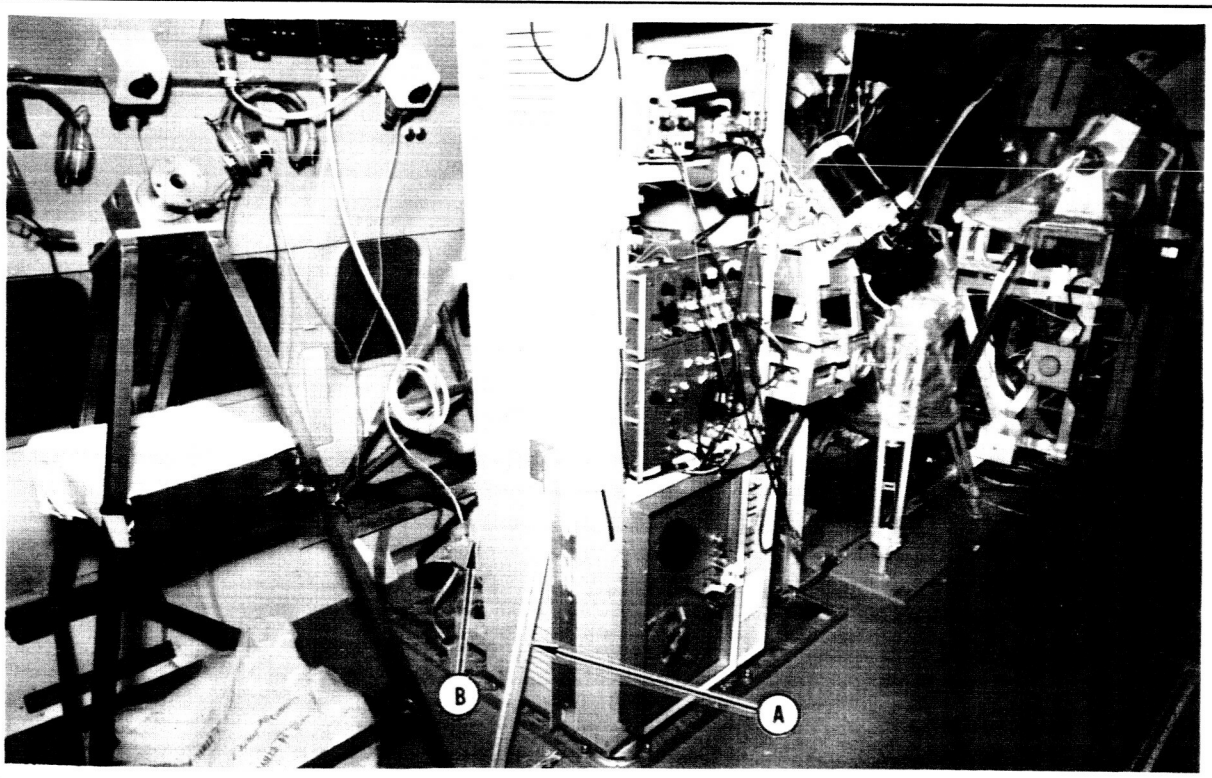

Figure 12. NASA – Goddard IR Corona Instrument (Aft View) A = SEAT RAIL CLAMP B = NITROGEN BOTTLE

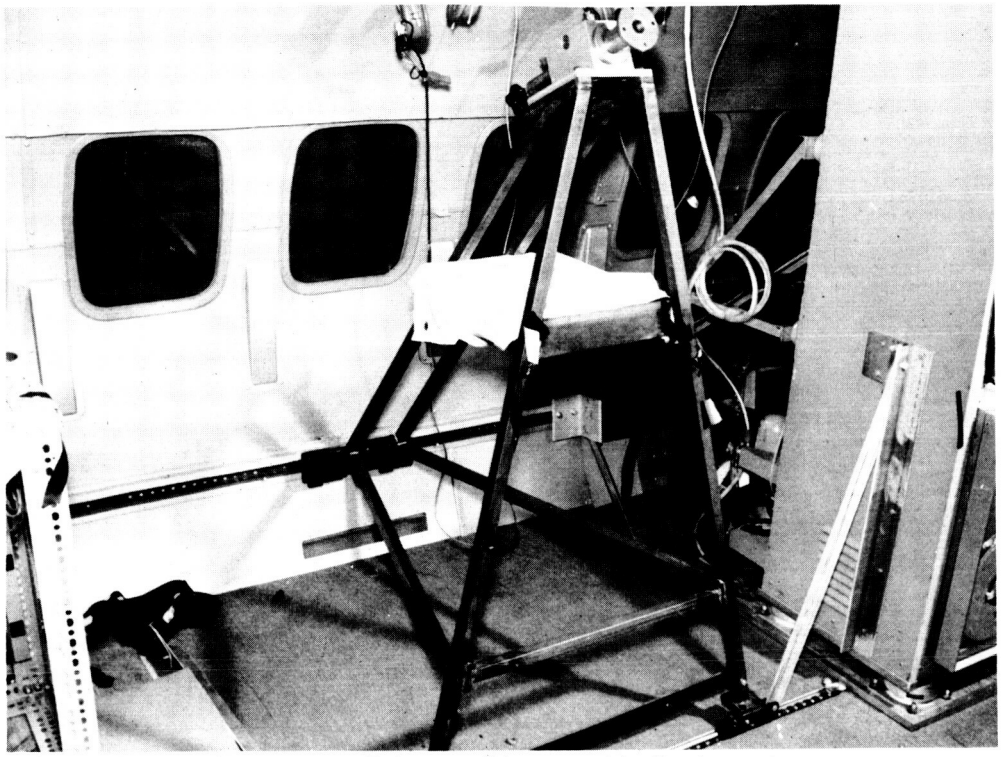

Figure 13. Swiss Federal Observatory Polar-Ray Photographic Equipment

A = INSTRUMENT STORAGE CONTAINER
B = SPECTROGRAPH MOUNT
C = BRACE MEMBERS
D = TIE-DOWN BELT

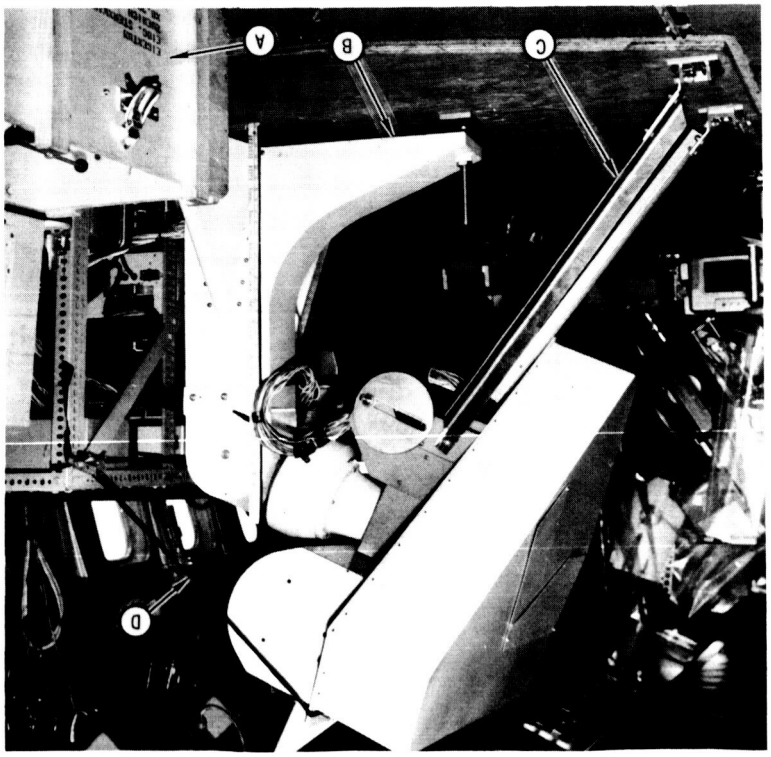

Figure 14. Sacramento Peak-University of Hawaii Equipment Installation (Forward View)

Station 5. --The spectrograph of Dunn and Cothern, station no. 5, was designed with three ball-socket feet and was attached to a wooden pallet. The load rating of each ball-socket assembly could not be obtained, and the plywood attachment to the floor track was not sufficiently strong. A bracket was then designed and fabricated to tie the spectrograph rear foot directly to the floor track fitting (fig. 15). The spectrograph electronics console was tied to the wooden pallet with sheet metal screws on the inboard side. However, a sufficient number of members were lacking on the outboard side. Bracketry was subsequently fabricated to tie the rear of this console to the floor-track fitting, and additional members were fabricated to completely tie the electronics console to the side wall track fitting. These members were designed to take forward shear, side loads, and the vertical reaction at the rear of the electronics console. Members were also fabricated to support the spectrograph since it was cantilevered and had a low natural resonance frequency. The members are shown in figs. 14 and 15. Without these members, failure could have occurred from fatiguing of the main spectrograph gimbal.

Station 6. --The equipment installed in station no. 6 (Fastie-Miller) was on the right-hand side of the aircraft and viewed through one of the standard 990 fuselage plexiglass windows. The c.g., and thus the loads of this equipment, were quite low to the floor. Two straps secured the tape recorder and another two straps tied down the Brush recorder (fig. 16). All other component parts were approved by visual inspection.

Station 7. --The equipment in station no. 7 (Smith-Torrey) was adequate, as installed, until an electronics cabinet and a storage cabinet were added. These additions overloaded the left floor-track clamp in the aft of the gimbal mount and necessitated the addition of one more aft floor-track clamp on the left-hand forward side of the gimbal mount (figs. 17 and 18). The shear loads were then within the limits of the clamps and the floor track.

Station 8. --The equipment in station no. 8 (De-Groot) was strengthened before shipment and needed only slight changes on installation. The members added are shown in fig. 19. Some of the Allen bolts were replaced with more reliable AN bolts. A member was added between the bottom of the stand and the side wall so that the side loads would go directly from the stand to the side wall. This eliminated bending of the bracket at the rear of the stand. Figure 20 shows how this angle was bolted. Spacers added between the floor, track clamps and the stand had to be analyzed because the fitting was eccentrically loaded and thus imposed shear and bending on the bolts.

Station 9. --Professor Righini's equipment, station no. 9, was installed as designed, except for the addition of one floor-track clamp to take horizontal shear, because the equipment weighed more than originally planned. This floor-track clamp and spacer are shown in fig. 21. Figure 22 shows two brackets added later to reduce vibration of the camera, which was mounted in the center of the top plate.

Stations 10 and 11. --The Deutsch-Cameron spectrograph, stations 10 and 11, was sufficient as designed and installed except that a bolt was replaced by

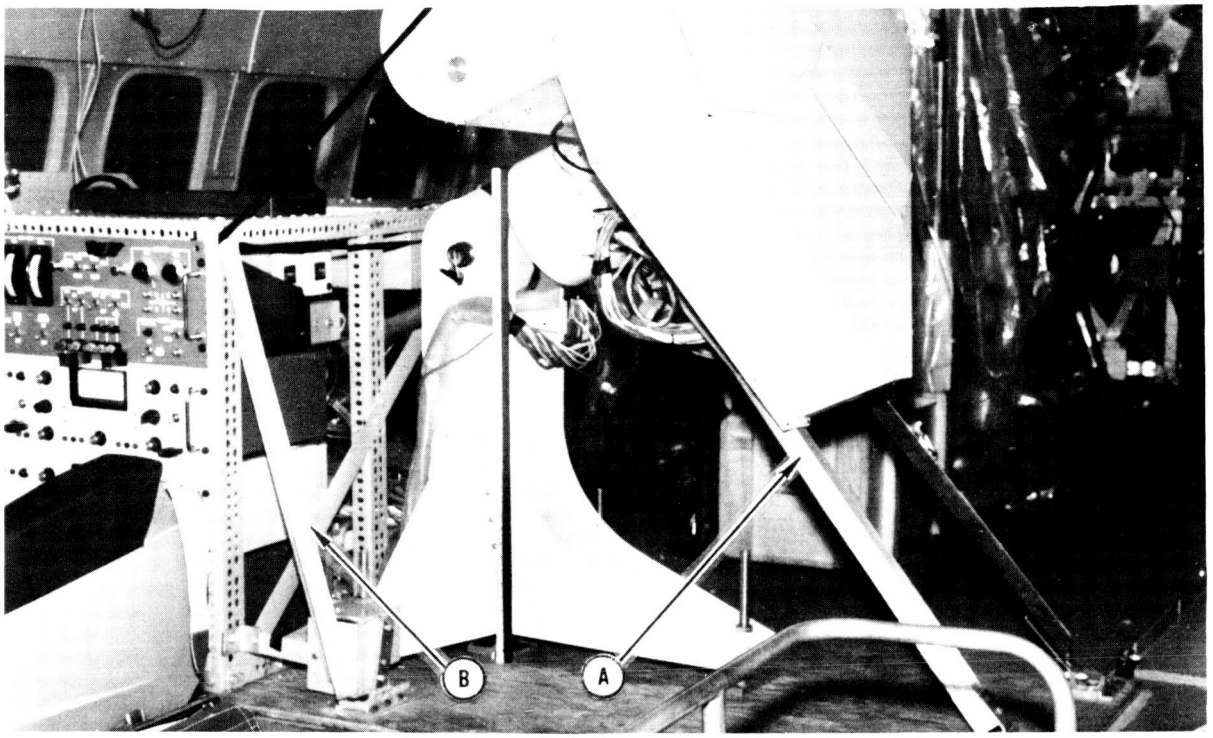

A = SPECTROGRAPH BRACE B = ELECTRONICS BRACE

Figure 15. Sacramento Peak-University of Hawaii Equipment Installation (Forward View)

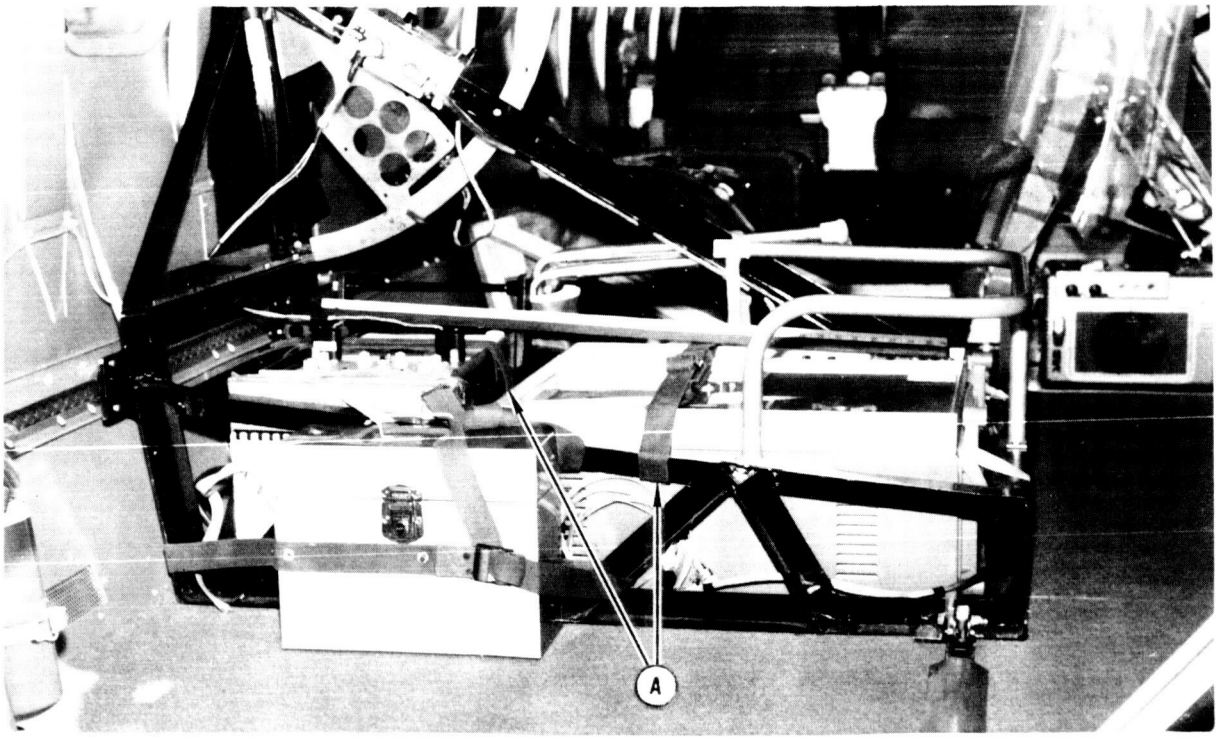

Figure 16. Installation of John Hopkins University Equipment

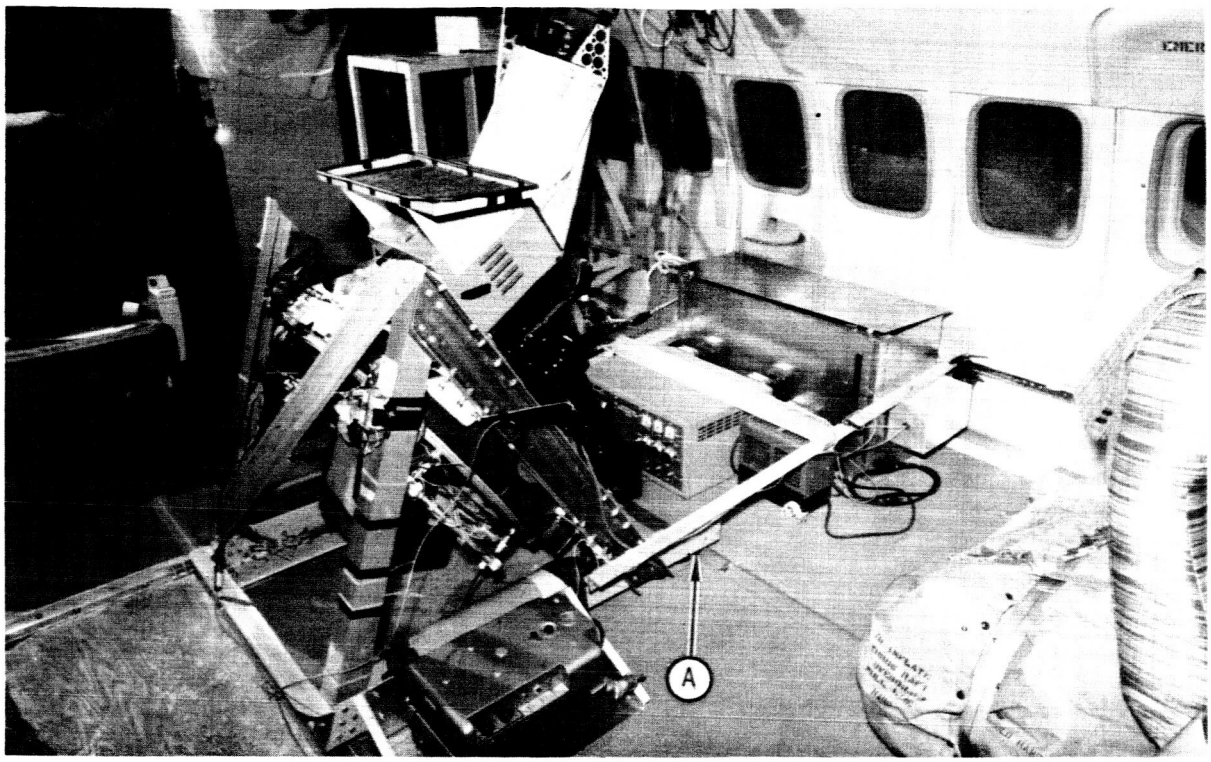

Figure 17. NASA – Ames Equipment Installation (Forward View)

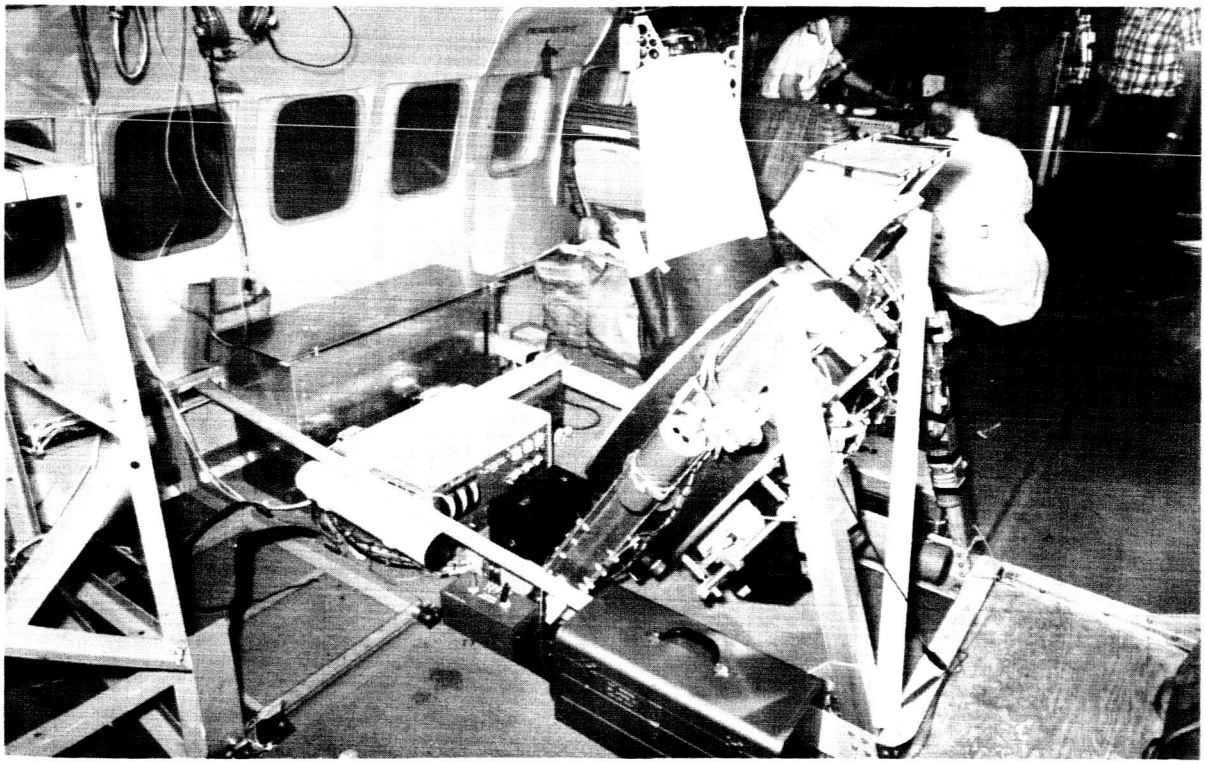

Figure 18. NASA- Ames Equipment Installation (Aft View)

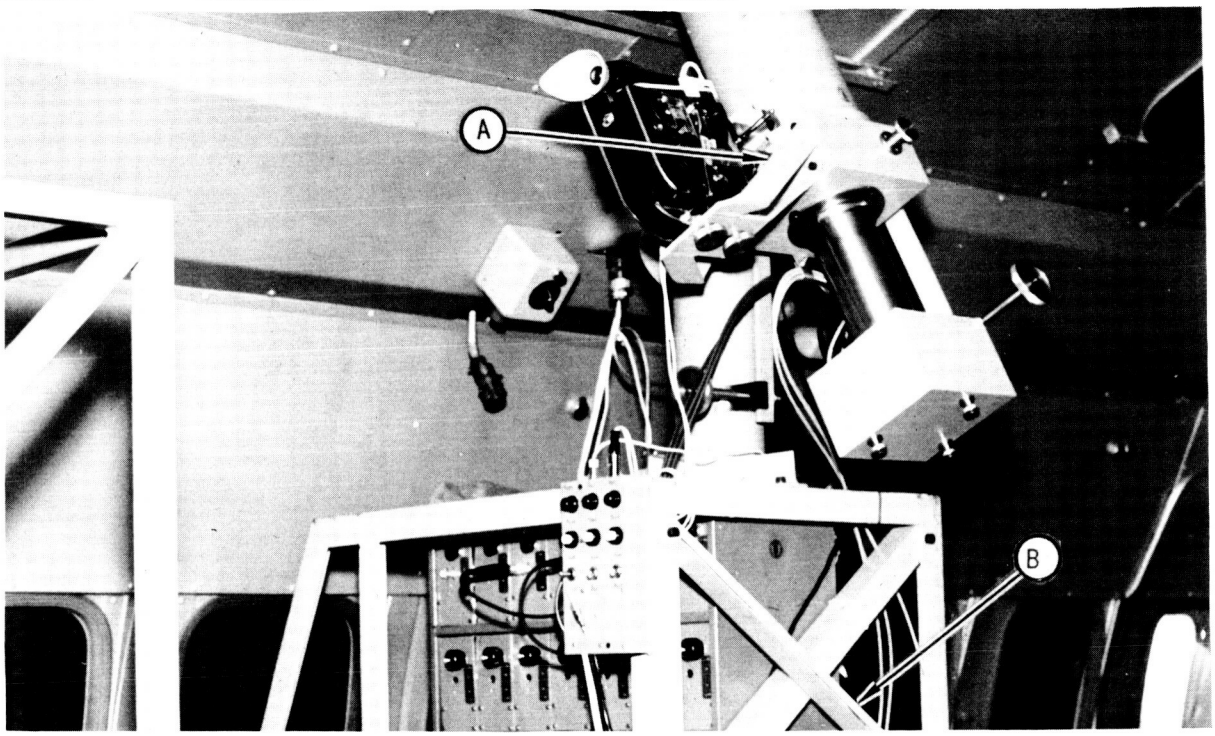

A = TELESCOPE SUPPORT MEMBER B = BASE CROSS-MEMBER

Figure 19. Observatory of Utrecht Equipment Installation (Forward View)

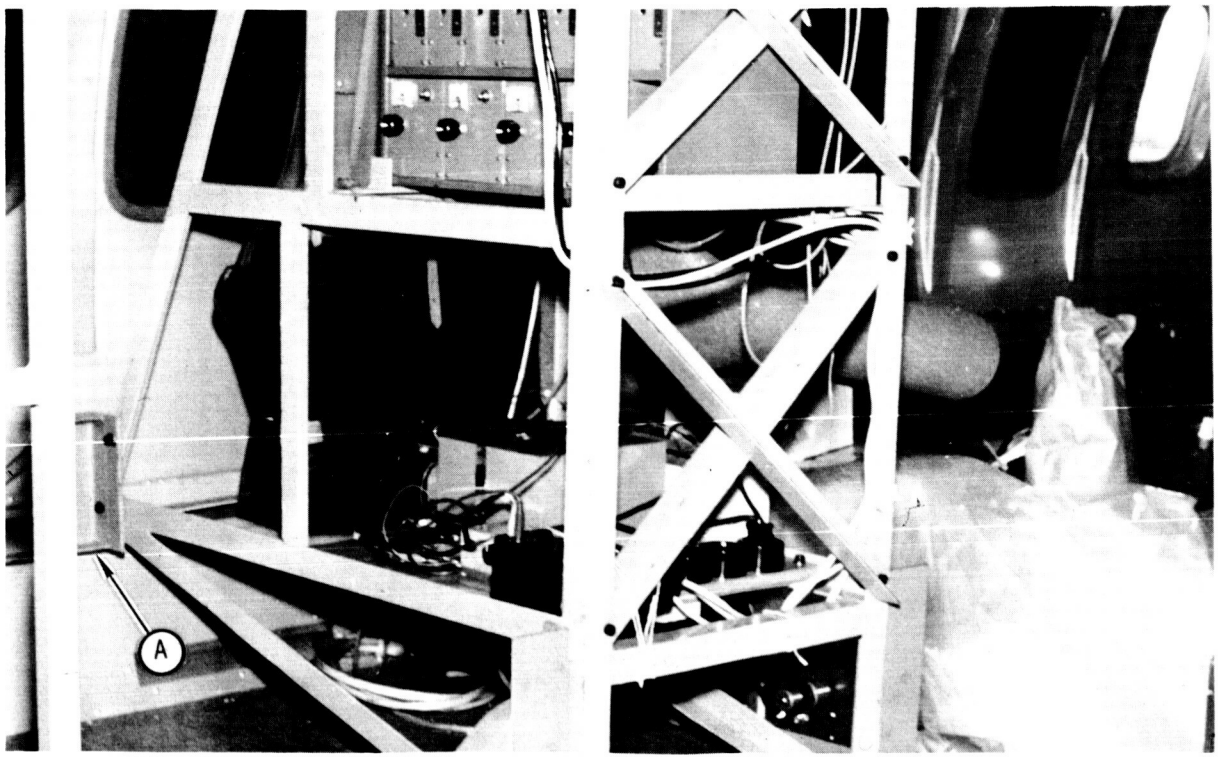

Figure 20. Observatory of Utrecht Equipment Installation (Aft View)

A = SIDEWALL CLAMP

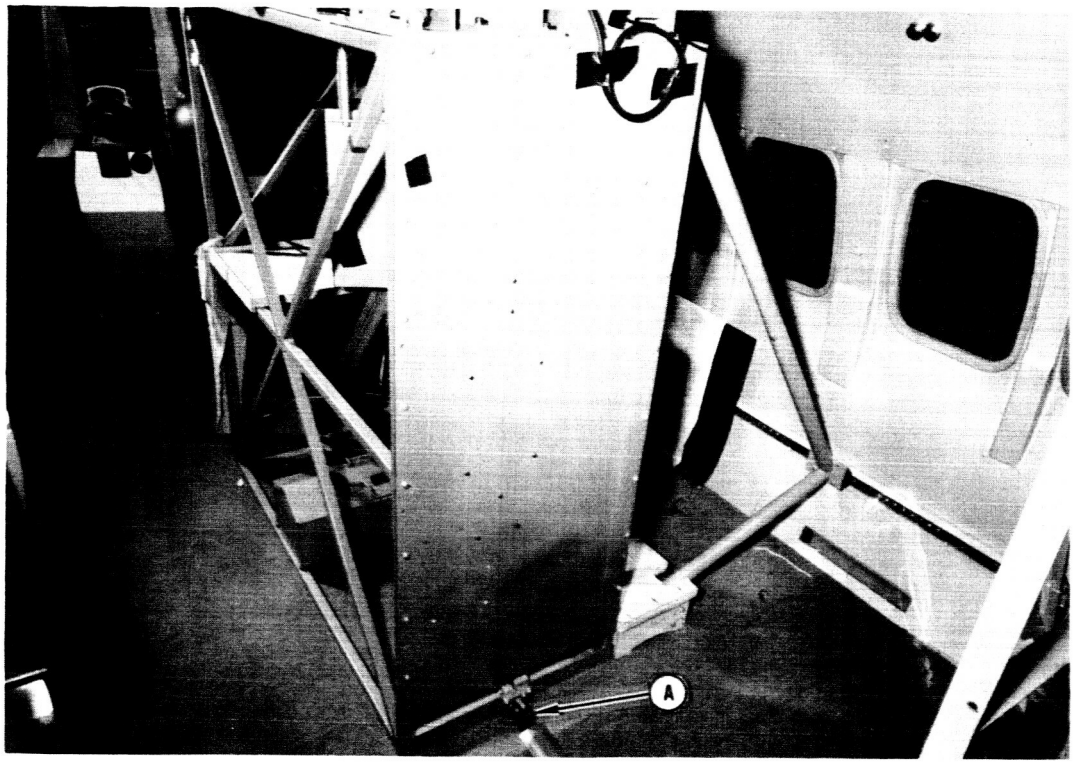

Figure 21. Observatory of Arcetri Equipment Installation (Forward View) A = FLOOR TRACK CLAMP

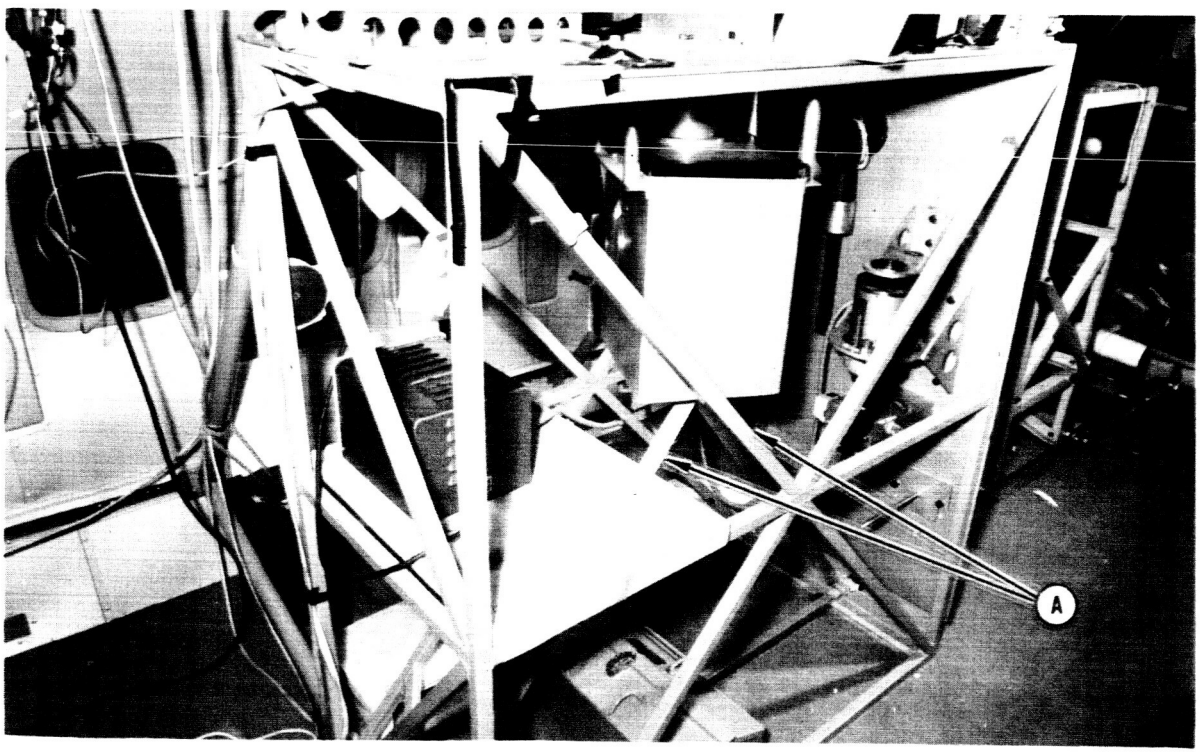

Figure 22. Observatory of Arcetric Equipment Installation (Aft View) A = CROSS BRACE MEMBERS

a quick release pin (figs. 23, 24,and 25) in the spectrograph arm. The electronics and refrigerator associated with this equipment are shown in fig. 26.

Station 12. --The equipment in station no. 12 (Dossin-Macar) required several modifications before flight. A limiting chain (fig. 27) was added to retard the vertical motion of the camera gimbal to prevent the lens from touching the optical glass. A safety cable (fig. 27) also was added to secure the camera assemblies for takeoff and landing. Because the stand for the cameras was very flexible, stiffening members were added. The loads caused by the weight of the cameras did not go directly to the floor track but went through channels in torsion, bending, tension, and compression. The optimum solution for this structural problem would have been to completely redesign and refabricate the mount. Since time did not permit redesign, Douglas decided to require only that the emergency loads were definitely to be taken by the floor track and were to be less than the maximum allowable loads (figs. 27 and 28). Braces were added to carry the loads in emergency conditions and to eliminate the low-frequency vibration of the apparatus on takeoff and landing.

Station 13. --The original Arnquist-Waddell equipment scheduled for installation in station no. 13 was to be stowed, except for the mounting stand, during takeoff and landing. However, the stowed portions proved to be too heavy to install safely in flight; the stand was not strong enough, even for flight loads, with the equipment attached, and the time required for removing the camera from the stand and stowing it was excessive. For these three reasons, the apparatus was not approved for installation. Subsequently, a new camera and stand were designed and installed. For takeoff and landing, the camera was secured, as mounted, with quick release locking pins and safety straps. These are shown in figs. 27 and 29.

Station 14. --The Carpenter-Mantis equipment in station no. 14 was safe for all loads when the locking bolt (fig. 30) was installed in the bottom of the camera.

Station 15. --The tripod and cameras for station no. 15 were not safe for takeoff and landing when set up and, therefore, they were stowed during that period of the flight. The pallet and tie-down straps are shown in fig. 30.

Miscellaneous

Two aerosol collector assemblies were installed on struts mounted on the nose tunnel access doors--one on each side. The struts were mounted to a 3/16-in. -thick, formed aluminum plate. Each plate was bolted to a door with 10 no. 8 flush-head screws and self-locking nut plates. The four screws attaching the collector to the struts were safety wired after each change of the collectors. This installation is illustrated in fig. 31.

A sun compass lens mount was fastened to the no. 1 left-hand standard window opening with an aluminum strap and two no. 10 screws. Below this a mirror was attached to the seat, the side-wall track, and the lens mount. A grid was mounted above the navigator's table, on the right-hand side of the aircraft.

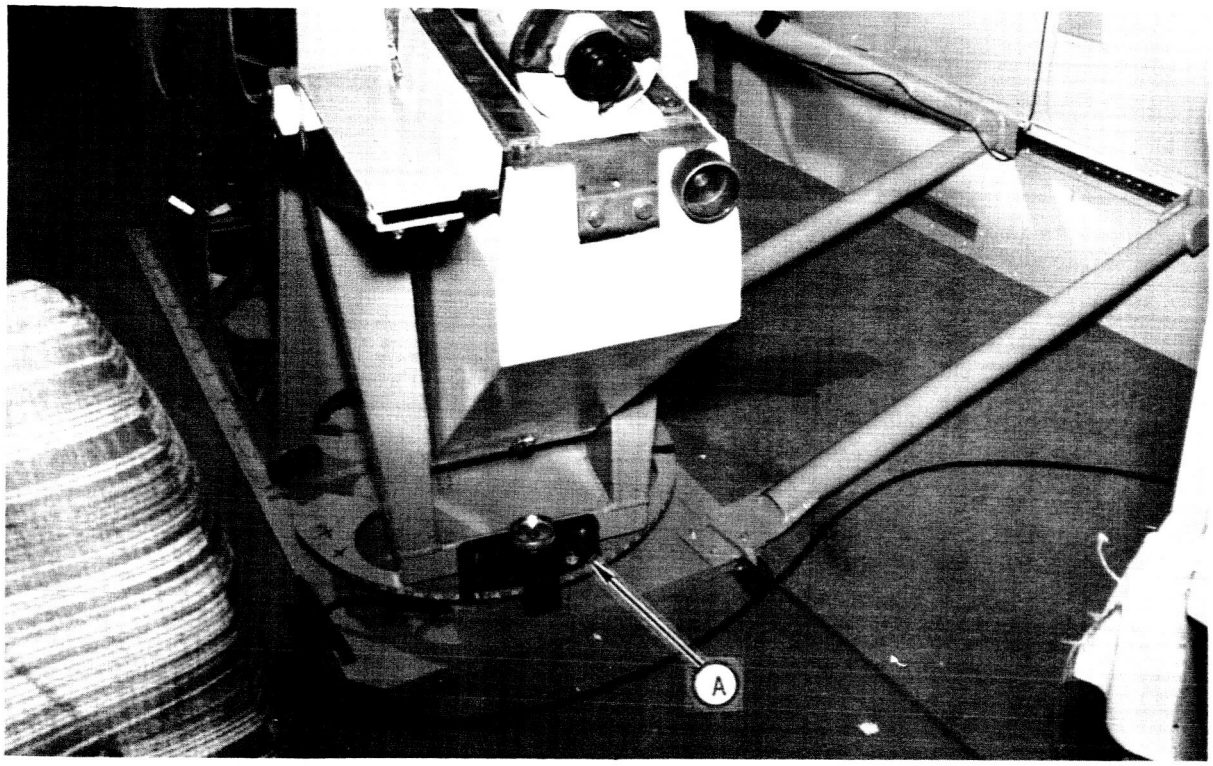

Figure 23. Douglas-Mt. Wilson Spectrograph Base Installation

A = BASE LOCKING PIN

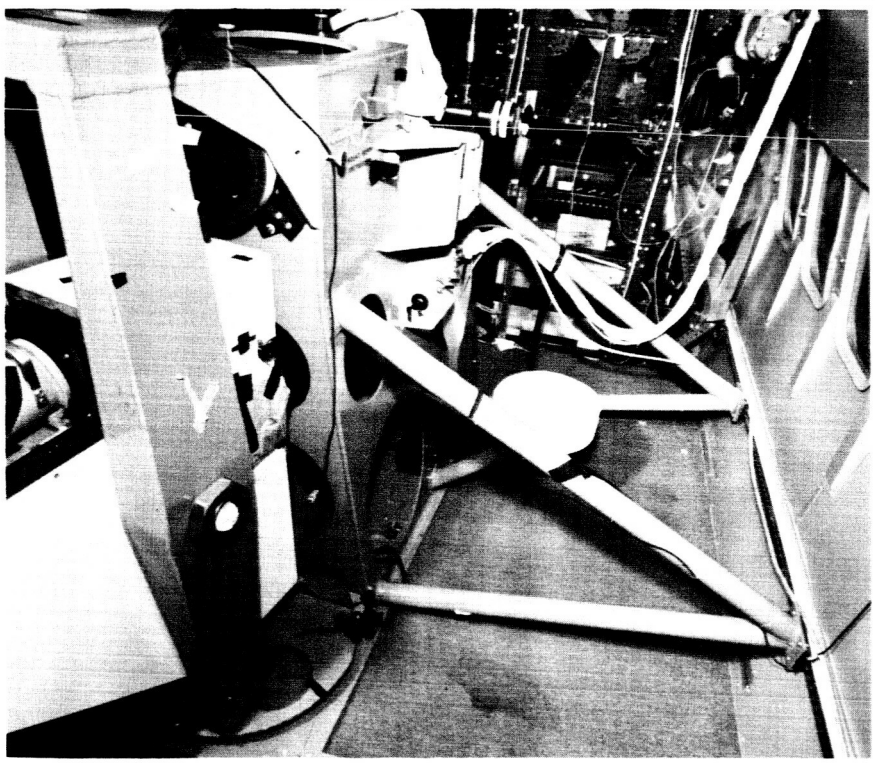

Figure 24. Douglas-Mt. Wilson Spectrograph Installation (Inboard View)

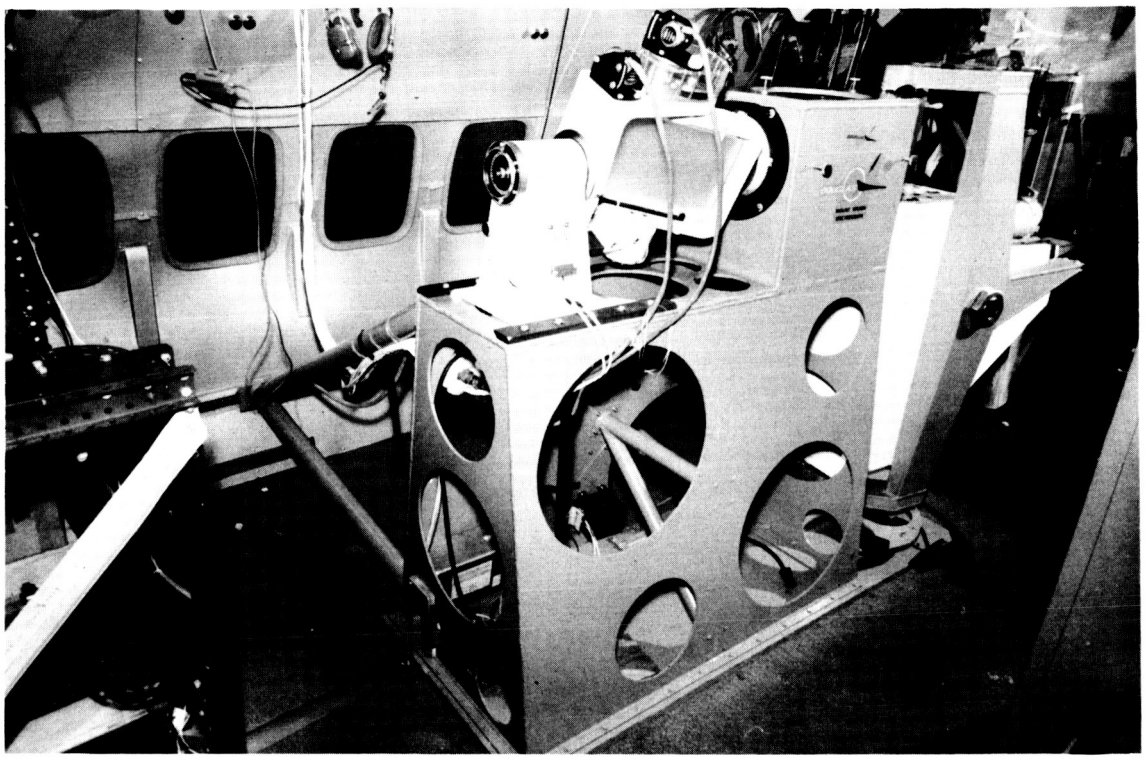

Figure 25. Douglas-Mt. Wilson Spectrograph Installation (Aft View)

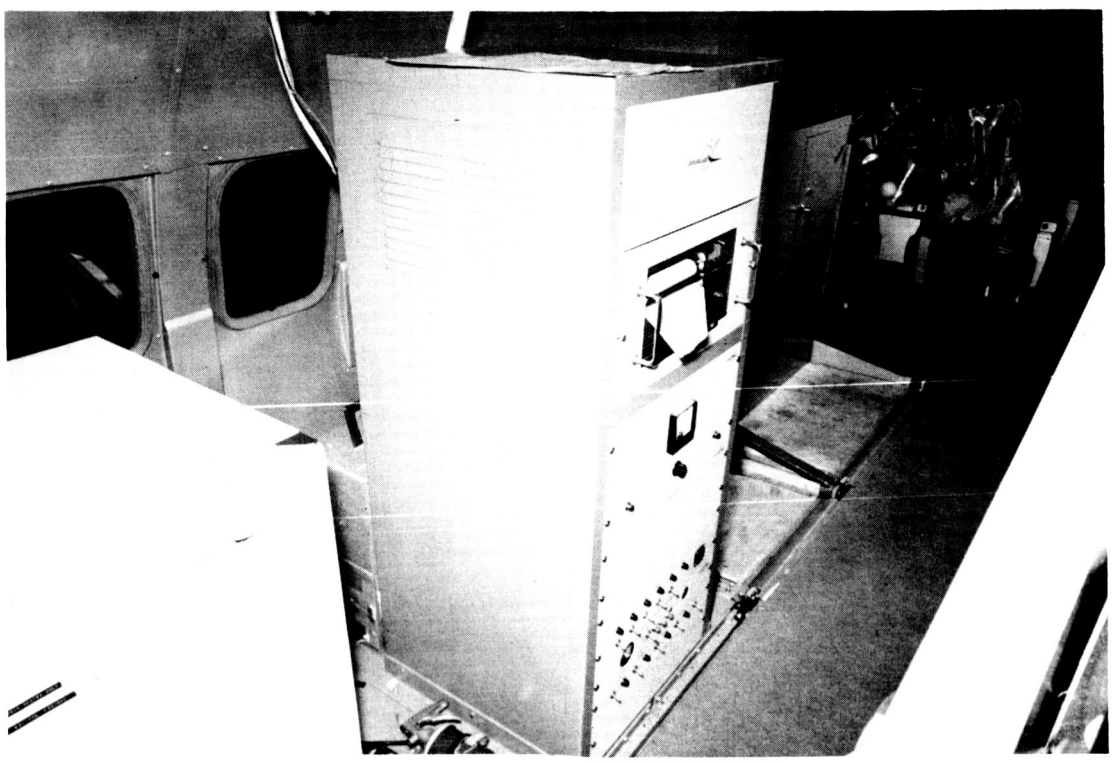

Figure 26. Douglas-Mt. Wilson Electronics Installation

A = MOUNT SUPPORT BRACE
B = MOUNT SUPPORT TIE-DOWN BRACE
C = RESTRAINING CABLE
D = RESTRAINING CHAIN
E = LOCKING PINS

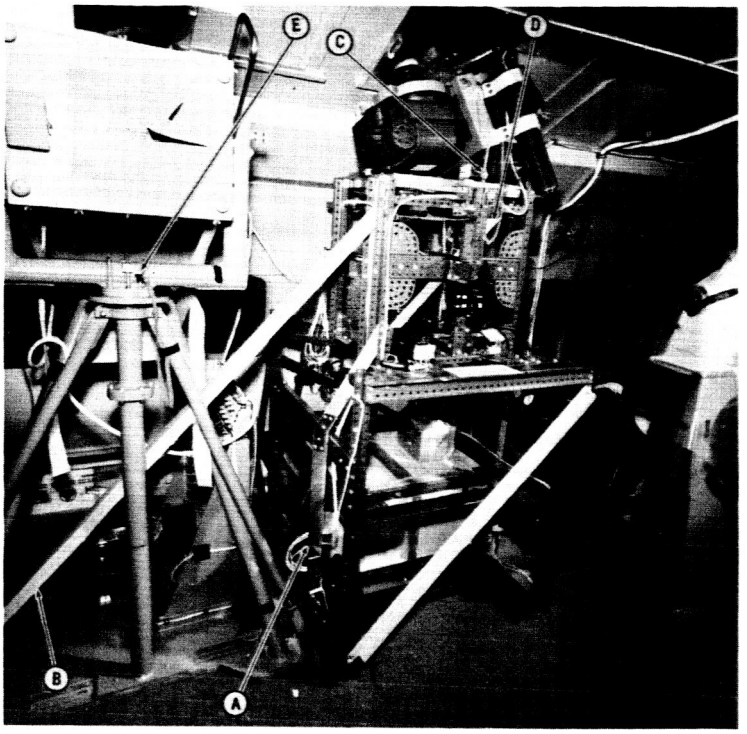

Figure 27. University of Liege and Douglas Polarization Equipment Installations (Side View)

A = FLOOR-TRACK ATTACHMENT
B = MOUNT MEMBER VERTICAL
C = MOUNT CROSS-MEMBER

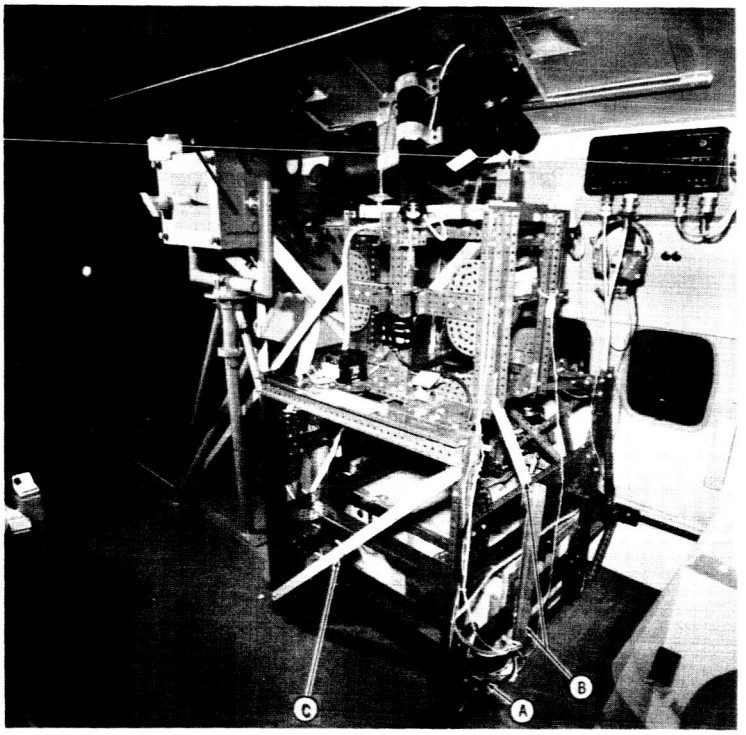

Figure 28. University of Liege and Douglas Polarization Equipment Installations (Forward View)

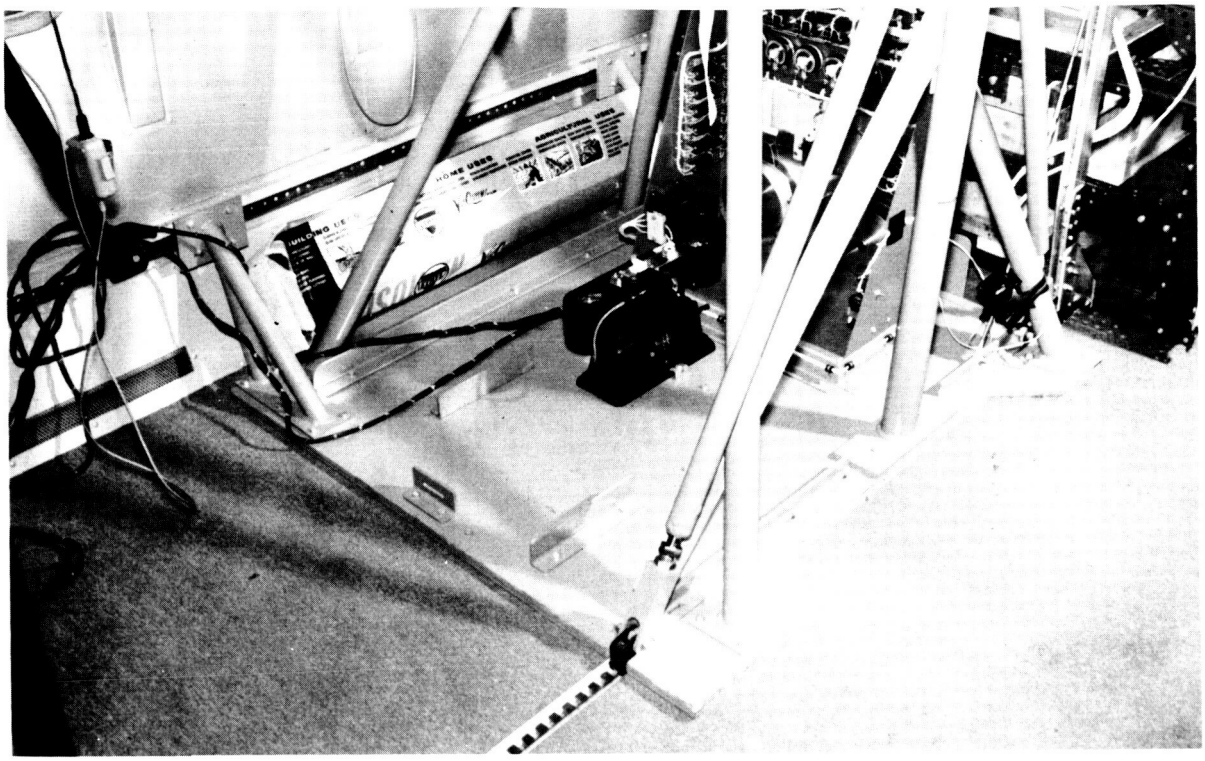

Figure 29. Base of Douglas Polarization Equipment

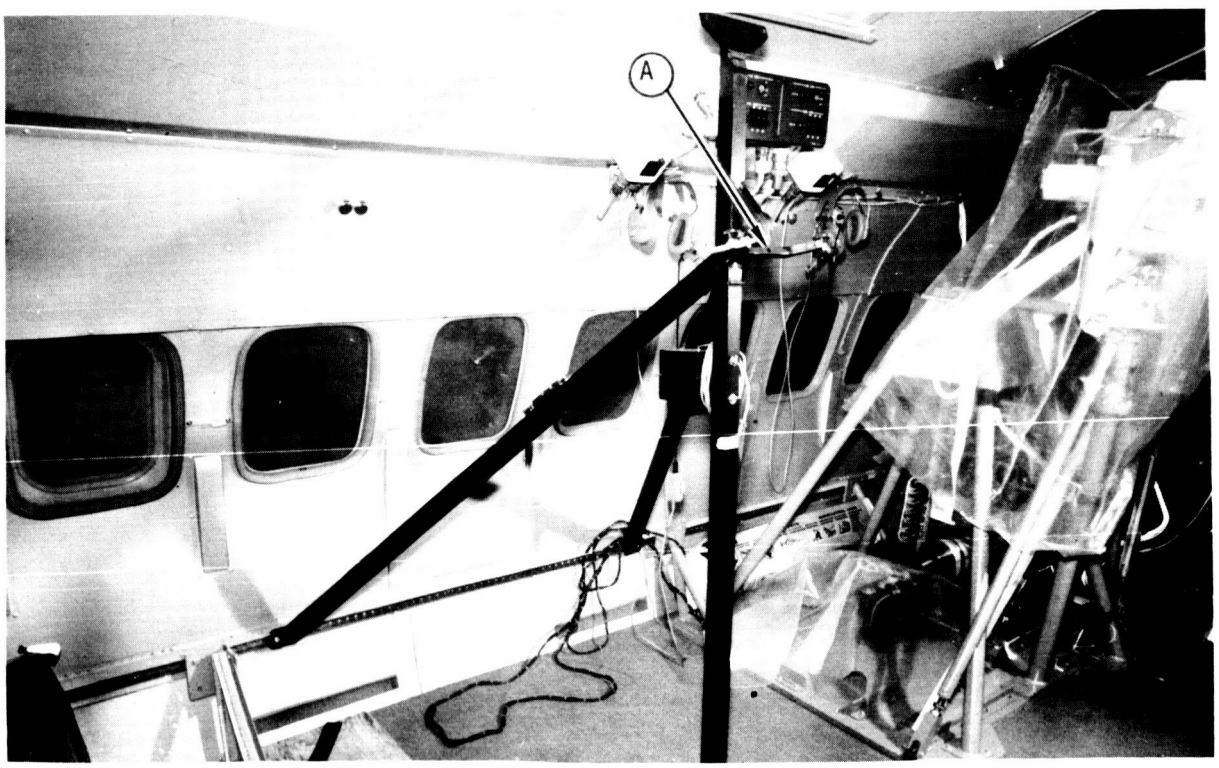

Figure 30. NASA-Houston Equipment Installation

A = TELESCOPE SUPPORT YOKE

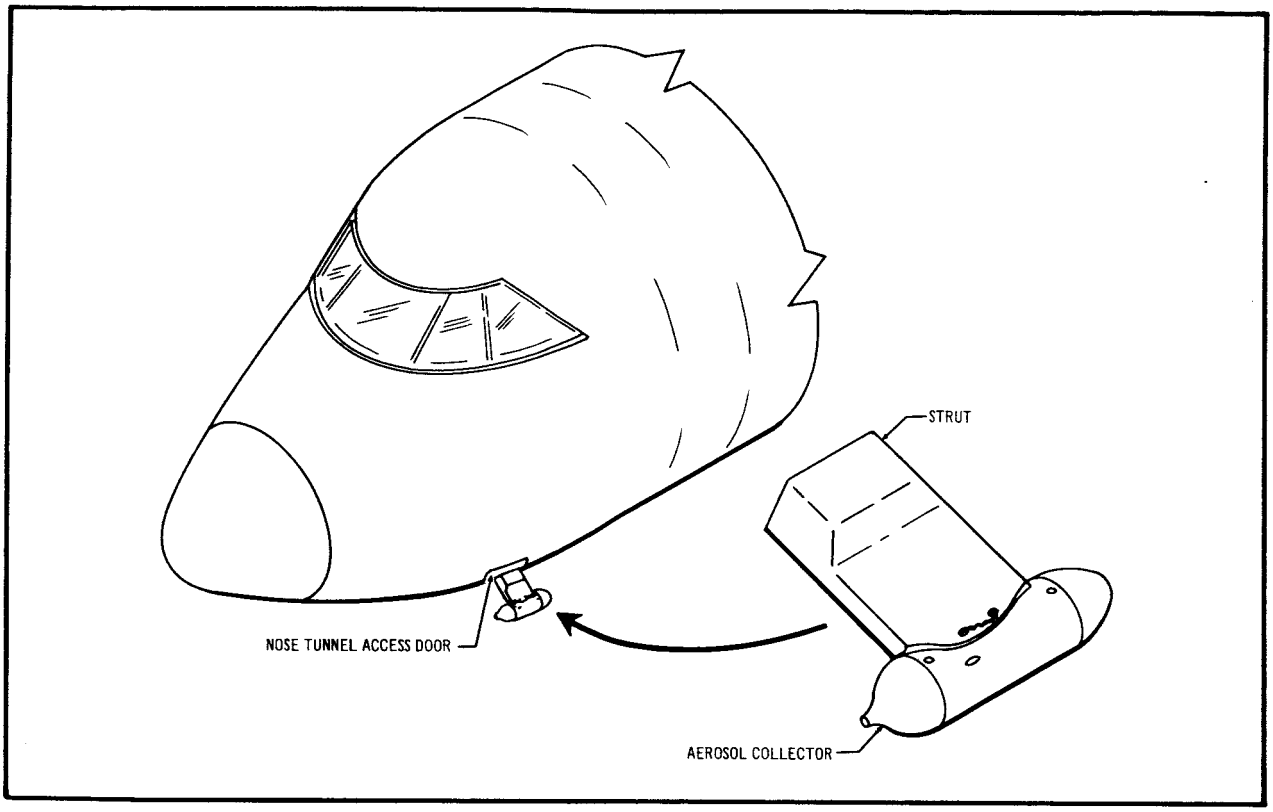

Figure 31. Douglas Aerosol Collector Installation

TASK III: NAVIGATIONAL STUDIES

Task III of the Douglas proposal to NASA (ref. 1) concerned the following:

(1) Prepare a revised edition of a map of French Polynesia showing the eclipse track corrected for the difference between ephemeris and geographic longitude

(2) Trace the umbra path of the eclipse on this map as it would appear to an observer at an altitude of 37,000 ft

(3) Show the shadow ellipses at an altitude of 37,000 ft at stations 20, 15, 10, 5, and 0 min before and after mid-maximal totality; also show sun-bearings for umbra stations at 5-min intervals

(4) Determine the correct sun elevations as seen from an altitude of 37,000 ft

(5) Illustrate the following flight paths on an oblique gnomonic projection tangent to the Earth at the point of mid-maximal totality:

   (A) A great circle on the Earth tangent to the umbra track at the point of mid-maximal totality

   (B) A loxodrome at constant bearing of the local meridian at the point of mid-maximal totality (a right turn)

   (C) A path following the umbra track (a right turn)

   (D) A -90° constant sun-bearing path intercepting the umbra track at the point of mid-maximal totality (a left turn)

A detailed study of each of the above flight paths was made, and a flight plan was recommended based on these findings. A table of physical constants used in this section is shown in Appendix A.

Subtask 3.1

The corrected map of French Polynesia showing the eclipse track is shown in fig. 32. The dashed line labeled sea-level is the path of the umbra as projected upon the Earth's surface, and the solid line just above the dashed line represents the track at an altitude of 37,000 ft. The track at 37,000 ft is 3 to 7 n.mi. North of the ground track, toward the direction of the sun.

The data used for plotting the umbra path (fig. 32) were taken directly from the United States Naval Observatory Circular No. 102 (ref. 9), supplemented by correspondence with the Naval Observatory (Appendix B and ref. 10). The arguments in the circular were given in Universal Time (U.T.) and the longitudes were referenced to the Greenwich meridian. The correction between Ephemeris and U.T. was considered in the circular.

The sun-bearing angle relative to the local meridian and the sun elevation angle (contained in the circle at the end of the azimuth arrows) are shown in fig. 32 at 5-min intervals along the track. The sun elevation at 37,000 ft differed by less than +6 min of arc from that seen at sea level. The sun elevation angle was required only to the nearest tenth of a degree. There was practically no difference between the elevation angles on the ground and those at altitude as given in fig. 32.

Choice of Eclipse Intercept Point

The duration of totality at the point of maximum totality is 316.5 sec, making this point a good choice of interception point. To minimize slueing problems for aircraft instruments, it is desirable that the sun be 90° abeam. These two points nearly coincided. In consultation with NASA-Ames, the point where the sun was 90° abeam was chosen as a nominal intercept point. This point's coordinates were: longitude, 131°55' W; latitude, $-1^{\circ}37'$ S; and U.T. $21^{h}23^{m}44^{s}$ (about 18 min after local noon). In the early planning stages (January through February 1965), the intended base of operations was Tahiti. The intercept point was 1,414 n.mi. northeast of this island. The French government later indicated that they would not allow the expedition to stage from their protectorate. The new base of operations was established at Hilo, Hawaii, which was 1,810 n.mi. northwest of the intercept point. The use of Tahiti as a stopover for refueling was granted, and the total distance was within the range of the aircraft. With the position of intercept determined, five possible flight paths were studied:

(1) Follow the center path of the umbra

(2) Fly a loxodrome course

(3) Fly a great circle course

(4) Fly a straight space trajectory

(5) Fly a course of constant sun-bearing

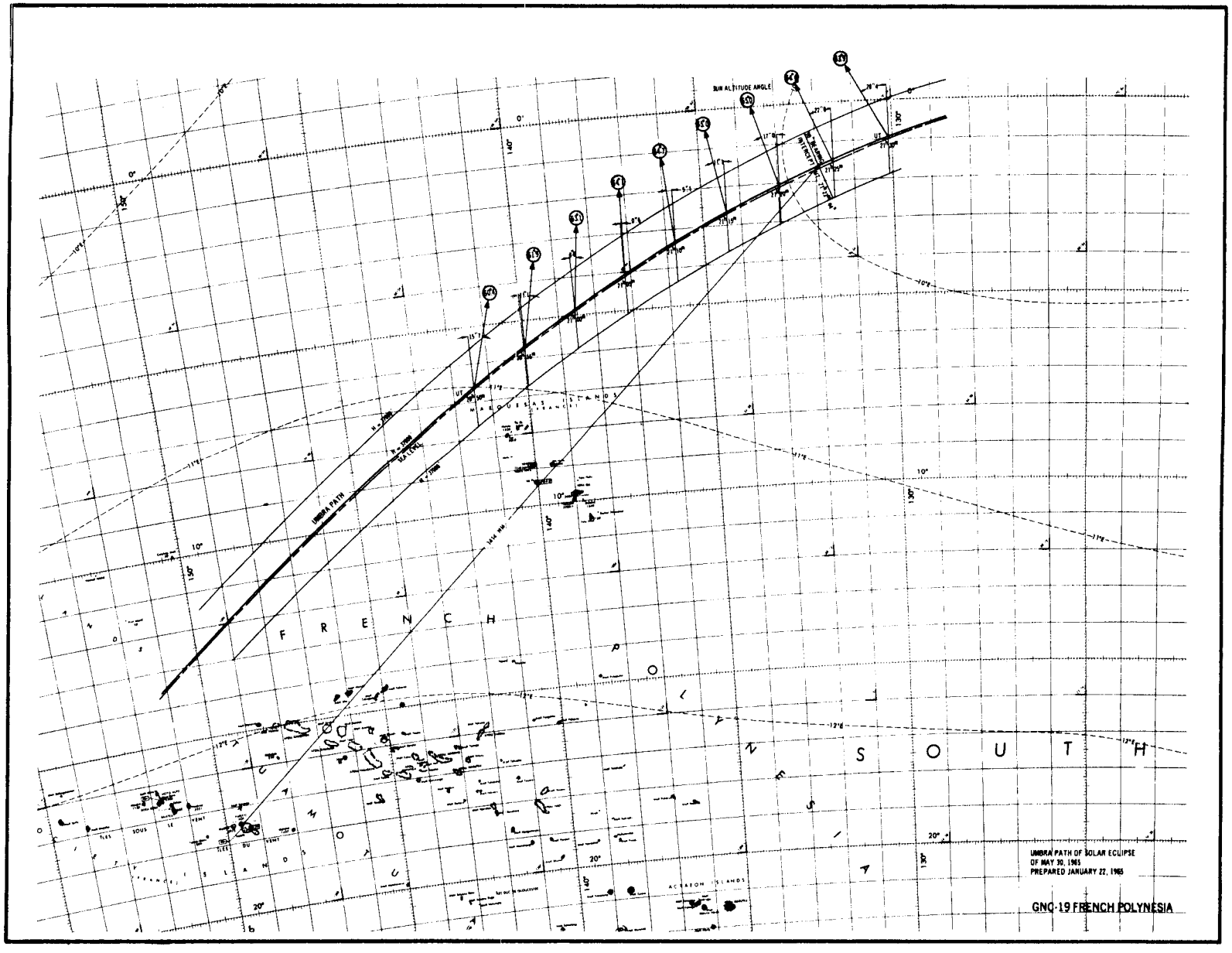

Figure 32. Umbra Path of Total Solar Eclipse of May 30, 1965

These flight paths were easily compared by drawing them on the oblique gnomonic projection at the point of intercept. This was accomplished by projecting the Earth's surface onto a plane which is tangent to the Earth's surface at the point of intercept by using rays drawn from the center of the Earth. Fig. 33 illustrates this projection.

A spherical Earth was assumed and the sea level plane rather than the plane at the aircraft altitude was used. In fig. 33, the point of tangency of plane ABCE is assumed to have a longitude λ_o and latitude ϕ_o. Longitude is measured positive West from Greenwich; latitude is measured positive North from the Equator. The general point, P, on the Earth's surface is located by the difference in longitude from λ_o, $\lambda - \lambda_o$, and by latitude, ϕ. It is projected to a point Q, with coordinates x, y on a plane ABCD. The x, y coordinates have their origin at the point of tangency; x is positive Westward and y is positive Northward. This is a left-handed coordinate system. The transformation equations from ref. 11, pp. 283-285 are:

$$\left.\begin{aligned} x &= \frac{R_o \sin(\lambda - \lambda_o)\cos\phi}{\cos\phi\cos\phi_o\cos(\lambda - \lambda_o) + \sin\phi\sin\phi_o} \\ y &= \frac{R_o(\sin\phi\cos\phi_o - \sin\phi_o\cos\phi\cos(\lambda - \lambda_o))}{\cos\phi\cos(\lambda - \lambda_o)\cos\phi_o + \sin\phi\sin\phi_o} \end{aligned}\right\} \quad (4)$$

where R_o is a scaling factor, 221.827 in. This gives a map scale of 3.87 in. = 60 n. mi. at the point of tangency. In ref. 11, x and y are interchangeable with ξ and η, and λ and ϕ are interchangeable with α and δ. Some algebraic manipulation was needed to obtain the equations given here.

The inverse equations from ref. 11 are:

$$\left.\begin{aligned} \lambda &= \lambda_o + \arctan\left(\frac{x}{R_o\cos\phi_o - y\sin\phi_o}\right) \\ \phi &= \arctan\left(\frac{R_o - \cos\phi_o(R_o\cos\phi_o - y\sin\phi_o)}{\sin\phi_o\sqrt{x^2 + (R_o\cos\phi_o - y\sin\phi_o)^2}}\right) \end{aligned}\right\} \quad (5a)$$

This inverse exists where the Jacobian:

$$J = \frac{(\cos\phi)R_o^2}{(\cos\phi_o\cos\phi\cos(\lambda - \lambda_o) + \sin\phi_o\sin\phi)^3} \quad (5b)$$

is non-zero, which will be true except in the immediate region of the poles.

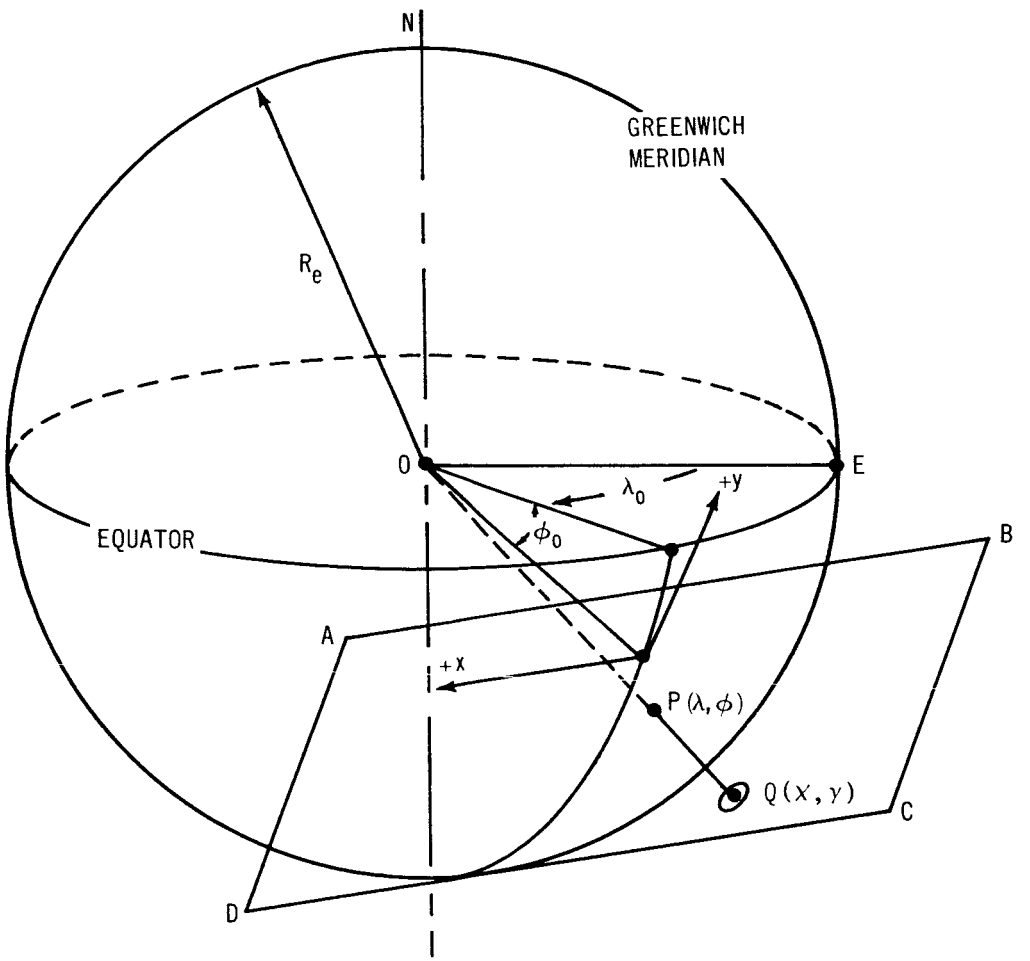

Figure 33. Mapping the Earth's Surface Into a Tangent Plane

This type of projection was convenient for the following reasons: (1) all great circle courses map into straight lines; (2) it gives reasonable perspective to the curvature of the various flight paths in the region of the point of intercept; (3) it represents the intercept region in much the same way as the pilots and navigators would see it; and (4) it was convenient in determining the second and third contact times and in developing an error matrix for the aircraft at intercept.

Choice of Flight Path

Fig. 34 shows the map with the alternate flight paths. One obvious choice was to follow the center path of the umbra. Geographic coordinates of the center of the umbra track given in ref. 9 were mapped into the tangent plane using equation (4). Maximum duration of totality will occur for this course, minimizing the effect of timing error on totality duration.

The sun bearing angle would have changed at the rate of approximately 1^{o}/min as seen from this course, and would have been altered by $1.^{o}6$/min of timing error. As many of the astronomical instruments were to be mounted pointing in a fixed direction, this sun bearing angle variation would have strained their slueing capacity and was therefore undesirable.

A second alternative was to fly a loxodrome, which is a path at constant azimuth angle with respect to the meridians of longitude. This is the simplest flight path for an autopilot to steer. A sufficiently sensitive inertial navigator precessed for latitude changes will follow this path. The equation for geographic coordinates of a loxodrome is (ref. 12, page 38):

$$\lambda - \lambda_o = -\tan \omega \log_e \left| \frac{\tan (\pi/4 + \phi/2)}{\tan (\pi/4 + \phi_o/2)} \right| , \qquad (6)$$

where λ_o and ϕ_o are the coordinates of the desired intercept point and ω is the azimuth angle. Fig. 34, shows a loxodrome course through the adopted intercept point and tangent to the umbra path. To obtain coordinates of this curve in the tangent plane of fig. 33, equation (6) was substituted in equation (4).

A great circle course is also easily steered by autopilot. It requires a constant aircraft heading change. In fig. 34, the great circle tangent to the umbra path at the adopted intercept point is shown. The undesirable feature of both loxodrome and great circle flight paths was the change in sun bearing angle from the aircraft. This angle varied approximately 8^{o} during the 9 min of anticipated totality.

Steering the aircraft along a straight space trajectory was considered, i.e. the path followed to keep the sun's bearing and elevation angles constant. The trajectory studied would be tangent to the umbra path at the intercept point and would have involved an initial dive and an exit climb of $1^{o}45'$. Excessive air speed variations probably would have made this maneuver undesirable from the eclipse observers' standpoint, unless compensatory jet thrust control were available. Necessary instrument modifications and flight testing caused the idea to be shelved.

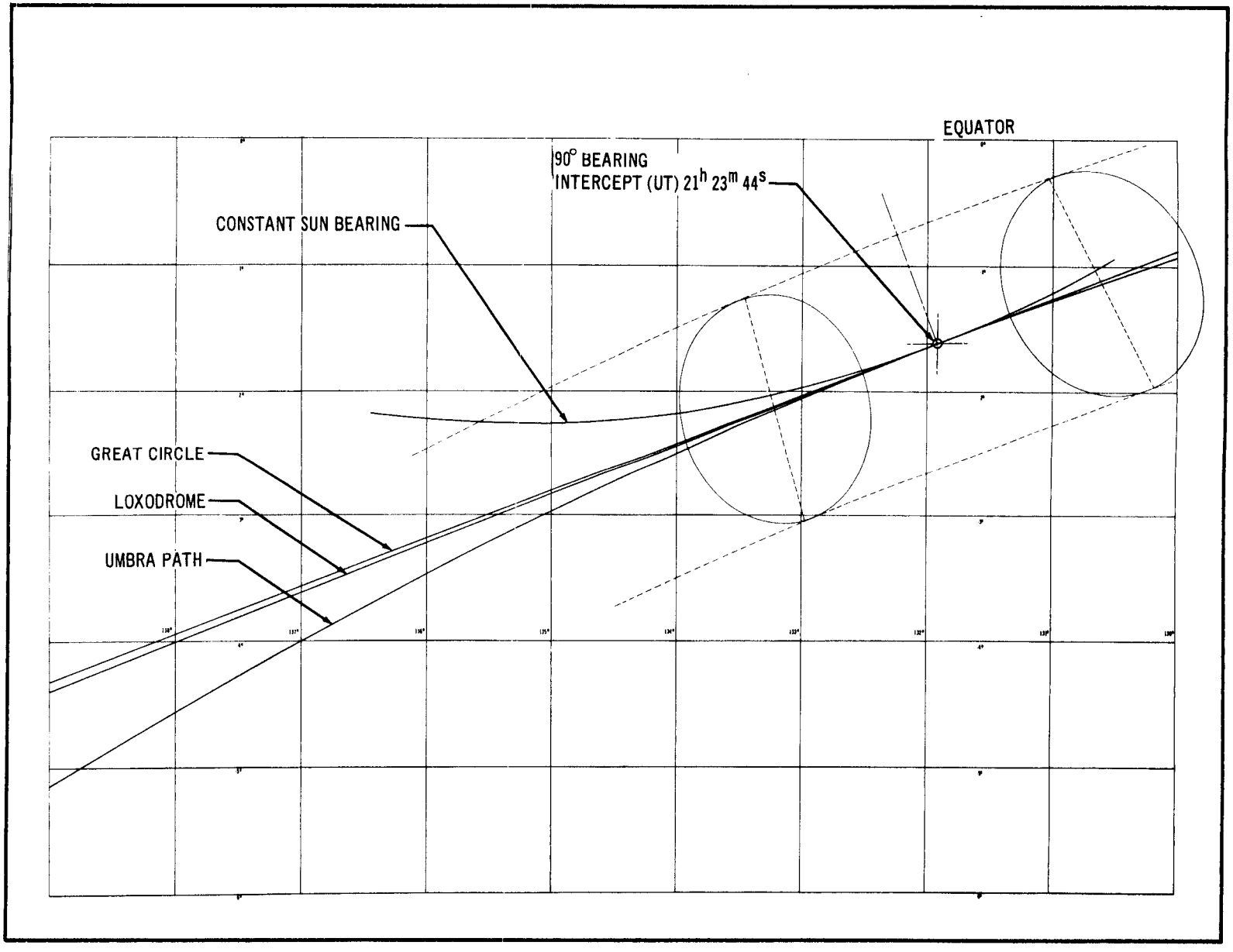

Figure 34. Alternate Flight Path in Gnomonic Projection

The most desirable flight path was one along which the sun bearing angle remained constant. The elevation change was small because the eclipse was observed near local noon. For the case of -90^{o} bearing angle, the aircraft heading (measured clockwise from North) was:

$$H = AZ + 90^{o}, \tag{7}$$

and the changes in longitude and latitude were:

$$\left.\begin{aligned} \Delta\lambda &= V \cos\phi \sin h \, \Delta t \,, \\ \Delta\phi &= V \cos h \, \Delta t \end{aligned}\right\} \tag{8}$$

where V is the aircraft speed and Δt is the elapsed time interval. The azimuth, AZ, is computed by the following formulae (see Appendix C):

$$U.T. = Z.t. \pm \lambda \tag{9}$$

$$h = GST_{o} + U.T. + \Delta t - \lambda - \alpha \tag{10}$$

$$\sin\epsilon = \sin\phi \sin\delta + \cos\phi \cos\delta \cosh \tag{11}$$

$$\sin AZ = -\sin h \cos\delta / \cos\epsilon \tag{12}$$

$$\cos AZ = \frac{\sin\delta - \sin\phi \sin\epsilon}{\cos\phi \cos\epsilon}$$

where

U.T. = Universal Time (Greenwich Mean Time)
Z.T. = Zone Time (Local Standard Time)
h = Hour angle of target object
GST_{o} = Greenwich sidereal time at 0^{H} U.T.
Δt = Correction of U.T. to corresponding sidereal time interval
α = Right ascension of target object
δ = Declination of target object
ϵ = Elevation angle of target object
λ, ϕ = Observer's longitude and latitude

Using a computer program, H, ϵ and AZ were evaluated at the adopted intercept point λ_{o}, ϕ_{o} by equations (10), (11), and (12). The aircraft heading then was determined by equation (7). This permitted extrapolation using equation (8) to a new point, λ, ϕ. The process was repeated to give additional coordinate points along the desired curve. The time steps, Δt, were sufficiently small to avoid noticeable variation in the derivatives of λ and ϕ. Here the U.T. was uniquely fixed by the choice of λ_{o}, ϕ_{o} on the eclipse track. The quantities

φ , δ, GST_0, and Δt were given by the American Ephemeris and Nautical Almanac (ref. 13). At each computed point in the constant bearing path, the longitude, latitude, aircraft heading, target elevation angle, and universal time were printed out.

The constant -90° sun bearing path computed for the solar eclipse intercept flight of May 30 resulted in a 1° change in sun elevation angle ($\epsilon = 64.^\circ 7$ at mid-intercept), which was within the slueing capability of the astronomical telescopes and cameras. This was a very minor inconvenience considering the relaxation of the azimuth-slueing requirement. This was chosen as the first approximation to the course to be followed.

Simulation of Constant Bearing Path

The constant bearing flight path adopted for the solar eclipse flight was not a simple geometric curve. It was found to be closely approximated by an arc of a circle in the tangent plane. This was fortunate because a precise execution of the constant bearing course would have required a variable heading change. The circular path approximation required a relatively simple maneuver called a coordinated banked turn. The equation defining the radius of curvature for the best circular fit to the constant bearing path indicated a value of 592 n.mi.

$$R = 0.955\ V/(\overline{dh/dt}) \quad \text{n.mi.} , \tag{13}$$

where dh/dt is expressed in degrees per min and V is in knots. The bank angle necessary to execute a turn with this curvature is:

$$\beta = \arctan (V^2/Rg) , \tag{14}$$

which is easily derived by equating the centrifugal force acting on the aircraft with the lift component opposing it. Taking a nominal ground speed V = 490 knots for the CV 990, the bank angle corresponding to R = 592 n.mi. is $0.^\circ 3$. After the final hot run flight strategy had been established , it was ascertained that the Sperry-Phoenix autopilot could not be tuned to execute such a shallow bank maneuver in the time available. This and other flight operation problems were outside the scope of Douglas responsibilities and are not discussed here.

Determination of Beginning and End of Totality

The times at which total solar eclipse would begin (second contact) and end (third contact), as seen from the aircraft following the constant -90° bearing course, were vital data to most of the experimenters. The pre- and post-intercept leg flight-maneuver strategy were also affected by these data. The motion of the aircraft and the umbra ellipse were computed analytically in the tangent plane as functions of time. A very small area of Earth's surface was involved and deviation from the tangent plane was negligible. The deviation of the umbra projected on the surface from a true ellipse was also slight. Likewise, the difference in ellipse semi-axes a and b of fig. 35 between sea level and 37,000 ft altitude and their variation during totality were ignored. In addition, the aircraft speed was assumed to be constant during the intercept run.

Fig. 35 shows the geometrical model for determination of the contact times. The origin, 0, 0, of the xy system is the tangency point of the tangent plane and a sphere of radius R_E + 37,000 ft. The center of the umbra ellipse lies at point, X_o, Y_o. At point B the leading edge of the umbra overtakes the aircraft (second contact), and at point E the trailing edge of the umbra passes the aircraft. The aircraft flies along the circular arc $\widehat{HI}$, whose center is at $\bar{x}$, $\bar{y}$. The angles Ω and Ω_o define the aircraft position on $\widehat{HI}$ relative to the intercept point and leading edge of the umbra, respectively. The angle, θ, is the angle between the major axis of the umbra and the local meridian (same as the sun's azimuth). The angle is measured positive East from North. Defining time to be zero at the mid-intercept (mid-totality) point, negative prior thereto, and positive after, the quantities X_o, Y_o, and θ were converted from Naval Observatory data (ref. 9 and 10) to this time system. Appendix B shows plots of these quantities in relation to the differential time. By the method of least squares, polynomials of adequate degree were fit to the resulting functions in the intercept region, viz., valid from U. T. $21^h\,15^m$ to $21^h\,30^m$. In a left-handed cartesian coordinate system with origin at the ellipse center and moving with the ellipse, points $(\bar{x}, \bar{y})$ on the ellipse satisfy:

$$\frac{\bar{x}^2}{b^2} + \frac{\bar{y}^2}{a^2} = 1 \tag{15}$$

and coordinates of these points are related to coordinates in the xy system by:

$$\left.\begin{aligned} \bar{x} &= (x - X_o)\cos\theta + (y - Y_o)\sin\theta \\ \bar{y} &= -(x - X_o)\sin\theta + (y - Y_o)\cos\theta \end{aligned}\right\} \tag{16}$$

Substituting equation (16) into (15), the equation of the umbra in the xy system is:

$$\begin{aligned} Ax^2 + By^2 - \left[2AX_o + CY_o\right] x - \left[2BY_o + CX_o\right] y + Cxy \\ + \left[AX_o^2 + BY_o^2 + CX_oY_o\right] - a^2b^2 = 0 \end{aligned} \tag{17}$$

where

$$\begin{aligned} A &= b^2\sin^2\theta + a^2\cos^2\theta \\ B &= b^2\cos^2\theta + a^2\sin^2\theta \\ C &= (a^2 - b^2)\sin 2\theta\,. \end{aligned}$$

The semi-minor axis b in fig. 35 was given in ref. 9 (the quantity L), and in the tangent plane, $a = b/\sin\epsilon$, where the sun elevation ϵ at mid-totality was used in the computations.

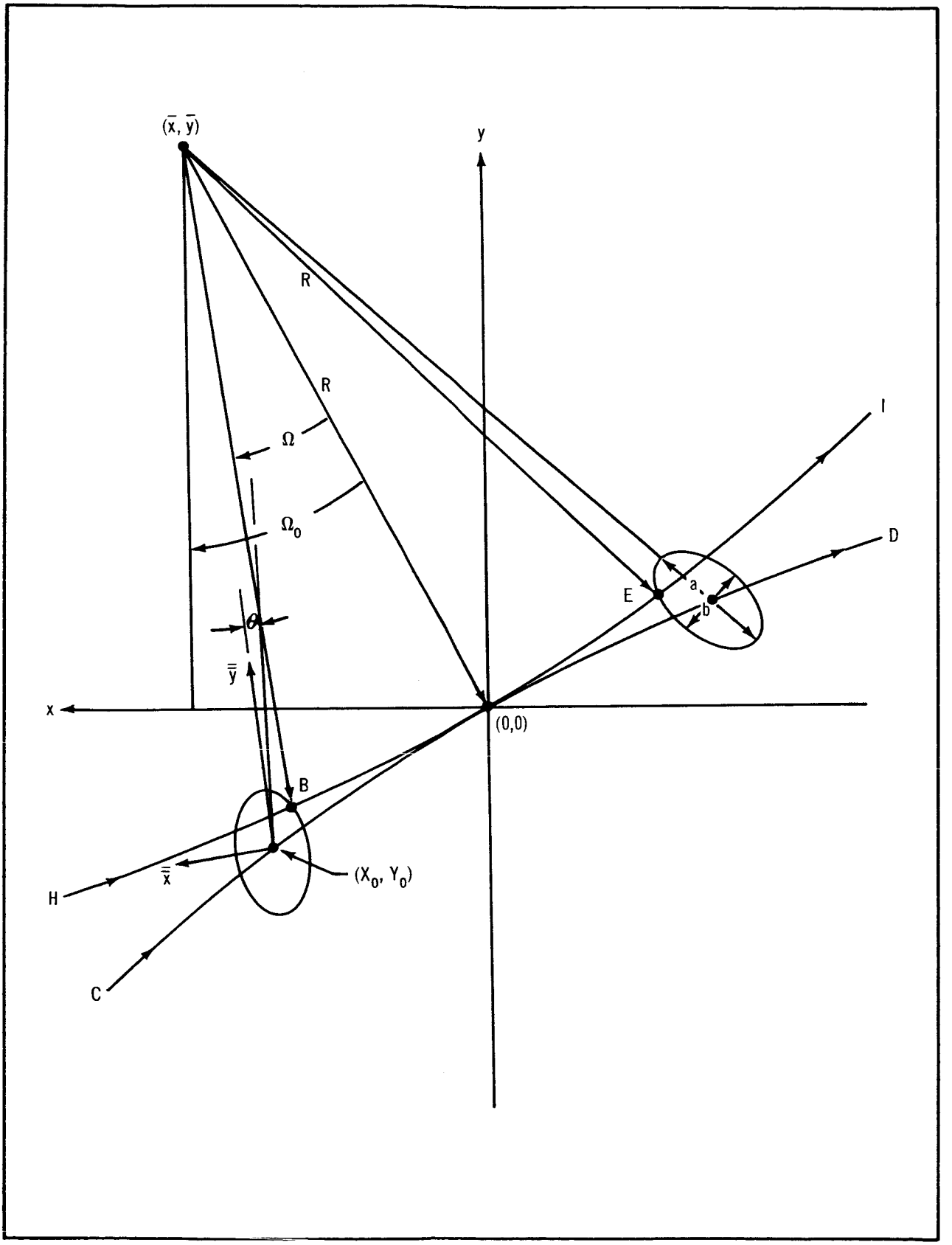

Figure 35. Geometry of Second and Third Contact Determination

The instantaneous position coordinates of the aircraft in the xy plane are:

$$\left.\begin{aligned} x_A &= \bar{x} + R \sin(\Omega - \Omega_o) \\ y_A &= \bar{y} - R \cos(\Omega - \Omega_o) \end{aligned}\right\} \tag{18}$$

where

$$\Omega = -\int V/R \; dt = -\frac{V}{3{,}600R} \; t \text{ radian.}$$

Here, V is in knots, R is in nautical miles, and T is in sec. At the beginning and end of totality the aircraft coordinates must satisfy equation (17). At arbitrary times equation(17)will not be equal to zero; the right-hand side will have residual Δ. Using a computer program, the contact times were determined by iteration with respect to time until Δ vanished. The aircraft position coordinates were obtained from equation(18)after the second and third contact times were known. Duration of totality was found to be 582 sec.

Flight Plan for the Solar Eclipse Flight

The general strategy of the flight plan was to fly from Hilo to a point West of the intercept point; in a single passage, intercept the eclipse on a course of -90^o sun bearing with mid-intercept occurring at position λ 131°55' W, ϕ 1°37' S. at $21^h23^m44^s$ U.T.; then proceed directly to Tahiti. Fig. 36 illustrates the eclipse intercept leg of the flight and table 1 gives the complete flight plan. The 20^o banked turns (points M to S and F to R in fig. 36) and the straight approach leg (S to A) were chosen to minimize autopilot gyro oscillations. The outbound and inbound great circle distances were computed by means of the spherical triangle identity:

$$D = R_E \arccos\left[\sin\phi_1 \sin\phi_2 + \cos\phi_1 \cos\phi_2 \cos(\lambda_1 - \lambda_2)\right] \tag{19}$$

where subscripts 1 and 2 denote the initial and final points of the course. The initial and terminal heading angles, h, follow from the identities:

$$\left.\begin{aligned} \sinh_1 &= \frac{\sin(\lambda_1 - \lambda_2)\cos\phi_2}{\sin(D/R_E)} \\ \sinh_2 &= \frac{\sin(\lambda_1 - \lambda_2)\cos\phi_1}{\sin(D/R_E)} \end{aligned}\right\} \tag{20}$$

The flight path segments preceeding and following the intercept leg were patched to the latter by geometric construction on the gnomonic projection.

Tables 2 and 3, respectively, list the aircraft heading angles and sun-elevation angles at the labelled points of fig. 36.

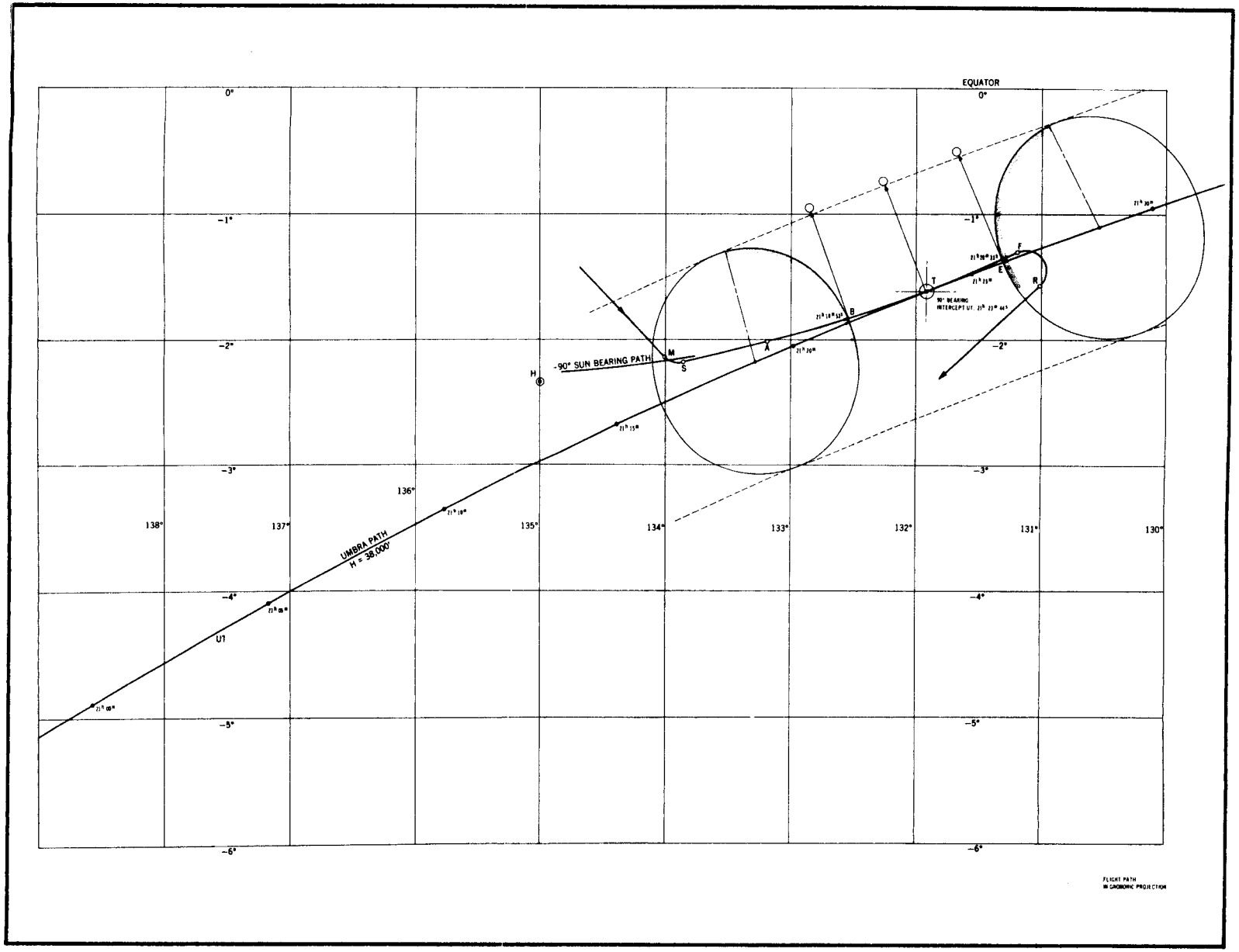

Figure 36. Flight Plan for Hot Run, May 30, 1965

TABLE 1

FLIGHT PLAN FOR HOT RUN OF MAY 30, 1965

Point	Station	Longitude	Latitude	Universal time	Maneuver	Duration	Distance n.mi.
H	Hilo airport	155°10'	19°45'				
M	Maneuver begins	134°01'	-2°08'	21:07:37.5	Outbound Great Circle course		1,810.0
S	Straight leg begins	133°51'	-2°11'	21:08:52.5	Left turn 20° bank	1^m15^s	10.2
A	Arc path begins	133°12'	-2°01'	21:13:52.5	Straight leg	5^m0^s	41.0
B	Beginning of totality	132°32'	-1°50'	21:18:52.5	Left turn 1/3° bank	5^m0^s	41.0
T	Target (mid-totality)	131°55'	-1°37'	21:23:44	Continue	$4^m51.5^s$	39.8
E	End of observation	131°19'	-1°22'	21:28:32.8	Continue	$4^m48.8^s$	39.5
F	Finish intercept run	131°12'	-1°18'	21:29:32.8	Continue	1^m0^s	8.2
R	Return leg begins	131°01'	-1°34'	21:32:54.8	Right turn 20° bank	3^m22^s	27.5
P	Airport at Tahiti	149°34'	-17°34'		Return trip Great Circle course		1,455.0
						Total	3,472.2

TABLE 2

FLIGHT PATH HEADING ANGLES FOR HOT RUN OF MAY 30, 1965

Point	Heading angle
S	$76.^{\circ}758$
A	$76.^{\circ}758$
B	$72.^{\circ}591$
T	$68.^{\circ}650$
E	$64.^{\circ}903$
F	$64.^{\circ}149$

TABLE 3

FLIGHT PATH SUN ELEVATION HISTORY FOR HOT RUN OF MAY 30, 1965

Point	Elevation angle to sun
S	$65.^{\circ}701$
A	$65.^{\circ}399$
B	$65.^{\circ}128$
T	$64.^{\circ}737$
E	$64.^{\circ}279$
F	$64.^{\circ}171$

Alternate Flight Paths

As a precaution against bad weather in the nominal eclipse intercept area, a second flight plan designated weather alternate was prepared for May 30. The same techniques as previously described were used. The position of the weather alternate mid-intercept point was based on reasonable proximity to the tentative radar tracking ship position. To be effective, the ship had to be stationed in a manner to assist with navigation by the aircraft of both courses. Fig. 37 shows the weather alternate flight path in the intercept area and table 4 gives the complete flight plan. Tables 5 and 6, respectively, list the aircraft heading and run elevation angles. A second alternate flight plan was prepared early in the planning stages when the use of Tahiti as a refuelling stopover was in doubt, and a non-stop flight (Hilo to Hilo) was anticipated. This situation never occurred and discussion of the flight plan is omitted. Duration of totality on the weather alternate was computed to be 557 sec. The second alternate intercept path duration would have been 498 sec.

Error Matrix for Contact Times

Navigation of the CV-990 precisely along the nominal intercept course was considered unlikely because of the limited navigational equipment on the aircraft, the impossibility of obtaining star fixes, remoteness from conventional ground-based radar and guidance beacons, and uncertainty concerning wind velocity. The flight navigators indicated that a time error of 5 min and a position error of 15 n.mi. were possible. Evaluation of the effect of these errors on the second and third contacts times was part of the navigation work.

To determine the variation of contact times with aircraft position and/or time errors, the values were computed along several constant sun-bearing flight paths concentric with the nominal path, allowing the aircraft to arrive at mid-intercept early or late by as much as 5 min. The total number of combinations of position and time errors for which equation (17) was solved by relaxation was 77 for the nominal eclipse intercept area and for the weather alternate. The results are tabulated in table 7. These numbers are based on the nominal aircraft ground speed of 490 knots. Additional computations with speed varying from 470 to 510 knots showed that the observers would gain 1 sec totality time for each knot speed in excess of nominal and would lose time at the same rate for speeds below nominal. Notes appended to the error matrix tables explain their utilization.

The Practice Flights

Due to the complexity of the 1965 ASEE mission, several practice flights from Moffett Field, California, and Hilo, Hawaii were planned. These flights were planned (1) to evaluate in-flight navigational capability with the aid or absence of ground based support, (2) to test communication with a radar tracking ship which was to aid navigation in the intercept area of the eclipse flight, (3) to permit the experimenters practice in use of their equipment under conditions simulating the eclipse flight acquisition conditions, and (4) to give the flight crew and, where necessary, the experimenters practice working together.

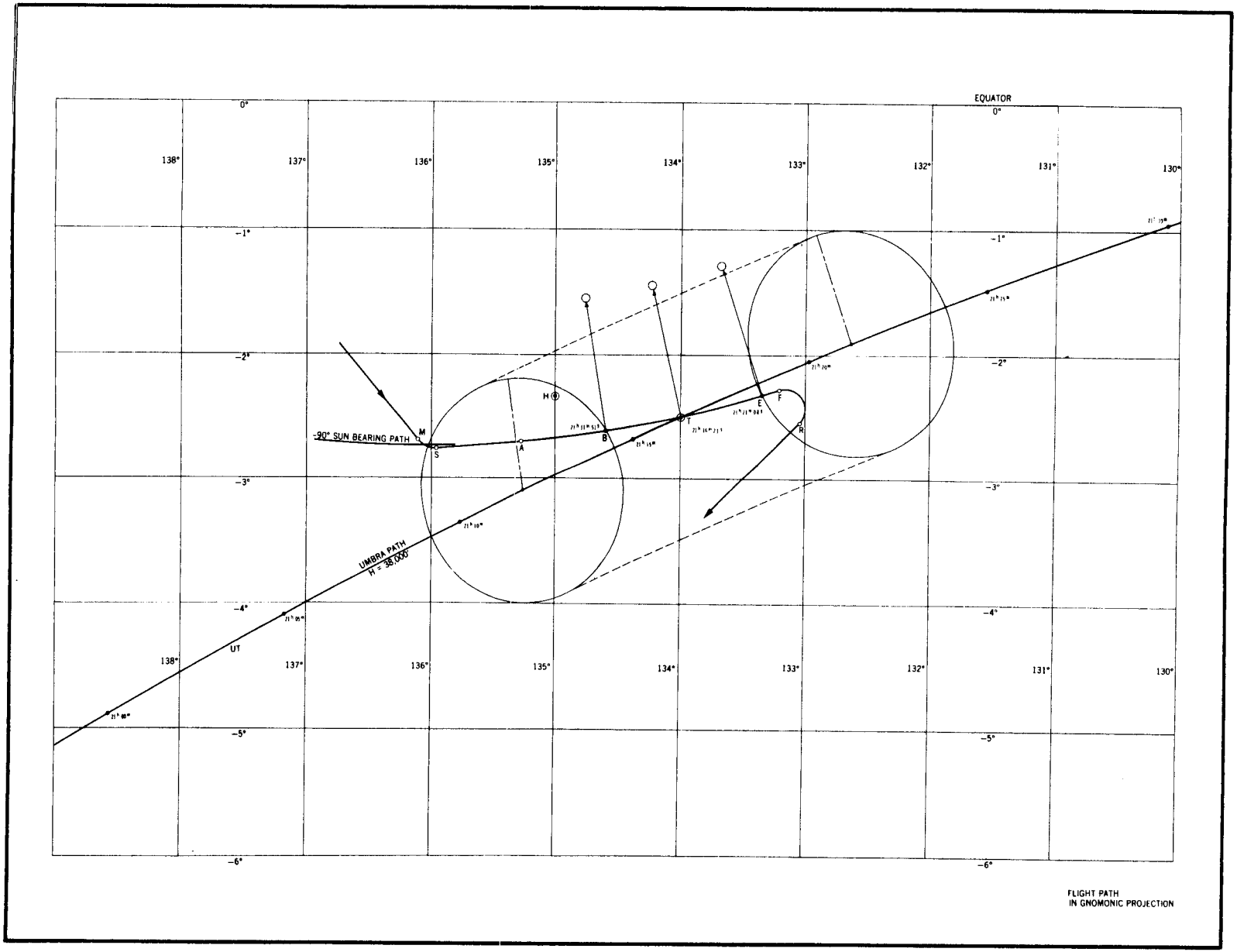

Figure 37. Flight Plan for Weather Alternate, May 30, 1965

TABLE 4

FLIGHT PLAN FOR WEATHER ALTERNATE FROM HILO MAY 30, 1965

Point	Station	Longitude	Latitude	Universal time	Maneuver	Duration	Distance n.mi.
H	Hilo airport	$155^{\circ}10'$	$19^{\circ}45'$				
M	Maneuver begins	$136^{\circ}06!5$	$-2^{\circ}40!8$	$21^{h}00^{m}39^{s}$	Outbound Great Circle course		1,752.9
S	Straight leg begins	$135^{\circ}57!6$	$-2^{\circ}45'$	$21^{h}01^{m}51.4^{s}$	Left turn 20° bank	$1^{m}12.4^{s}$	9.86
A	Arc path begins	$135^{\circ}16!8$	$-2^{\circ}41!4$	$21^{h}06^{m}51.4^{s}$	Straight leg	$5^{m}00^{s}$	41.00
B	Beginning of totality	$134^{\circ}35!9$	$-2^{\circ}36!5$	$21^{h}11^{m}51.4^{s}$	Left turn $1/3^{\circ}$ bank	$5^{m}00^{s}$	41.00
T	Middle of observation	$134^{\circ}00'$	$-2^{\circ}29'$	$21^{h}16^{m}23^{s}$	Continue	$4^{m}31.6^{s}$	36.97
E	End of observation	$133^{\circ}21'$	$-2^{\circ}19!2$	$21^{h}21^{m}08.2^{s}$	Continue	$4^{m}45.2^{s}$	38.82
F	Finish intercept run	$133^{\circ}13!4$	$-2^{\circ}16!4$	$21^{h}22^{m}08.2^{s}$	Continue	$1^{m}00^{s}$	8.20
R	Return leg begins	$133^{\circ}02!7$	$-2^{\circ}32!3$	$21^{h}25^{m}14.2^{s}$	Right turn 20° bank	$3^{m}06^{s}$	25.31
P	Airport at Tahiti	$149^{\circ}34'$	$-17^{\circ}34'$		Return trip Great Circle course		1,326.60
						Total	3,280.70

TABLE 5

HEADING ANGLES FOR WEATHER ALTERNATE FLIGHT OF MAY 30, 1965

Point	Heading Angle
S	85.°100
A	85.°100
B	80.°983
T	77.°275
E	73.°313
F	72.°483

TABLE 6

SUN ELEVATION HISTORY FOR MAY 30, 1965, WEATHER ALTERNATE FLIGHT

Point	Elevation angle to sun
S	65.459°
A	65.416°
B	65.279°
T	65.051°
E	64.734°
F	64.332°

TABLE 7

VARIATION OF CONTACT & TOTALITY TIME WITH TIME AND POSITION ERROR WEATHER ALTERNATE ECLIPSE FLIGHT-MAY 30, 1965

Position Error		Minutes late					On track	Minutes early				
	490 Knots	-5	-4	-3	-2	-1	0	+1	+2	+3	+4	+5
		21:15:00	21:15:47	21:16:35	21:17:23	21:18:12	21:19:01	21:19:50	21:20:39	21:21:27	21:22:14	21:23:01
	15 S.	21:24:20	21:25:07	21:25:55	21:26:44	21:27:33	21:28:23	21:29:14	21:30:05	21:30:56	21:31:47	21:32:36
		560	560	560	561	561	561	564	566	569	573	575
		21:15:00	21:15:45	21:16:32	21:17:19	21:18:07	21:18:56	21:19:44	21:20:32	21:21:20	21:22:08	21:22:56
	10 S.	21:24:25	21:25:13	21:26:01	21:26:50	21:27:39	21:28:29	21:29:19	21:30:09	21:30:59	21:31:48	21:32:36
		565	568	569	571	572	573	575	577	579	580	580
		21:15:02	21:15:46	21:16:32	21:17:18	21:18:05	21:18:53	21:19:41	21:20:29	21:21:17	21:22:04	21:22:52
	5 S.	21:24:29	21:25:17	21:26:05	21:26:54	21:27:43	21:28:32	21:29:22	21:30:11	21:30:59	21:31:47	21:32:34
		567	571	573	576	578	579	581	582	582	583	582
		21:15:07	21:15:49	21:16:34	21:17:19	21:18:06	21:18:53	21:19:40	21:20:28	21:21:15	21:22:03	21:22:52
	0	21:24:29	21:25:18	21:26:06	21:26:55	21:27:43	21:28:33	21:29:22	21:30:10	21:30:57	21:31:44	21:32:29
		562	569	572	576	577	580	582	582	582	581	577
	5 N.	21:15:14	21:15:55	21:16:38	21:17:23	21:18:08	21:18:54	21:19:41	21:20:29	21:21:17	21:22:05	21:22:54
		21:24:27	21:25:16	21:26:05	21:26:54	21:27:42	21:28:31	21:29:19	21:30:06	21:30:53	21:31:38	21:32:22
		553	561	567	571	574	577	578	577	576	573	568
		21:15:23	21:16:03	21:16:45	21:17:29	21:18:13	21:18:59	21:19:45	21:20:33	21:21:20	21:22:09	21:22:58
	10 N.	21:24:23	21:25:12	21:26:01	21:26:50	21:27:38	21:28:26	21:29:12	21:30:00	21:30:46	21:31:30	21:32:12
		540	549	556	571	565	567	567	567	566	561	554
		21:15:35	21:16:14	21:16:55	21:17:37	21:18:21	21:19:05	21:19:52	21:20:39	21:21:27	21:22:15	21:23:04
	15 N.	21:24:16	21:25:06	21:25:55	21:26:44	21:27:32	21:28:19	21:29:06	21:29:52	21:30:36	21:31:19	21:31:59
		521	532	540	547	551	554	554	553	549	544	535

Note: To correct intercept times for an error in ground speed, proceed as follows:

(A) If actual ground speed is greater than 490 knots, subtract 0.5 sec (per knot over 490) from time of second contact; add 0.5 sec (per knot over 490) to time of third contact.

(B) If actual ground speed is less than 490 knots, add 0.5 sec (per knot less than 490) to time of second contact; subtract 0.5 sec (per knot less than 490) from time of third contact.

Position Error		Minutes late					On track	Minutes early				
	490 Knots	-5	-4	-3	-2	-1	0	+1	+2	+3	+4	+5
	15 S.	21:08:17 21:17:04 527	21:08:50 21:17:48 538	21:09:27 21:18:31 544	21:10:06 21:19:14 548	21:10:48 21:19:58 550	21:11:32 21:20:42 550	21:12:18 21:21:26 552	21:13:05 21:22:12 547	21:13:54 21:22:58 544	21:14:43 21:23:46 543	21:15:32 21:24:34 542
	10 S.	21:08:30 21:17:09 519	21:09:01 21:17:58 537	21:09:36 21:18:39 543	21:10:14 21:19:23 549	21:10:54 21:20:08 554	21:11:36 21:20:53 557	21:12:21 21:21:38 557	21:13:07 21:22:24 557	21:13:53 21:23:11 558	21:14:41 21:23:59 558	21:15:30 21:24:47 557
	5 S.	21:08:46 21:17:12 506	21:09:15 21:17:58 523	21:09:48 21:18:44 536	21:10:23 21:19:30 547	21:11:02 21:20:16 554	21:11:43 21:21:02 559	21:12:26 21:21:48 562	21:13:10 21:22:35 565	21:13:56 21:23:22 566	21:14:42 21:24:10 568	21:15:30 21:24:58 568
	0	21:09:06 21:17:12 486	21:09:30 21:18:00 510	21:10:01 21:18:48 527	21:10:35 21:19:35 540	21:11:12 21:20:21 549	21:11:51 21:21:08 557	21:12:33 21:21:55 562	21:13:16 21:22:43 567	21:14:00 21:23:30 570	21:14:46 21:24:18 572	21:15:32 21:25:06 574
	5 N.	21:09:18 21:17:10 472	21:09:48 21:18:00 492	21:10:17 21:18:49 512	21:10:49 21:18:37 528	21:11:24 21:20:25 541	21:12:02 21:21:13 551	21:12:42 21:22:00 558	21:13:23 21:22:48 565	21:14:07 21:23:35 568	21:14:51 21:24:23 572	21:15:37 21:25:11 574
	10 N.	21:09:46 21:17:05 439	21:10:08 21:17:57 469	21:10:35 21:18:47 492	21:11:05 21:19:37 512	21:11:38 21:20:26 532	21:12:15 21:21:14 539	21:12:53 21:22:03 550	21:13:33 21:22:51 558	21:14:16 21:23:39 563	21:14:59 21:24:27 568	21:15:44 21:25:15 571
	15 N.	21:10:07 21:16:56 409	21:10:31 21:17:51 440	21:10:55 12:18:43 468	21:11:23 21:19:34 491	21:11:55 21:20:24 509	21:12:30 21:21:14 524	21:13:07 21:22:03 536	21:13:46 21:22:51 545	21:14:27 21:23:40 553	21:15:09 21:24:28 559	21:15:53 21:25:15 562

Note: To correct intercept times for an error in ground speed, proceed as follows:

(A) If actual ground speed is greater than 490 knots, subtract 0.5 sec (per knot over 490) from time of second contact; add 0.5 sec (per knot over 490) to time of third contact.

(B) If actual ground speed is less than 490 knots, add 0.5 sec (per knot less than 490) to time of second contact; subtract 0.5 sec (per knot less than 490) from time of third contact.

The sun and moon offered the most logical simulation targets for the practice flights, and originally the authors were requested to prepare constant 90° bearing flight paths to observe these objects on seven dates in May 1965, so that at mid-intercept on the observation leg the object sought would have an elevation angle 64.7°. At the conclusion of the solar eclipse program, 12 complete flight plans had been prepared and two additional ones had been partially completed. The pressure of time, particularly in the case of practice flights scheduled after initiation of the project (for which complete flight plans were needed on 1 to 2 days notice), demanded a rapid procedure to determine the flight paths. The following techniques were adopted.

Solution of equation (11) for the observer's latitude yields:

$$\phi = \arcsin\left(\frac{\sin\epsilon\,\sin\delta \pm \cos\delta\,\cos H\sqrt{\sin^2\delta - \sin^2\epsilon + \cos^2\delta\,\cos^2 H}}{\sin^2\delta + \cos^2\delta\,\cos^2 H}\right) \qquad (21)$$

where equation (10) gave $H = GST_o + U.T. + \Delta t - \lambda - \alpha$. Lacking finite object parallax, specification of U.T. determines α, δ, and Δt, whereas GST_o is a function only of the date. Substitution of equation (10) into (21) thus results in a relation $f(\lambda,\phi) =$ constant, i.e., a locus of coordinate points on Earth's surface which may be evaluated once the elevation ϵ is given. It is well known in celestial navigation that this locus is a circle of arc radius $\zeta = 90 - \epsilon$ degrees (see fig. 38). The center of the circle is that point on Earth's surface where the object is seen directly overhead, i.e., in the zenith. The coordinates at this point on Earth are:

$$\lambda_s = GST_o + U.T. + \Delta t - \alpha \qquad (22)$$

$$\phi_s = \delta \qquad (23)$$

obtained from equations (10) and (21) by setting $H = 0$, $\epsilon = 90°$. Since it was desired to find those geographic points where the sun or moon would have $\epsilon = 64.°7$, the arc radius of this circle was 25.°3 = 1,513 n.mi., or about 7% of Earth's circumference. This situation plus the laborious computation and drafting involved in rigorously constructing constant-elevation loci on ai, ϕ grid suggested a simplification in selecting the mid-intercept point for the practice flights which proved to be adequate. A procedure was followed to compute and plot the track of the sub-solar or sub-lunar point on a rectangular grid in the plane tangent to Earth's surface at that point. Circles of radius 25.°3 were constructed at 5 to 15 min U.T. intervals, representing fairly close approximations to the true constant elevation loci (the difference was due to deviation of the tangent plane from the Earth's surface). The correction necessary to obtain the exact locus is easily evaluated (see Appendix D) and was applied to all practice flight planning except for the May 6 and 7 flights.

In order to choose one mid-intercept point from the constant elevation curves, additional restrictions had to be imposed. These restrictions were based on flight capability, scheduling to ensure adequate time for evaluation of results, and various degrees of desired duplication of the eclipse flight path. Table 8 summarizes the requirements for those dates on which practice flights

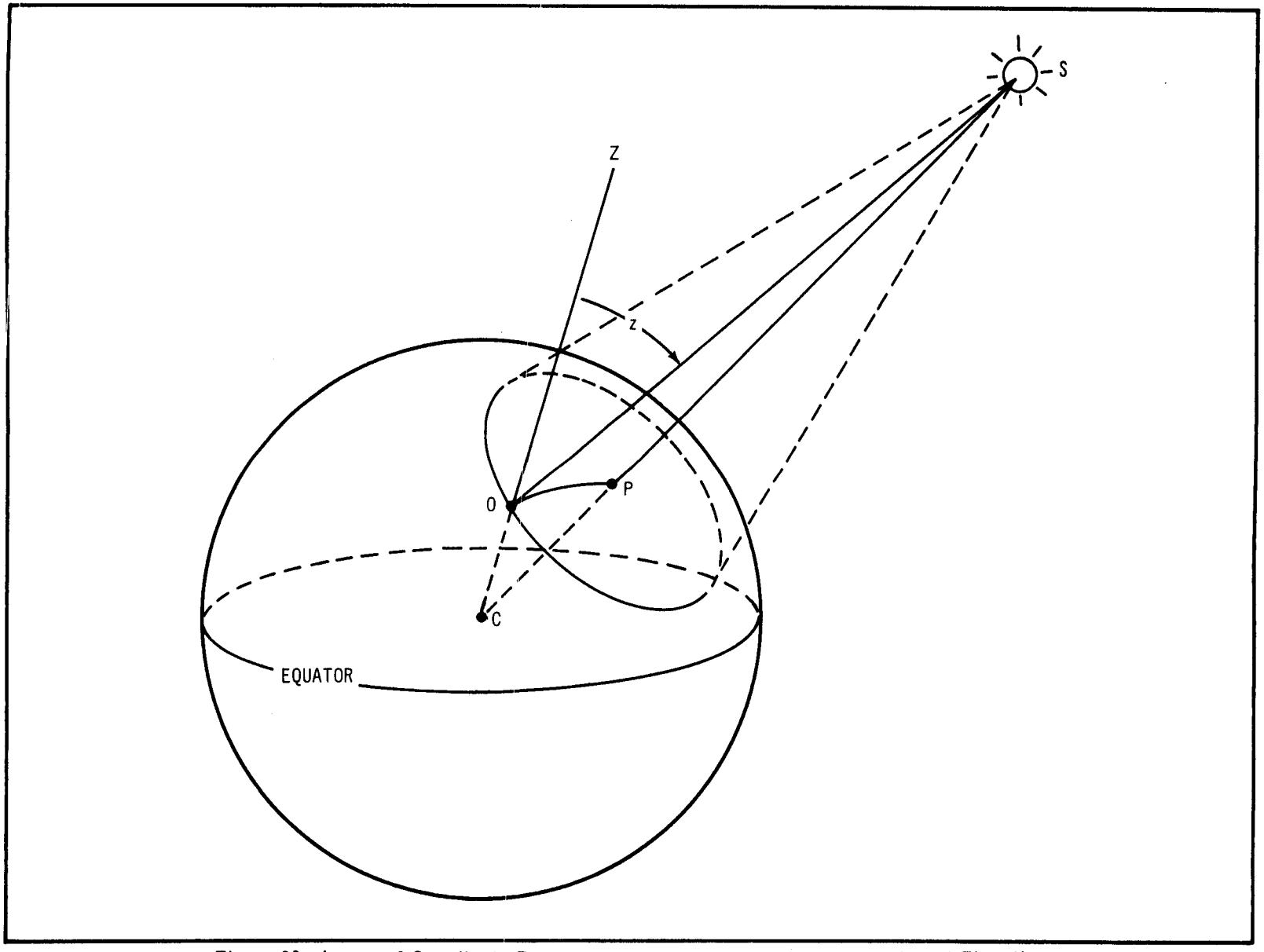

Figure 38. Locus of Coordinate Points on the Earth's Surface as a Function of Elevation

TABLE 8

PRACTICE FLIGHT REQUIREMENTS

Date	Observer target	Flight base*	Restrictions affecting choice of mid-intercept point
1965			
May 6	Sun	Moffett	Mid-morning intercept near $\lambda = 122^{\circ}W$
7	Sun	Moffett	Mid-morning intercept near $\lambda = 122^{\circ}W$
9	Moon	Moffett	Mid-evening at meridian transit, $\lambda = 122^{\circ}W$
10	Moon	Moffett	Same as May 9
12	Sun	Moffett	Same as May 6 and 7
13	Sun	Moffett	Same as May 6 and 7
14	Sun	Moffett	Same as May 6 and 7
15	Sun	Moffett	Mid-afternoon intercept near $\lambda = 122^{\circ}W$
24	Sun	Hilo	Duplicate closely eclipse flight outbound leg and intercept run; intercept run within steaming range of tracking ship from latter's eclipse station. Simulate hot run bank turn
24	Moon	Hilo	Acquire on outbound leg of sun observation flight at elevation 60° to 65° **
25	Moon	Hilo	Same as May 24, Moon
26	Sun	Hilo	Same as May 24, Sun
28	Sun	Hilo	Same as May 24, Sun
30	Moon and Sun	Hilo	Solar Eclipse flight; details elsewhere
June 1	Sun	Hilo	Begin intercept run near Christmas Island (λ 157°W, ϕ 2°N); calibration flight

* Moffett: Moffett Field, Mountain View, California

Hilo: Hilo Airport, Hilo, Hawaii

** Unfavorable astronomical circumstances rendered the May 24 and 25 Moon observations not feasible, and no flight plans were prepared for this purpose.

were planned, and figs. 39, 40, and 41 show the constant elevation plots with mid-intercept points and aircraft departure points indicated for May 7 and 28 (solar observation), and May 10 (moon observation).

To calculate the constant lunar elevation loci, it was necessary to include the effects of finite parallax. A computer program was used to precisely evaluate equations (10) and (21). The moon's right ascension and declination were assumed to vary linearly with time during a normal 6-hour data interval, coefficients being determined by fits to ephemeris data. The program steps in λ and U. T., solve equation(10)for $H(\lambda, U.T.)$, then solves equation(21)for $\phi(\lambda, U.T.)$, with $\epsilon = 64.^{\circ}7$. The resulting latitudes and corresponding hour angles are then introduced into these equations for corrections ΔH and $\Delta\delta$ due to parallax derived in ref. 11, p. 204, yielding corrected values H' and δ'. Substitution of H' and δ' into equation (21) then gives improved latitudes ϕ'; the process may be repeated by iteration until $|\phi' - \phi|$ is a suitably small value. Actual computations showed convergence to $0.^{\circ}01$ after only two iterations. Any further improvement in accuracy would have been spurious because of neglect of atmospheric refraction and non-linearity in $\alpha(U.T.)$ and $\delta(U.T.)$.

Constant 90°-bearing flight paths through the adopted mid-intercept points were computed and constructed on appropriate maps together with nominal approach and departure legs as described for the solar eclipse flight planning. Reproductions of the flight charts and flight plans prepared are contained in Appendix E.

The flight paths determined are valid only for zero aircraft pitch angle and negligible wind velocity. The actual non-zero pitch angle was corrected for by pre-slueing the telescopes in azimuth during installation and is not relevant to the present discussion (see Appendix F.). The effect of a pitch angle of 1 to 2° on the observed elevation angle was found to be essentially negligible ($0.^{\circ}07$). The effect of winds on the flight navigator's ability to follow a prescribed course as critical as the eclipse path caused much concern. The 1963 airborne solar eclipse expedition experienced such related difficulties.

Winds were expected to affect (1) the arrival time and position of the aircraft in the intercept area and (2) accuracy in navigating the observation leg as prescribed. Problems associated with (1) above are handled by standard flight navigation techniques. The radar tracking ship stationed near the initial point, S, of the intercept path was intended to guide the NASA CV 990 to this point at the correct time with the proper ground heading (track). Douglas was concerned primarily with (2) above, and an elaborate analysis of wind effects on the observation leg of the flight path was conducted.

The aim of this analysis was to provide the navigator with data to correct the aircraft heading at point S (practice flights) or point A (May 30 eclipse flight) so that the aircraft would arrive at mid-point T on time, assuming availability of wind velocity data. Points S and A were the respective critical points of the practice and eclipse flight paths at which fixed flight maneuvers were required, no further alterations being possible until the end of observation. Space and time limitations preclude a complete discussion of this work.

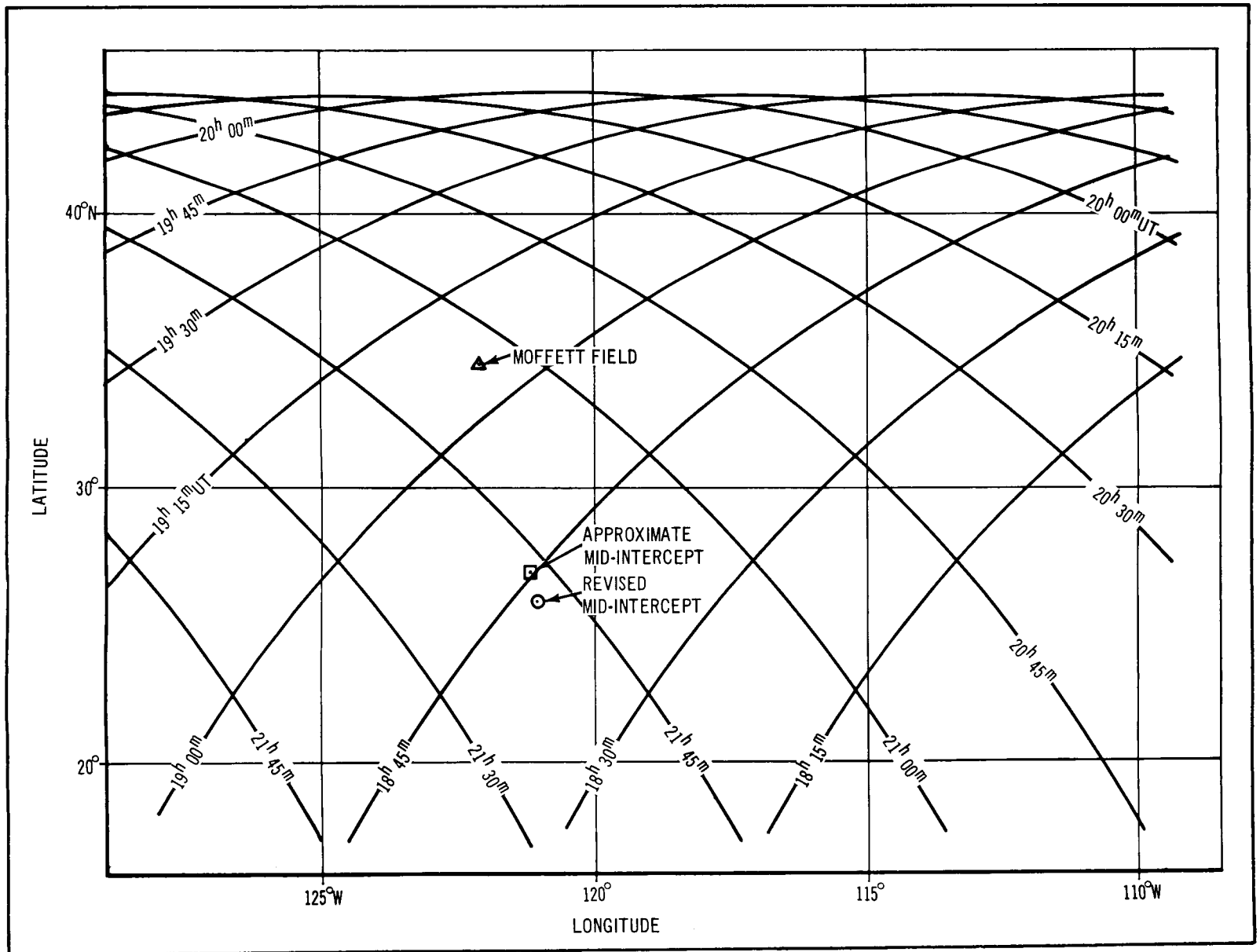

Figure 39. Approximate 64°.7 Solar Elevation LOCI, May 7, 1965 (Mid-Morning to Mid-Afternoon)

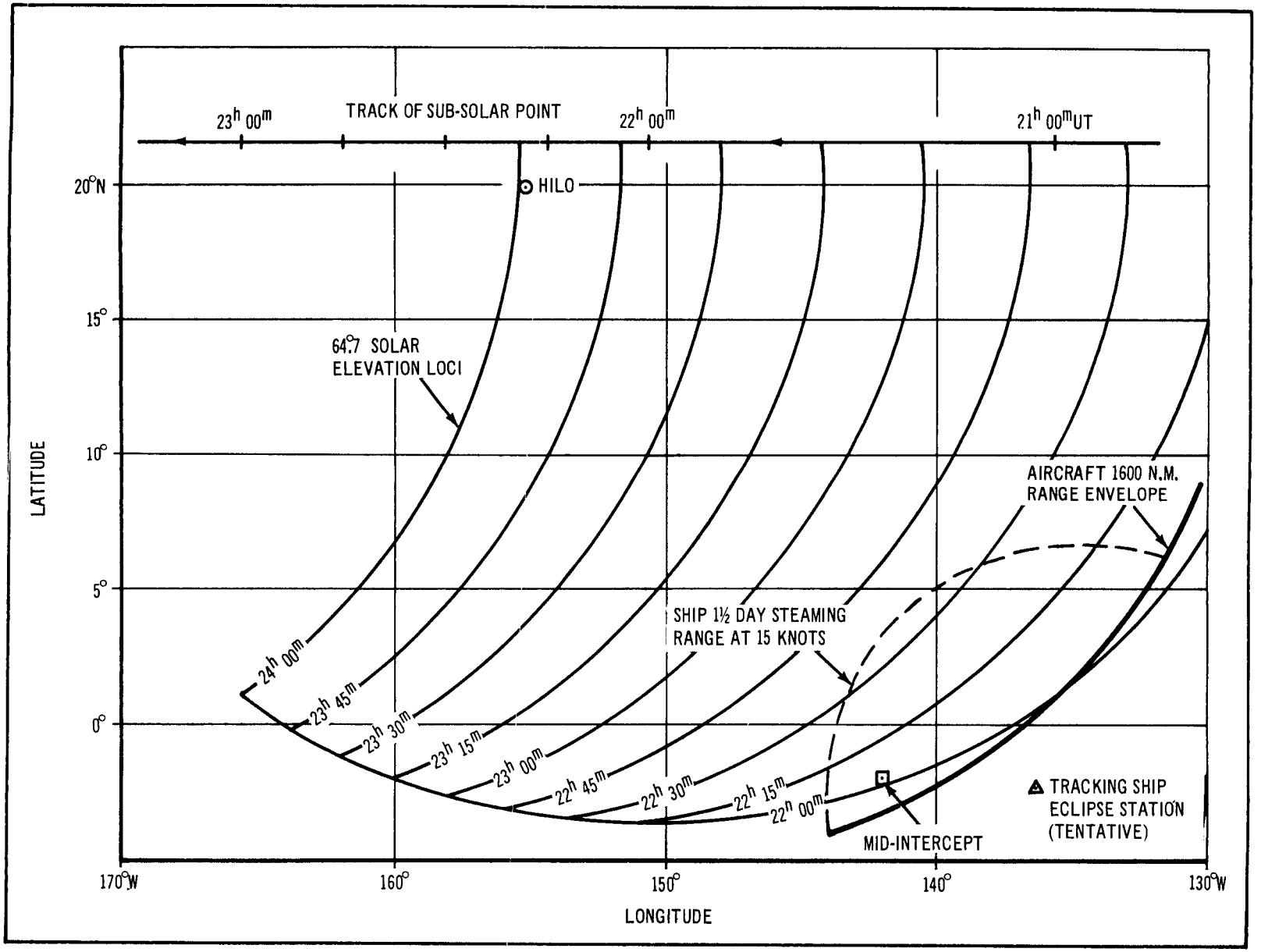

Figure 40. Practice Flight Capability Map, May 28, 1965 (Afternoon)

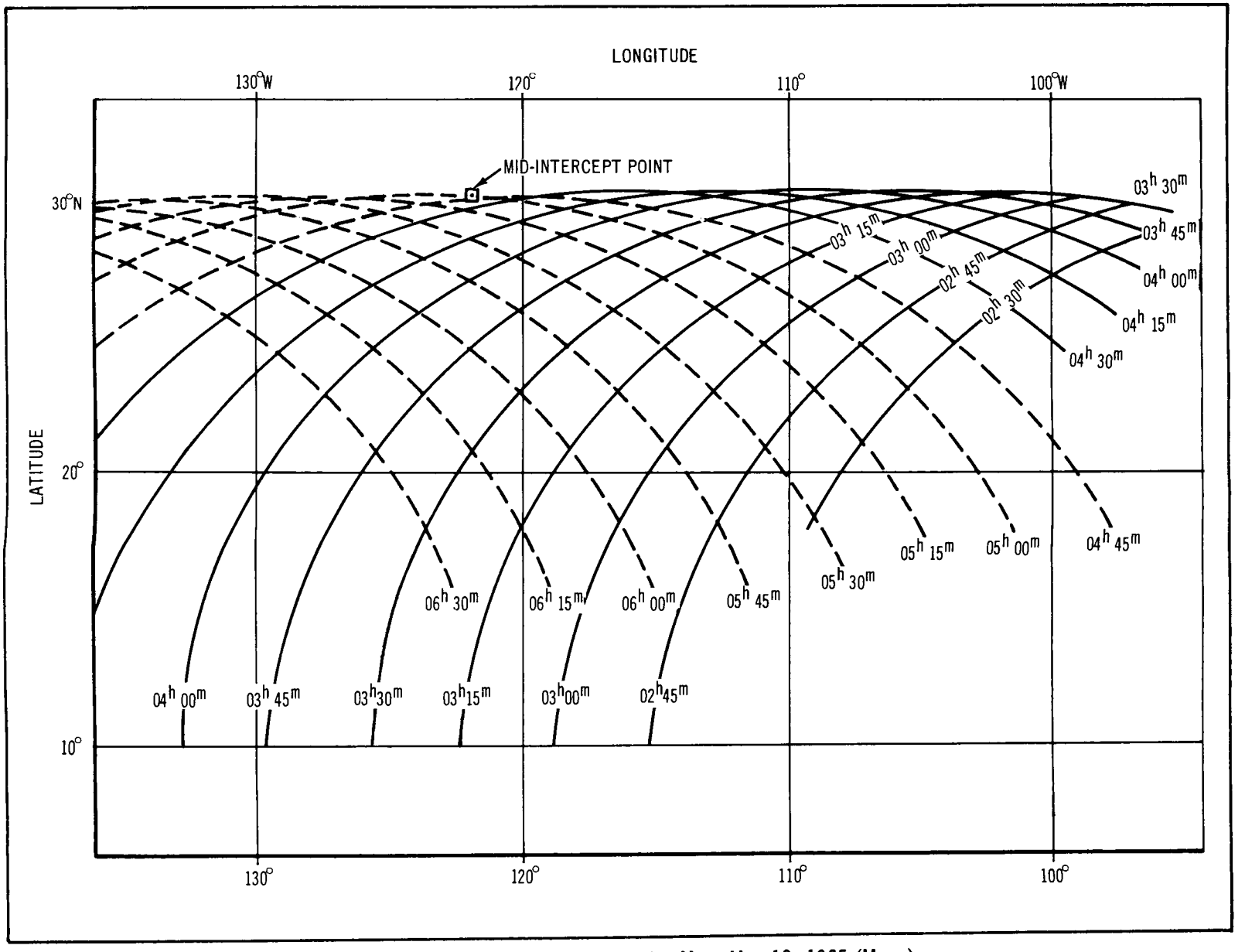

Figure 41. Practice Flight Capability Map, May 10, 1965 (Moon)

Wind speeds of 10 to 15 knots were anticipated in the eclipse intercept area and speeds up to 100 knots were expected for the practice flights from Moffett Field. Graphs were plotted showing the geographical variation of point S or A with wind velocity and the proper heading to fly at these points (figs. 42 and 43) for the May 30 eclipse flight. Variations in the aircraft track up to $+12^{\circ}$ from the ideal (zero wind) heading were possible during the flights from Moffett Field, while the initial point S of the intercept leg, corrected for the wind, could have differed in position by as much as 100 n. mi. from the ideal point. In view of the lower wind speed expected in the eclipse intercept area, the potential variations for the flights from Hilo were smaller, yet the more stringent time schedule made the wind problem equally serious.

Airborne Navigation Aids

Two airborne navigation aids, the sun compass and cusp navigation, were considered. Only the sun compass was used during the expedition, but both are described in the following paragraphs.

The Sun Compass. — Use of the focussed solar image projected on a calibrated grid for navigation dates back at least to the 1929 South polar flight by Admiral Byrd. Such a device (Sun Compass) was installed on the DC-8 aircraft which made the 1963 solar eclipse flight and proved so helpful to the navigator that a larger and more accurate system was conceived for the 1965 eclipse program.

The 1965 sun compass consisted of a 6-in. objective lens with focal length of 120 in., a front-surfaced plane mirror, and a grid card approximately 3 sq ft, plus mounting hardware. The lens was mounted in an aluminum housing which was bolted to the anacoustic pane of the standard forward left-hand fuselage window in the NASA CV-990. The mounted lens was oriented so that the incoming beam of sunlight was normal to the lens with the aircraft at 1.8° pitch angle, $1/3^{\circ}$ left bank, and the sun at $64.^{\circ}7$ elevation. A sheet aluminum diaphragm with a 1/4 in. hole in the center was installed directly behind the lens, which reduced the image intensity and aberrations due to transmission through two curved plexiglass windows. Below the lens mount and diaphragm assembly, the plane mirror was attached to the side-wall seat track and left-hand forward seat. The grid card was mounted above the navigator's desk on the opposite (i.e., forward right) side of the aircraft. Light from the sun passed through the standard window, through the 6-in. lens and diaphragm onto the plane mirror, which directed the beam nearly horizontally across the aircraft interior to the grid card. Fig. 44 shows the sun compass as installed in the CV-990. Fig. 45 is a reproduction of the grid.

The vertical grid scale (68 arc sec/mm) was marked in 1° intervals to show aircraft bank-angle left or right from the nominal $1/3^{\circ}$ left, and the horizontal scale (68 cos ϵ arc sec/mm), also in 1° intervals, indicated sun bearing fore or aft of 90° left. Alignment of the sun compass was to be accomplished by adjusting the mirror; however, the necessary fine adjustment of the plane mirror in its mount could not be made, hence alignment was obtained by moving a section of the grid on the master card. To establish the alignment,

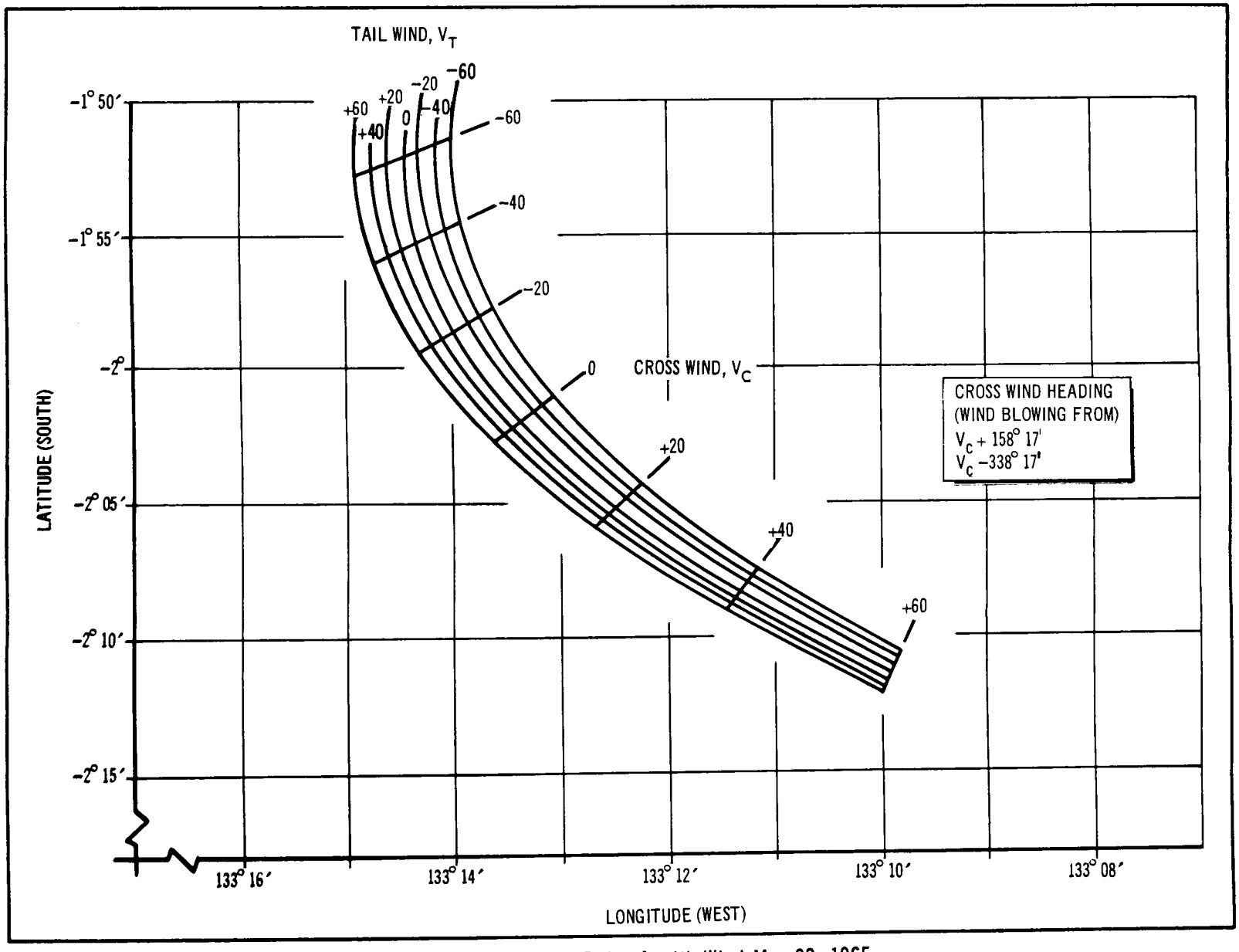

Figure 42. Variation of Point A with Wind, May 30, 1965

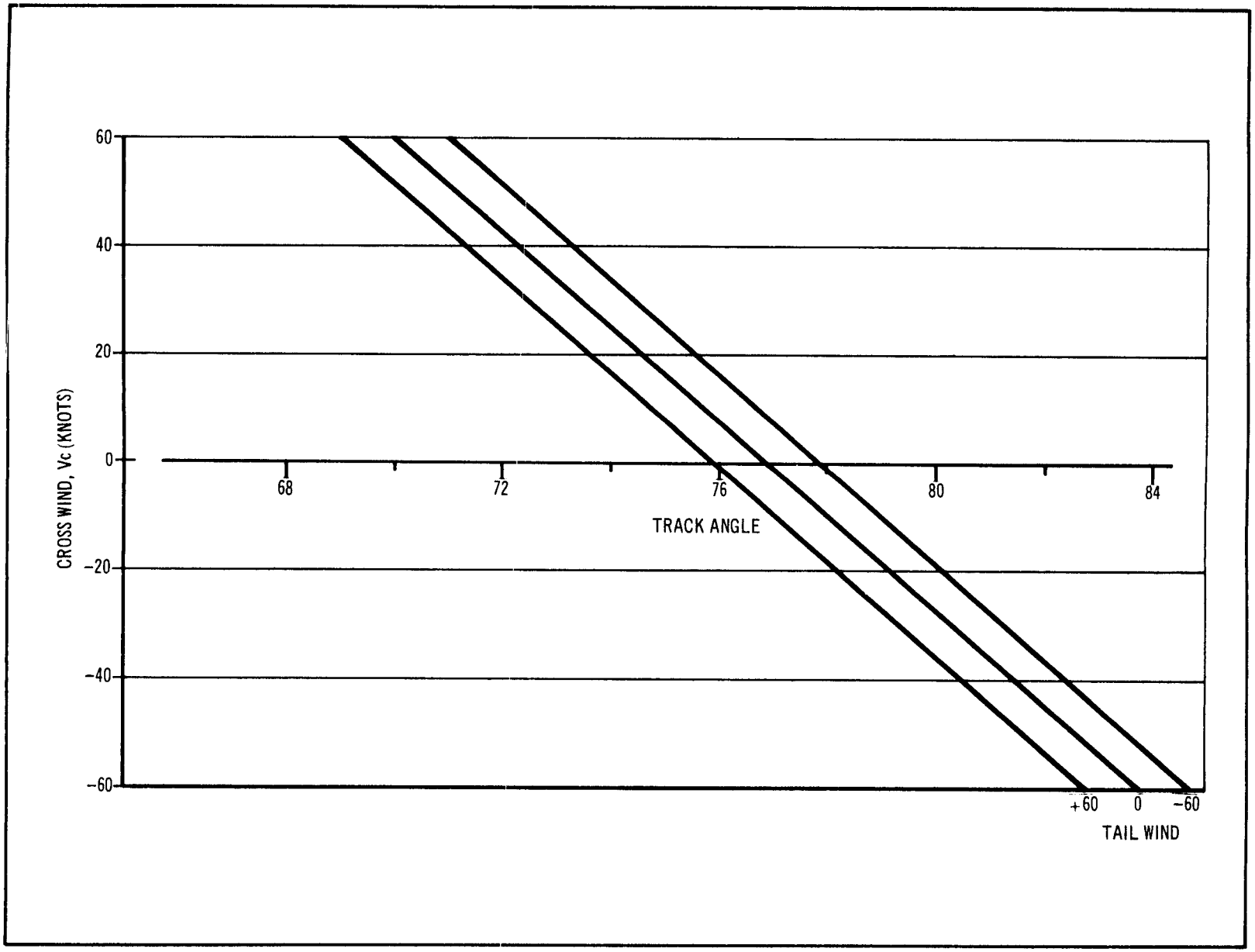

Figure 43. Variation of Track at Point A with Wind, May 30, 1965

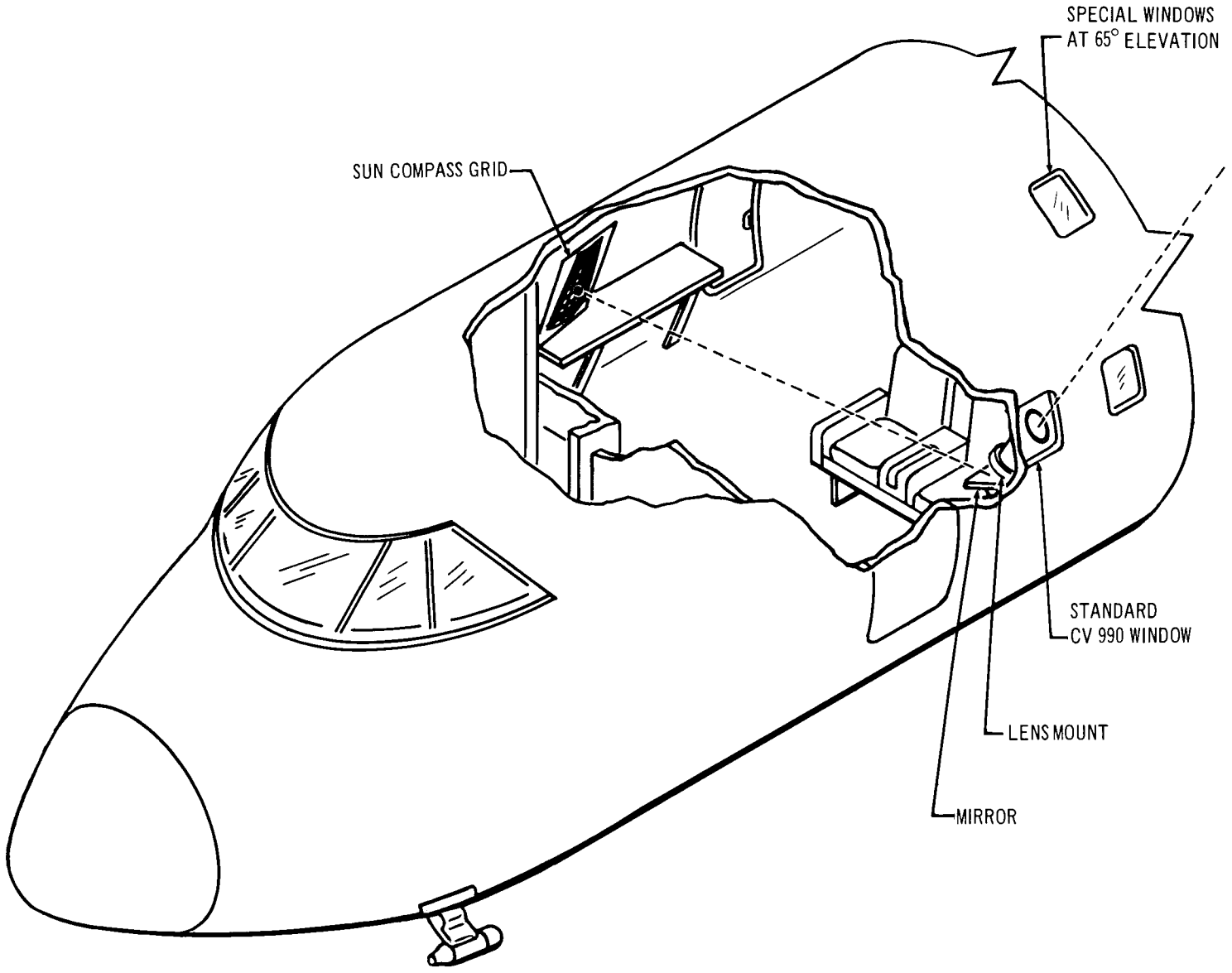

Figure 44. Sun Compass Installation in NASA CV-990 Aircraft

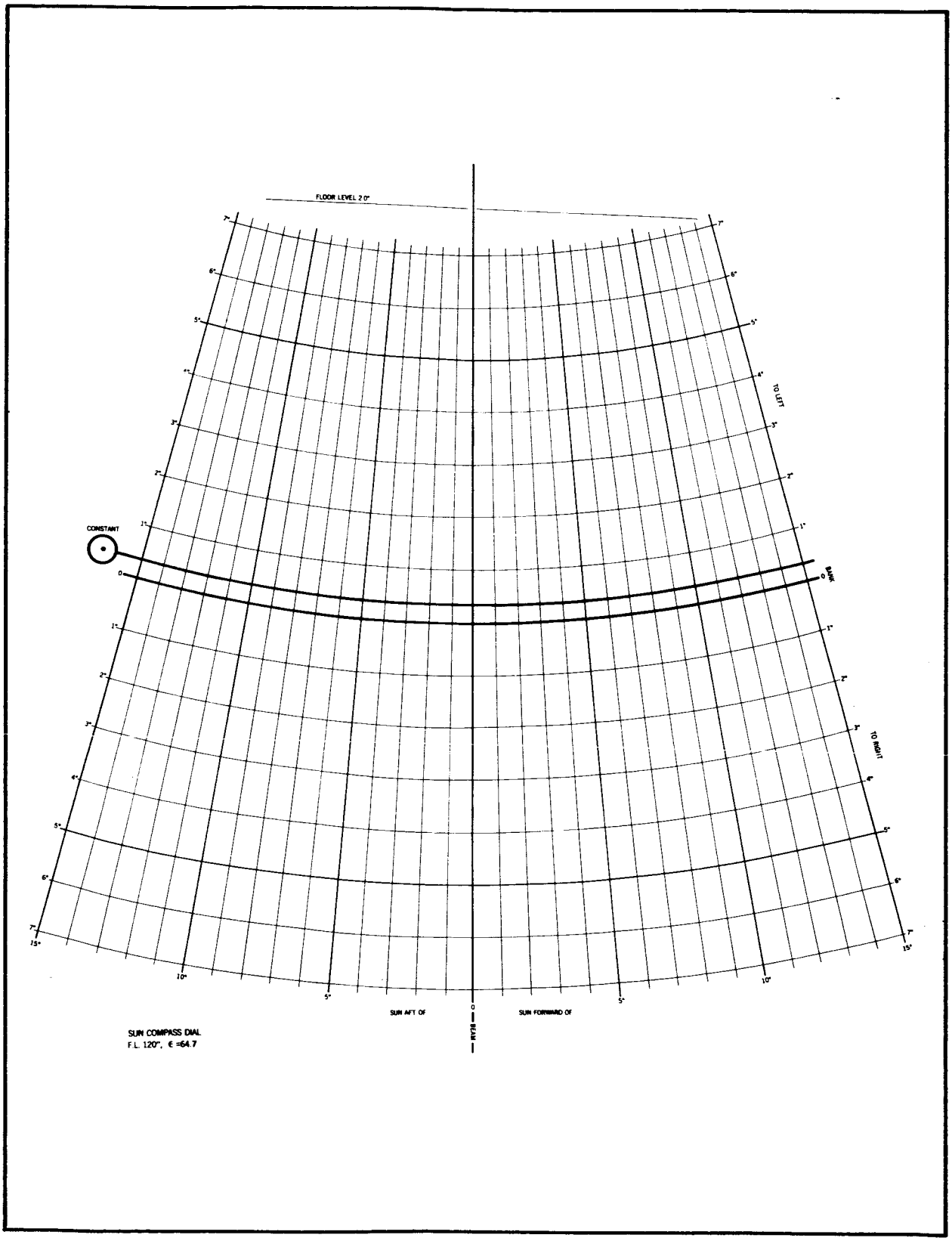

Figure 45. Sun Compass Grid

the aircraft heading, pitch angle, and bank angle were measured while the aircraft was parked at Hilo airport. Twice on each day while the aircraft was at Hilo, the sun attained $\epsilon = 64.^{\circ}7$; the relevant calculations are summarized in table 9. Using this information, plus the known parked aircraft attitude, the projected solar image could be zeroed on the movable grid overlay section. Another method of checking the sun compass alignment was to orient a theodolite in a direction simulating the incoming beam of the sun during mid-totality, accounting for differing pitch and bank angles of the parked aircraft.

During the solar eclipse flight and some of the practice flights, the sun compass was used to assist in navigation of the CV-990. The observation leg of the June 1 calibration flight was steered for 35 min along the constant Sun bearing course by this device. In addition, the Sun compass was an aid in tuning the Sperry-Phoenix autopilot.

Navigation by Cusps. — The feasibility of using cusps of the partially eclipsed sun as a second backup to conventional navigation techniques during airborne eclipse flights was investigated (ref. 14). Several factors, evolving mainly from lack of time and funds to construct the necessary measuring instrument, or to alter an existing sextant, precluded implementation on the 1965 solar eclipse flight. A brief summary of the feasibility study results are presented here. The reader may refer to the original paper for details.

To deduce geographic position by observations of eclipse cusps, two measurements on the cusps are necessary. The optimum pair are the angle subtended by the cusp line from the local vertical and the uneclipsed solar crescent thickness. Typical probable errors in measuring these quantities are estimated at 1° and 10 arc sec, respectively, yielding position uncertainty of about 11 n. mi. in a direction parallel to the umbra track and 7 n. mi. in a direction perpendicular to the umbra track , assuming the May 30, 1965 eclipse circumstances. Considerably better cross track accuracy (2 to 3 n. mi.) could be achieved a few minutes before mid-totality if the aircraft is near the umbra path, even though the umbra itself is at a distance up or down track. Because of the position errors found, it is concluded that this method has only marginal value but deserves further attention.

TABLE 9

PREDICTED INSTANTS OF 64.°7 SOLAR ELEVATION AT HILO, HAWAII, FOR PARKED AIRCRAFT WITH 4°0 SUN COMPASS LENS SLUE FORWARD OF 90° BEARING FROM AIRCRAFT CENTERLINE

Date	Universal Time	Zone Time 150° Meridian	Aircraft Heading
May 23, 1965	$20^h29^m42^s$	$10^h29^m42^s$ AM	172.°0
	$24^h04^m52^s$	$2^h04^m52^s$ PM	5.°0
May 25, 1965	$20^h29^m46^s$	$10^h29^m46^s$ AM	177.°2
	$24^h05^m10^s$	$2^h05^m10^s$ PM	6.°4
May 27, 1965	$20^h29^m56^s$	$10^h29^m36^s$ AM	170.°4
	$24^h05^m24^s$	$2^h05^m24^s$ PM	7.°2
May 29, 1965	$20^h30^m11^s$	$10^h30^m11^s$ AM	169.°6
	$24^h05^m38^s$	$2^h05^m38^s$ PM	8.°0

TASK IV: AIR FORCE HELIOSTATIC SYSTEM

Introduction

In December 1964, the Guidance and Control Laboratory of the Engineering Laboratories and Services Department began the design of a heliostatic system (see Appendix G for a glossary of terms) to be used on the Douglas-Mt. Wilson spectrograph experiment in conjunction with Project ASEE. The function of the optical electromechanical system was to position an image of a section of the solar corona on the slit of a spectrograph and to maintain this position throughout totality, despite the motions of the aircraft. The heliostat was conceived to be a two-axis, gyroscopically stabilized platform on which an optically suitable mirror would be mounted. The heliostat system would consist of a servo-driven heliostat and the electronics and controls required for operating it successfully. Early in 1965, the construction of a second system was undertaken for use by the Aerospace Research Laboratory (ARL), Wright-Patterson Air Force Base, Ohio, as Task IV of Contract NAS2-2703.

This section is concerned primarily with the fabrication and operation of the ARL instrument. It reviews design philosophy, based on the Douglas instrument, and gives results of laboratory tests and of the actual hot-run ASEE flight. During this flight, the system successfully maintained image stability within predicted performance tolerances throughout the period of totality.

System Design

The design problem was to mount a telescope rigidly to the airplane structure and to provide an optical-electromechanical system that would ensure that the telescope's line-of-sight or look direction always pointed at the sun. The same specifications, dictated by the Douglas-Mt. Wilson spectrograph experiment, were adopted for Task IV, namely, that the variations in look direction should vary no more than 1 min of arc, rms, for periods of 120 sec or longer. The following paragraphs present general information about the system design.

Gimbal design. — To provide pointing capability for the system, a gimbal was used in the orientation shown in fig. 46. The outer axis, referred to as the elevation axis, was made parallel to the telescope's actual line-of-sight, and the inner axis, referred to as the azimuth axis, was positioned in a plane perpendicular to the elevation axis and nominally containing the center of the sun. The terms azimuth and elevation are used here for convenience and do not carry their astronomical application.

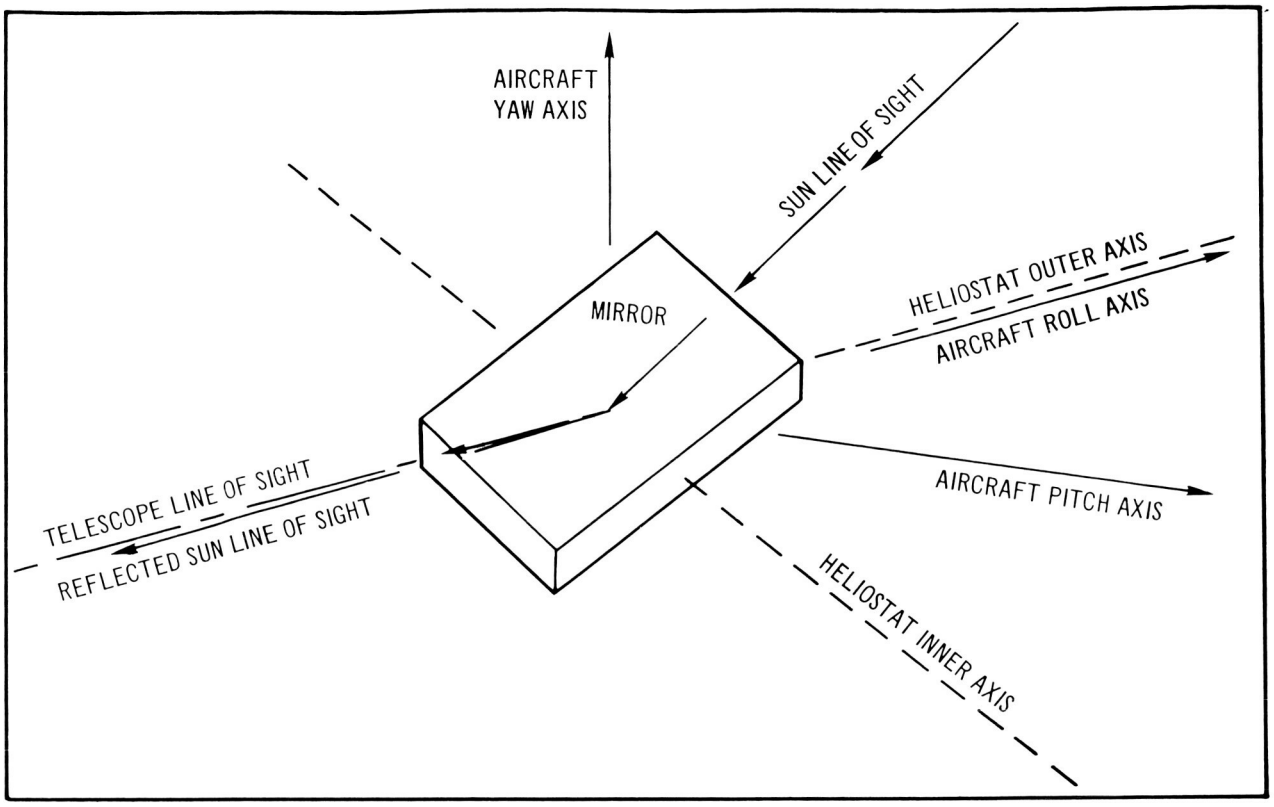

Figure 46. Heliostat Axis Orientation

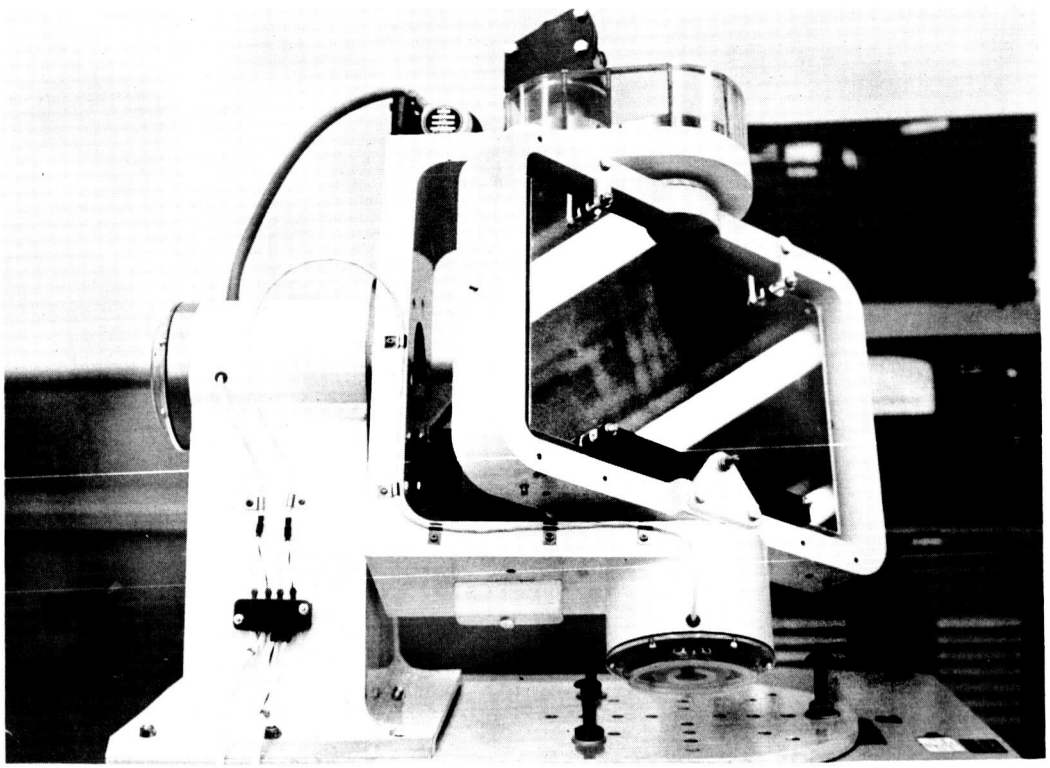

Figure 47. Heliostat Gimbal Assembly

The gimbal was designed (fig. 47) with direct-drive torque motors integrated into the axes to provide rotation for the gimbal frame. Provisions were made for mounting a mirror on the gimbal frame, and for mounting integrating-rate gyros to sense rotation about each axis.

A rigid, yet light-weight, gimbal assembly was constructed by machining the inner-axis frame and the outer-axis yoke from aluminum. The pedestal of the assembly was welded aluminum plate and tubing. Shielded, rather than sealed, bearings were used to minimize friction.

The inner axis of the platform must move at one-half the aircraft rate about that axis because of the double-angle reflection property of a mirror. To accomplish this, a one-to-two drive ratio from the mirror to the gyro was required. The only drive method determined that would meet the accuracy requirements was an arrangement which used mechanical pulleys with a steel band drive.

Mirror support. — The surface of the heliostat mirror must be adjusted precisely parallel to the inner axis. Also, the mirror must be solidly supported to reduce mirror bending. For mirror adjustment, a three-point suspension is ideal, but a four-point suspension gives better support. The support arrangement derived for use on the heliostat (fig. 47) combined the best features of both methods.

Drive motor selection. — Direct-current torque motors with a stall torque rating of 1.2 lb-ft were selected for both the elevation and the azimuth axis drives. The drive motors could have been of smaller torque rating, particularly in the elevation axis where only frictional and mass unbalance forces would have to be overcome. However, the additional motor torque capability, obtained without compromising system performance, added versatility to the system for future increased loads. In addition, the use of the same motor for both elevation and azimuth drives reduced the spare parts inventory requirements.

Servoloop design. — Initial loop studies on Type I servo systems which used both Bode plot methods and analog equipment, indicated that the loop could not be stabilized at a gain high enough to meet the dynamic accuracy requirements.

A Type II servosystem was then considered, but at the same time, an attempt was made to reduce the coupling caused by back EMF and thereby to reduce the dynamic error. The back EMF coupling was markedly reduced by driving the motor with a current source. This also reduced the effect of the electrical time constant of the motor. With motor damping (feedback proportional to angular rate) reduced to a negligible value, the servoloop became, for practical purposes, a Type III system.

Appendix H explains the characteristics of a Type III servosystem and gives more detailed information about the servosystem used for the heliostat.

Only forward loop compensation was used to stabilize the system. The compensation problem was analyzed with IBM 7094 (digital) equipment. This analysis resulted in the use of a compensation transfer function with three lead and three lag terms. This transfer function was obtained through use of an operational amplifier and resistor-capacitor combinations. Compensation details are presented in Douglas Report SM-48335 (ref. 2).

Static tests. — The bearing and motor-brush friction were checked on each axis of the system after installation of the torque motor. The friction measured approximately 3 oz.-in. Motor torque was within specified tolerances.

Each of the two gimbal axes was statically mass balanced after the complete heliostat system was assembled. Mechanical assembly and electrical operating procedures are described in Appendix I.

The two axes on the gimbal were found to be 0.00278° off perpendicularity.

Dynamic tests. — To determine the response characteristics of the completed system, simulated aircraft motions were applied to the heliostat. This simulation was performed on one axis at a time, with an oscillating rate table to apply the sinusoidal motions.

Fig. 48 depicts the heliostat mounted on the oscillating rate table in position for dynamically testing the inner axis of the heliostatic system. The heliostat electronics and aircraft attitude monitoring and recording equipment are in the console at the right side of the photograph. The console directly behind the oscillating rate table contains the electronics equipment for the table.

The mirror was installed, the gyros were aligned, and each of the axes was carefully mass balanced prior to the dynamic tests. The gain of each loop was adjusted until the response to a step input indicated a damping ratio of approximately 0.7. Each axis was subjected to the input frequencies and amplitudes tabulated in table 10. The system performance was measured by recording the output of the gyro of each axis under test. This output electrically represents the loop dynamic error from an inertial (gyroscope) reference. These errors are tabulated in table 10. Several typical wave-forms of the error signal are illustrated in fig. 49.

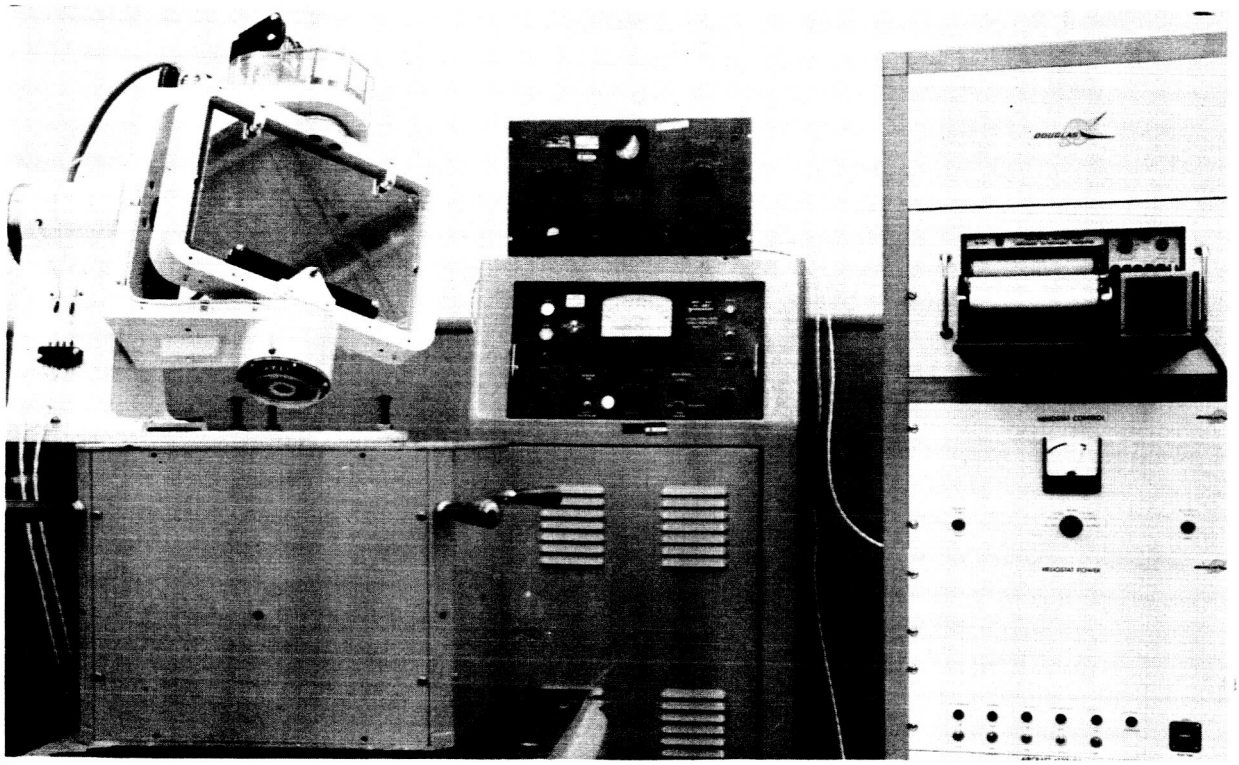

Figure 48. Heliostat System Dynamic Test Facility

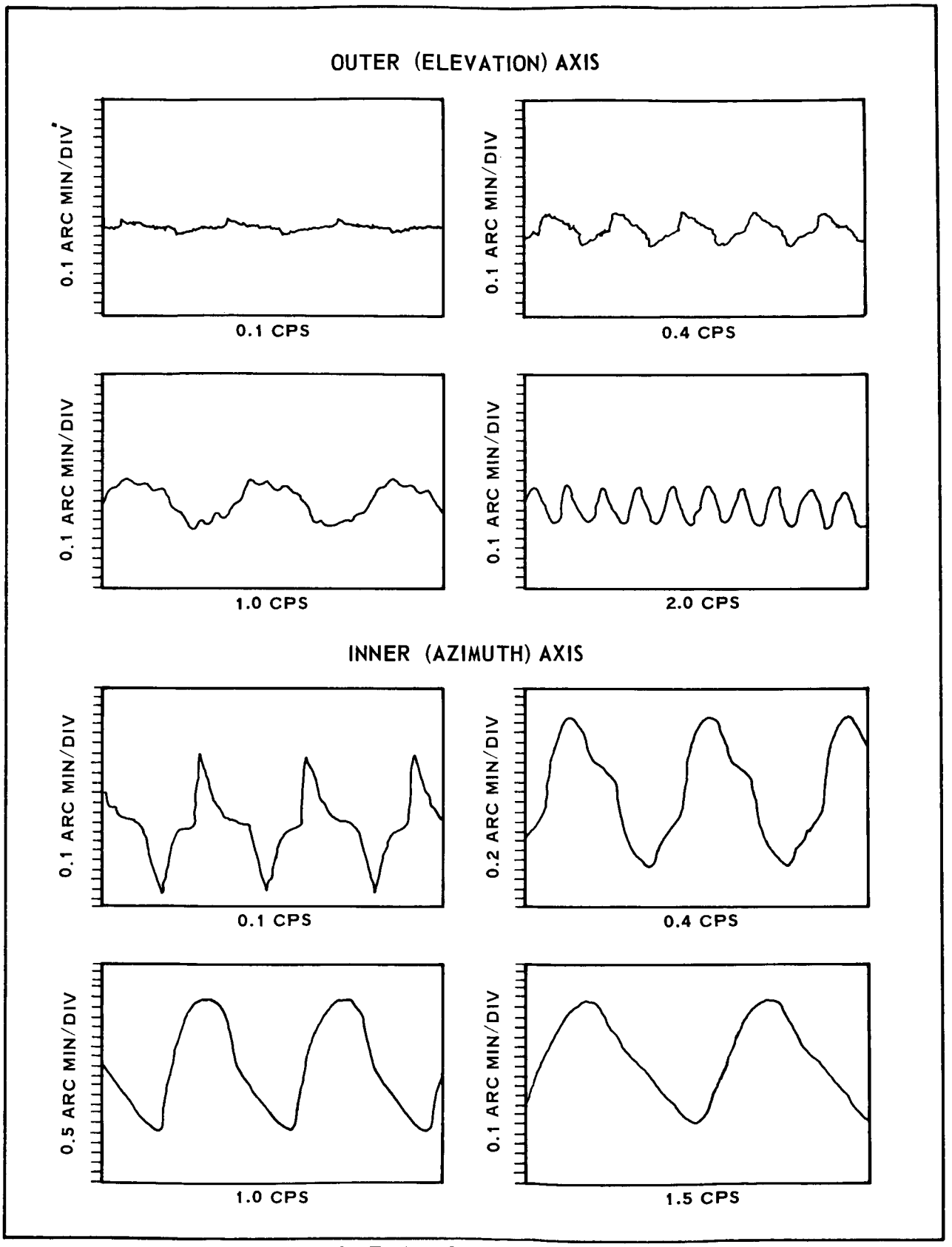

Figure 49. Typical Dynamic Error Waveforms

TABLE 10. DYNAMIC TEST RESULTS

Input frequency (cps)	Input amplitude (deg pk-pk)	Outer axis error (arc min pk-pk)	Inner axis error (arc min pk-pk)
0.1	2	0.124	1.21
0.2	2	0.247	1.67
0.4	2	0.247	2.66
0.6	2	0.330	3.49
0.8	2	0.371	4.37
1.0	2	0.371	5.81
1.2	2	---	7.67
1.5	2	---	13.00
2.0	2	0.371	14.18
4.0	2	0.330	---
6.0	2	0.206	---
8.0	2	0.206	---
10.0	2	0.206	---

Although the gimbal was space stabilized about the outer axis and, therefore, presented only frictional and mass unbalance loads to the outer axis motor, the gimbal necessarily rotated about the inner axis in inertial space and, thus, presented a much larger load to the inner axis motor. The effects of this basic difference are readily noted in the magnitudes of the errors of the axes.

The inner axis loop dynamic error continued to increase with increasing input frequency because of the increasing torque required to accelerate the load. The outer axis loop dynamic error showed the effect of auto-stabilization which, because it is more pronounced at high frequencies, kept the error small, especially in the region above the system response.

Flight Performance

During the flight in which the shadow of the moon was intercepted, a record was made of the heliostatic system performance and the angular motions of the aircraft.

To monitor the motions of the Convair CV990 aircraft, wide-angle, rate-integrating gyroscopes were rigidly attached to the aircraft structure and approximately aligned to each of the principal aircraft axes. These gyros were completely independent of the heliostatic system. The output of the gyros indicated the angular deviation of the aircraft axes from a set of inertial reference axes established by the gyros. Each of the gyros was connected to a recording galvanometer in an oscillograph recorder.

From the oscillograph record, three predominant aircraft angular-motion frequencies were observed. Table 11 lists these frequencies and the amplitudes for each of the major aircraft axes.

TABLE 11. AIRCRAFT ANGULAR MOTIONS DURING HOT RUN

Frequency (cps)	Roll (deg pk-pk)	Pitch (deg pk-pk)	Yaw (deg pk-pk)
5	0.2	0.08	0.04
0.2	0.4	0.1	0.2
0.01	1.4	0.2	0.8

The outer axis of the ARL heliostat was approximately parallel with the roll axis of the airplane. The inner axis was rotated nominally 25° from the airplane pitch axis in the pitch axis/yaw axis plane. The inner axis servo, therefore, received mostly pitch motions of the aircraft.

As in the dynamic tests of the heliostatic system, the output of each gyro of the heliostatic system was recorded to provide a continuous record of the instantaneous gyro-platform stabilization error.

From the oscillograph record, an approximate root-mean-square error was derived. The outer axis platform error of the ARL instrument was in the order of 0.07 arc min, rms, and the inner axis platform error was in the order of 0.25 arc min, rms.

These errors do not necessarily represent the exact optical line-of-sight stability; there are several other factors to consider. The primary factor is the optical alignment of the observing instrument. Discussion of line-of-sight stability is presented in Douglas Report SM-48335 (ref. 2).

Additional Information

Appendix J briefly describes the components that were selected or designed to match the requirements specified in the analytical study of the servoloop. Appendix K contains related vendor literature describing the electronic components. Appendix L contains schematics of the electronic circuitry.

APPENDIX A

ADOPTED NUMERICAL CONSTANTS

Distances and Conversion Factors

Distance conversion factors:	1 n.mi.	= 6,080 ft
		= 1.152 statute mi.
		= 1.853 km
Radius of Earth:	R_E	= 3,440 n.mi.

Aircraft Flight Parameters (CV-990)

Nominal ground speed,		
long range cruise:	V	= 455 knots
observation legs:	V	= 490 knots
		= 8.2 n. mi/min
Nominal altitude, observation legs:	37,000 ft	= 6.08 n.mi.
Nominal pitch angle, observation legs:		= 1.9° (nose up)

Target Object Aspect

Bearing, relative to aircraft longitudinal axis (centerline), positive in direction of motion:	= -90° (port, i.e. left)
Elevation angle, mid-intercept points:	= 64.7°

Geographic Coordinates

Moffett Field, Mountain View, California	λ	= 122° 10' W
	ϕ	= 37° 26' N
Hilo Airport, Hilo, Hawaii	λ	= 155° 10' W
	ϕ	= 19° 45' N
Papeete Airport, Tahiti, Society Islands, French Polynesia	λ	= 149° 34'W
	ϕ	= 17° 34'S
Christmas Island	λ	= 157° 28'W
	ϕ	= 1° 58' N

APPENDIX B

PERSONAL CORRESPONDENCE FROM THE U.S. NAVAL OBSERVATORY

The following is a copy of a letter from R. L. Duncombe, Director of the Nautical Almanac Office, U.S. Naval Observatory. It contains data which were transformed into the plots shown in figs. B-1, B-2, and B-3.

APPENDIX B

NAVY DEPARTMENT
U.S. NAVAL OBSERVATORY
WASHINGTON, D.C. 20390

5 November 1964

Dear Dr. Klemperer,

In reply to your letter of 15 October 1964, we have calculated the following data for the central line of the path of the total Solar Eclipse of 30 May 1965 for an altitude of 40,000 feet:

Universal Time	Sun's Altitude	Sun's Azimuth	Azimuth of Path	Velocity of Shadow
20^h50^m	60°23.6	015°.7	57°.0	1246 Kts
20 55	61 53.7	011.1	58.3	1208
21 00	63 07.7	006.0	59.8	1176
21 05	64 04.3	000.6	61.4	1151
21 10	64 42.1	354.9	63.1	1132
21 15	65 00.3	348.9	65.0	1119
21 20	64 58.2	343.0	67.1	1111
21 25	64 36.0	337.2	69.2	1110
21 30	63 54.2	331.6	71.6	1115

UT	Latitude	Longitude	L	Totality
20^h50^m	06°38.4S	141°24.5W	.014095	$5^m03^s.8$
20 55	05 43.9S	139 58.5W	.014159	5 08.6
21 00	04 52.9S	138 33.8W	.014211	5 12.7
21 05	04 05.4S	137 09.9W	.014252	5 16.0
21 10	03 21.3S	135 46.4W	.014280	5 18.6
21 15	02 40.4S	134 22.7W	.014298	5 20.2
21 20	02 02.7S	132 58.5W	.014304	5 21.1
21 25	01 28.3S	131 33.4W	.014299	5 21.1
21 30	00 57.2S	130 07.0W	.014282	5 20.3

APPENDIX B

The quantity L is the radius of the shadow on the plane through the observer and parallel to the fundamental plane. It is equivalent to the term you have defined as the "semi-axis of the shadow eclipse." The major-axis may be calculated by forming the product of the cosecant of the sun's altitude and the semi-axis. The unit is the equatorial radius of the earth.

The above values for the duration are the differences between the second and third contacts computed using the semidiameter which appears in the Lunar Ephemeris. These are consistent with the local circumstances given in Circular No. 102.

Sincerely yours,

R. L. DUNCOMBE
Director
Nautical Almanac Office

Dr. W. B. Klemperer
Douglas Aircraft Company, Inc.
Missile and Space Systems Division
3000 Ocean Park Boulevard
Santa Monica, California, 90406

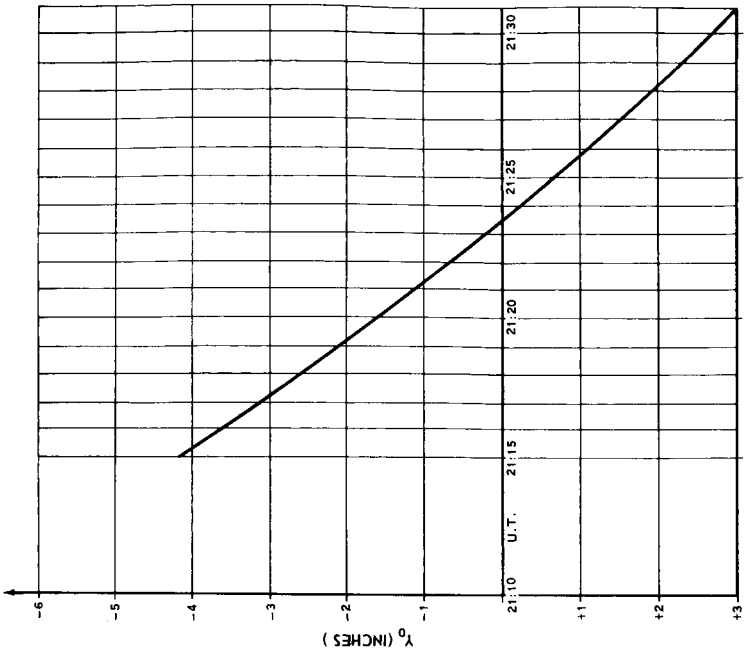

Figure B-1. Y_0 Coordinates of Umbra Path as a Function of U.T. in Gnomic Projection

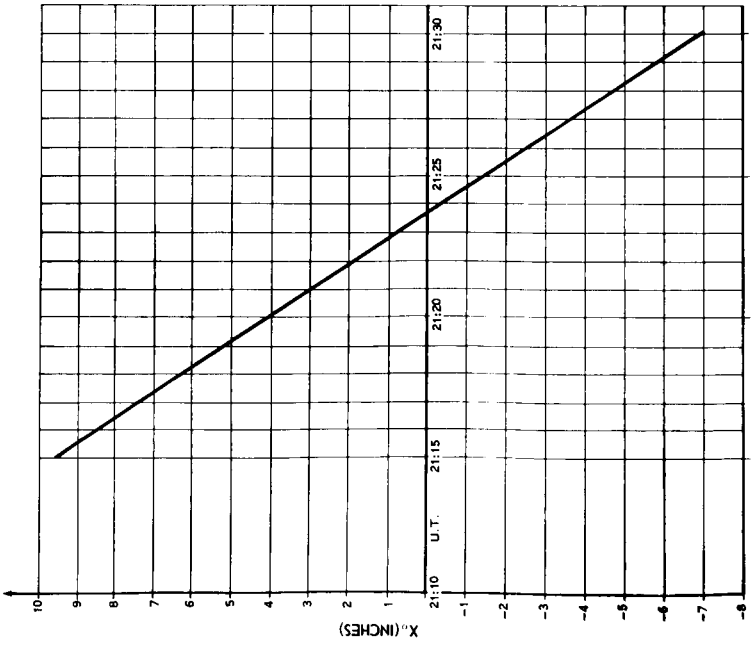

Figure B-2. X_0 Coordinates of Umbra Path as a Function of U.T. in Gnomic Projection

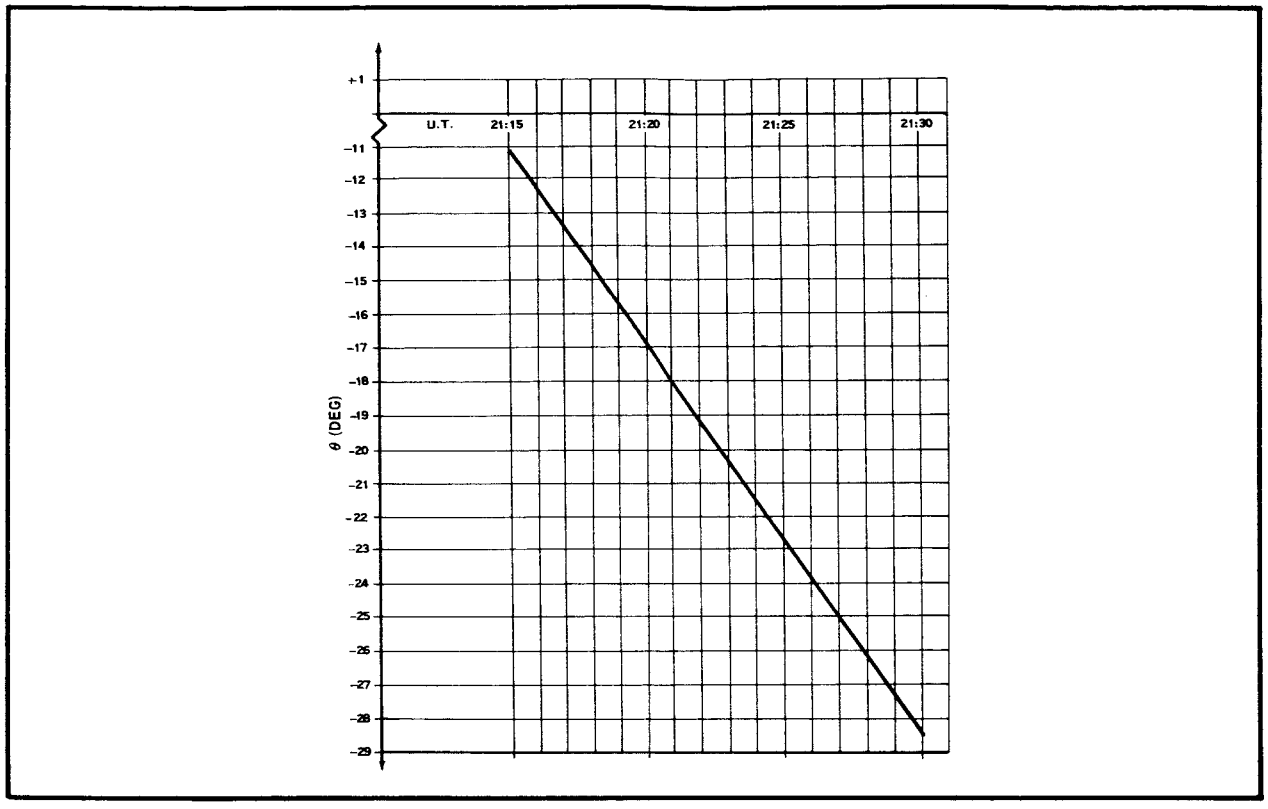

Figure B-3. Azimuth of Major Axis of Umbra Ellipse Along Umbra Track

APPENDIX C

BASIC EQUATIONS OF SPHERICAL ASTRONOMY

Celestial objects appear projected on an immense sphere termed the celestial sphere. Imagine the Earth's equator produced to infinity in all directions, intersecting the celestial sphere in a great circle and termed the celestial equator (Q). Imagine also the north and south geographic poles of Earth extended to infinity, intersecting the celestial sphere in two points, the celestial north (CNP) and the celestial south (CSP) poles. Because of the orbital motion of Earth about the sun, the latter appears to trace out a great circle, the ecliptic, on the celestial sphere, with a complete circuit requiring one year. The ecliptic intersects the celestial equator in two points, the vernal, Υ, and autumnal equinoxes. The great circle through CNP, Υ, and CSP may be termed the prime-hour circle. Because the stars, and to a first approximation the sun and the planets, lie at very great distances compared to the radius of Earth, their positions in the sky as seen from any point on Earth may be described by two coordinates which measure arc distances from some origin. The most commonly used coordinates are the right ascension, α, and declination, δ

where

α = Arc distance of astronomical object, S, from prime-hour circle, measured eastward parallel to Q, usually expressed in time units 0 to 24 hr

δ = Perpendicular arc distance of S from Q, positive if S lies between Q and CSP

Figure C-1 illustrates this system of coordinates.

Consider an observer located at longitude, λ, from the Greenwich meridian and latitude, ϕ; to be more definite, take λ West and ϕ North. Produce the line from Earth's center through the observer to meet the celestial sphere at Z, the zenith. The great circle through Z, CSP, and CNP is the observer's meridian. Denoting CNP by P, the spherical triangle PZS is the astronomical triangle. In fig. C-2 the arc $\overset{\frown}{FS}$ is the elevation, ϵ, of S, and since the arc $\overset{\frown}{FZ} = 90°$, then $\overset{\frown}{ZS} = 90° - \epsilon = \zeta$, the zenith distance of S. It is easily shown that $\overset{\frown}{NP} = \phi$, hence $\overset{\frown}{PZ} = 90° - \phi$. Similarly, since $\overset{\frown}{PD} = 90°$, then $\overset{\frown}{PS} = 90° - \delta$. The spherical angle $\angle PZS = \overset{\frown}{NF}$ is the azimuth, AZ, of S and the spherical angle $\angle ZPS$ is the hour angle, H, of S. Equations (11) and (12) of the text are identities in the triangle PZS. In the analyses conducted, $\angle PZS \equiv 360° - AZ$ so that azimuth is measured in the conventional navigational sense, Eastward from North, 0° to 360°.

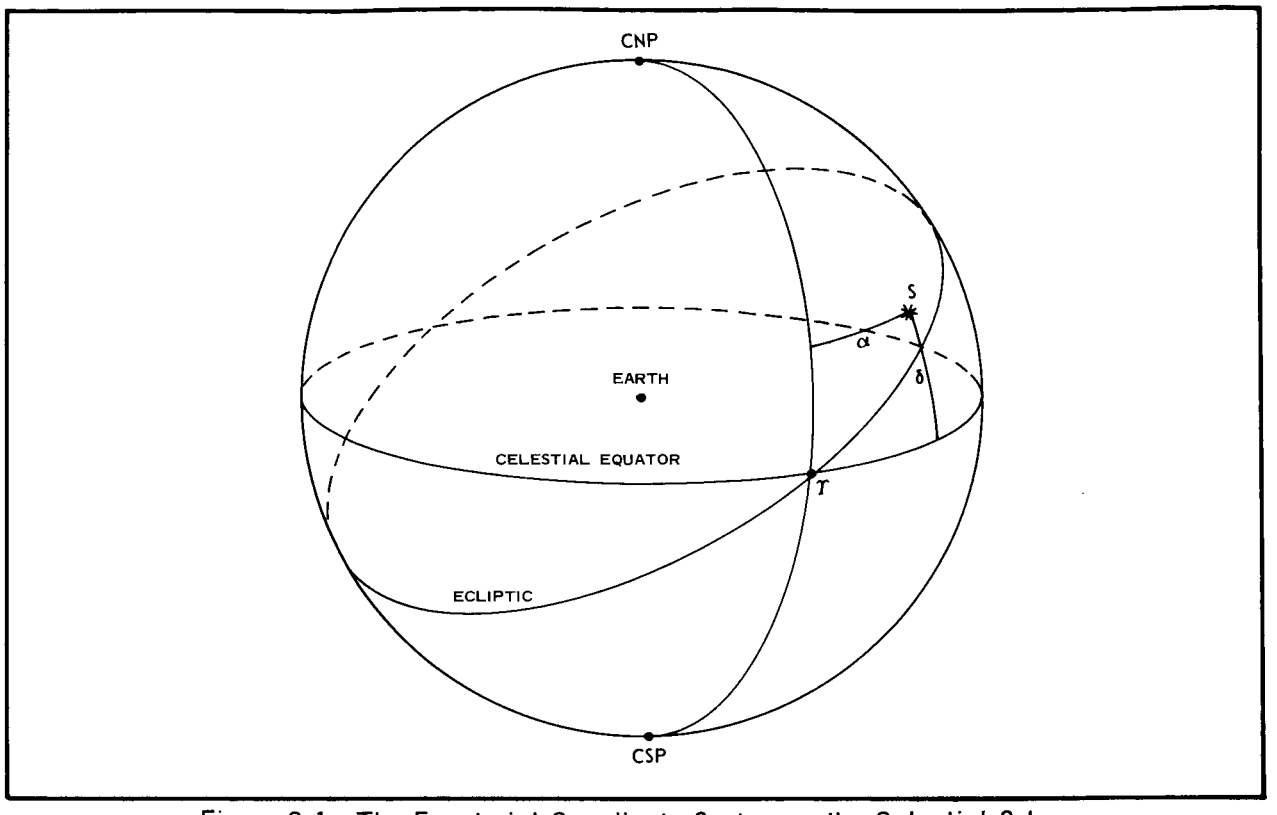

Figure C-1. The Equatorial Coordinate System on the Celestial Sphere

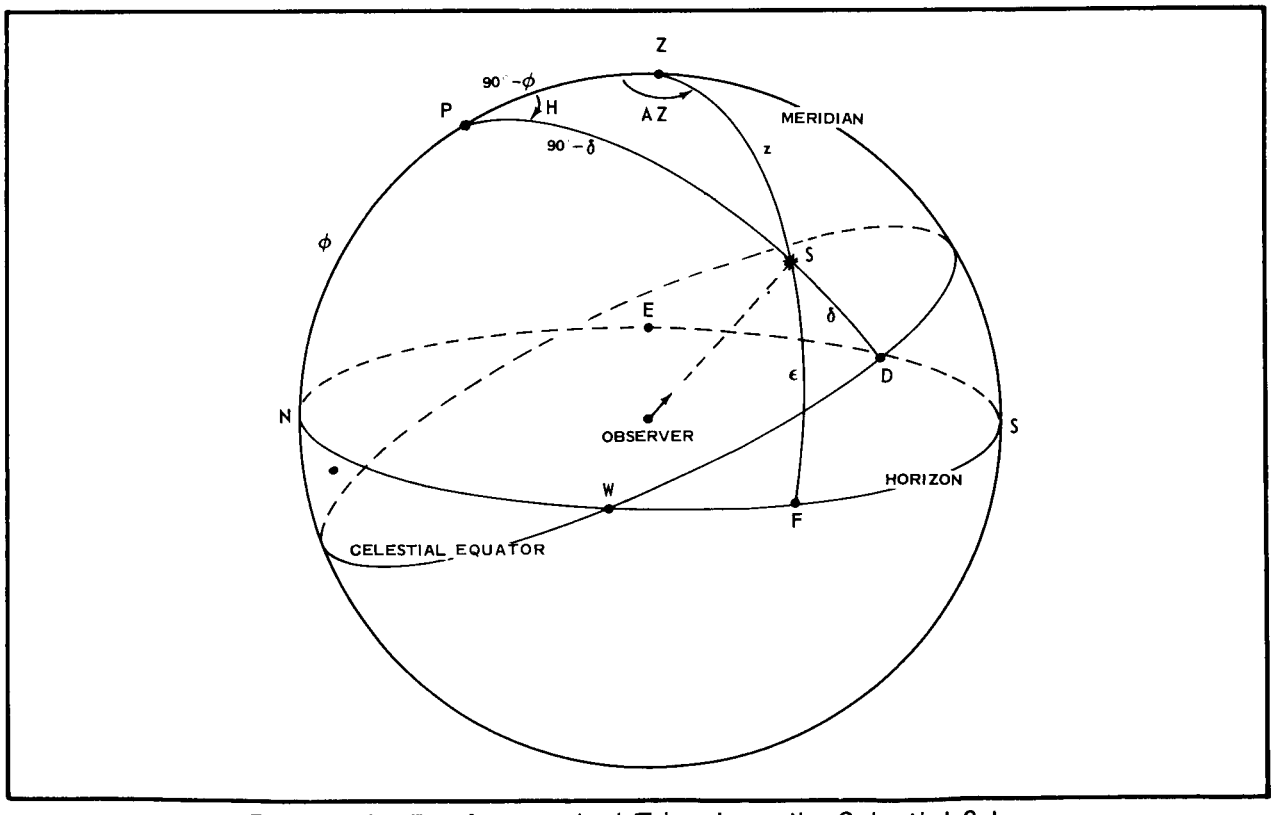

Figure C-2. The Astronomical Triangle on the Celestial Sphere

APPENDIX C

The hour angle of the vernal equinox Υ is the local sidereal time, and constitutes the fundamental clock of spherical astronomy. To sufficient accuracy, a sidereal day is the period of one Earth rotation, namely, $23^h56^m04^s$. Since the ordinary civil, or mean solar day, is 24^h, the sidereal clock runs ahead of the civil clock by an amount $\Delta T = 3^m56^s/24$ hour. Precise tables for converting mean solar to sidereal time intervals are given in ref. 13. The uniform system of civil time employed in practical astronomy and navigation is universal time, U.T., also known as Greenwich civil time, and Greenwich mean time. If Z. T. denotes the observer's local standard zone time, then, from equation (9) of Task III,

$$U.T. = Z.T. \pm \lambda .$$

where λ is expressed in time units, the plus sign being taken for points west and the negative for points east of Greenwich. It is evident from the above definitions of right ascension and sidereal time, LST, that the hour angle, H, of any object is

$$H = LST - \alpha .$$

This relation holds on the Greenwich meridian, i. e.

$$GHA = GST - \alpha ,$$

where GHA is the object's hour angle seen from the Greenwich meridian ($\lambda = 0°$), and GST is the Greenwich sidereal time.

The foregoing relation suggests a simple standard daily reference point for sidereal time, and therefore:

$$GST = GST_o + T\ (SID),$$

or

$$GST = GST_o + U.T. + \Delta t$$

where GST_o = Greenwich sidereal time at 0^h U. T., and T(SID) = sidereal time interval elapsed from 0^h U. T. to the U. T. at which GST is desired.

GST_o is given for every day of the year in ref. 13. Since the hour angle at which the observer sees the astronomical object is related to the hour angle GHA of the same object seen at Greenwich by

$$H = GHA - \lambda,$$

it follows that $H = GST_o + U.T. + \Delta T - \lambda - \alpha$ which is equation (10) of Task III.

APPENDIX D

ACCURACY OF CONSTANT-ELEVATION CIRCLES ON A PLANE TANGENT TO EARTH AT SUB-ASTRAL POINT

Let C be the center of Earth, assumed spherical, and O an observer at the surface. In fig. D-1, an astronomical object at a distance much greater than OC is overhead at point S, and is seen at zenith distance, ζ , by observer, O, whose zenith is in the direction of Z. The plane tangent to Earth at S intersects the line of sight from O to the astronomical object at O', where a flat Earth observer corresponding to O is located. The zenith distance, ζ', of the astonomical body measured at O' differs from ζ in general because the horizon planes O' T' and OT are not parallel. Given a value of ζ', it is desired to find the corresponding zenith distance ζ (or elevation angle $\epsilon = (90^\circ - \zeta)$ measured by the real observer at O.

Fig. D-1 illustrates the difference in zenith distances $\Delta\zeta = \zeta - \zeta'$. in relation to Earth's radius, R_E, and the line segment OP by $OP = R_E \tan \Delta\zeta$. In the small triangle OPO', $< POO' = \epsilon = 90^\circ - \zeta$, and $PO'O = \zeta'$. The side $OO' = R_E(1 - \cos \zeta)$ is related to OP by the law of sines as follows:

$$\frac{OO'}{OP} = \frac{\sin 180 - (\zeta' + \epsilon)}{\sin \zeta'}$$

By substituting the known expressions for OO' and OP into the left-hand side of the above equation and expanding the right-hand side, the following equation results:

$$\tan \zeta' = \sin \zeta$$

From this simple relation, one can determine ζ from ζ' or vice-versa, Table D-1 lists a series of true zenith distances, the corresponding projected zenith distances, and the differences. The table shows that an observer on the plane SO' always sees an astronomical object nearer the zenith (i.e., at higher elevation angle) than the corresponding real observer on Earth. For an initial survey of constant-elevation loci on Earth, the circle construction on the tangent plane SO' is apparently useful up to, but not exceeding, 30° true zenith distance, i.e., for elevations greater than 60° . Elevation angles $\geq 60^\circ$ restrict the arc OS to a small enough length relative to Earth's circumference that the λ, ϕ coordinate grid maps into a rectangular system on the SO' plane with little distortion, in equatorial and temperate latitudes. For lower elevations, the correct loci could be constructed by simply subtracting the differences $\Delta\zeta$ from the arc length SO (i.e., from ζ) to determine the circle radius, but here a rigorous mapping (e.g., gnomonic projection) of latitude and longitude into the tangent plane would be required. The whole effort could be equally well invested in a computer program to solve equations (10) and (21) of Task III point by point for the precise loci of constant ϵ on the Earth's surface.

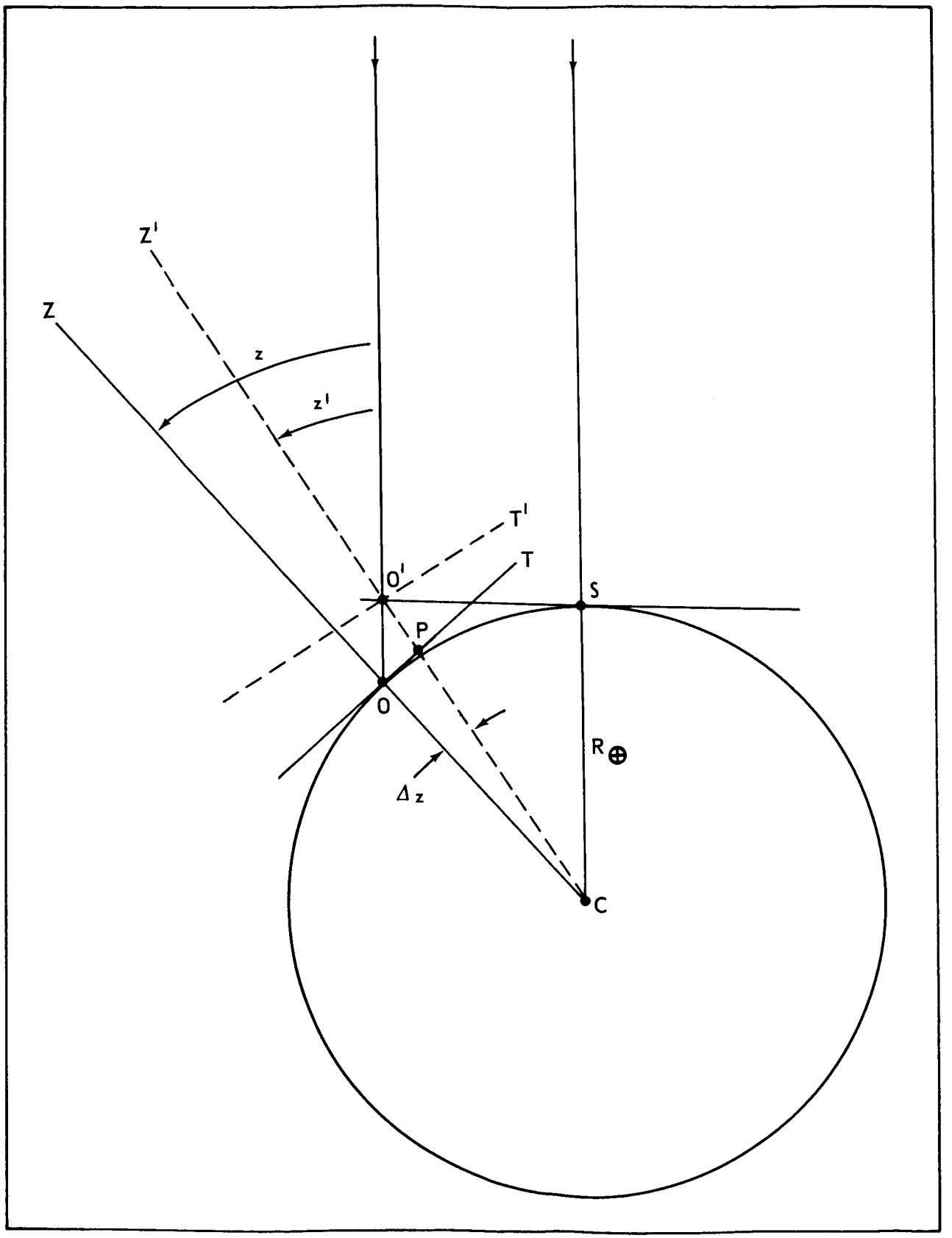

Figure D-1. Constant-Elevation Loci on Plane Tangent at Sub-Astral Point

APPENDIX D

TABLE D-I

TRUE AND PROJECTED ZENITH DISTANCES

True Elevation Angle (ϵ)	True Zenith Distance (ζ)	Projected Zenith Distance (ζ')	Difference $\Delta\zeta = -\Delta\epsilon$
90.0	0.0	0.0	0.0
85.0	5.0	4.98	0.02
80.0	10.0	9.85	0.15
75.0	15.0	14.52	0.48
70.0	20.0	18.88	1.12
65.0	25.0	22.92	2.08
60.0	30.0	26.55	3.45
45.0	45.0	35.30	9.70
30.0	60.0	40.88	19.12
15.0	75.0	44.00	31.00
0.0	90.0	45.0	45.0

APPENDIX E

FLIGHT PLANS FOR THE PRACTICE FLIGHTS

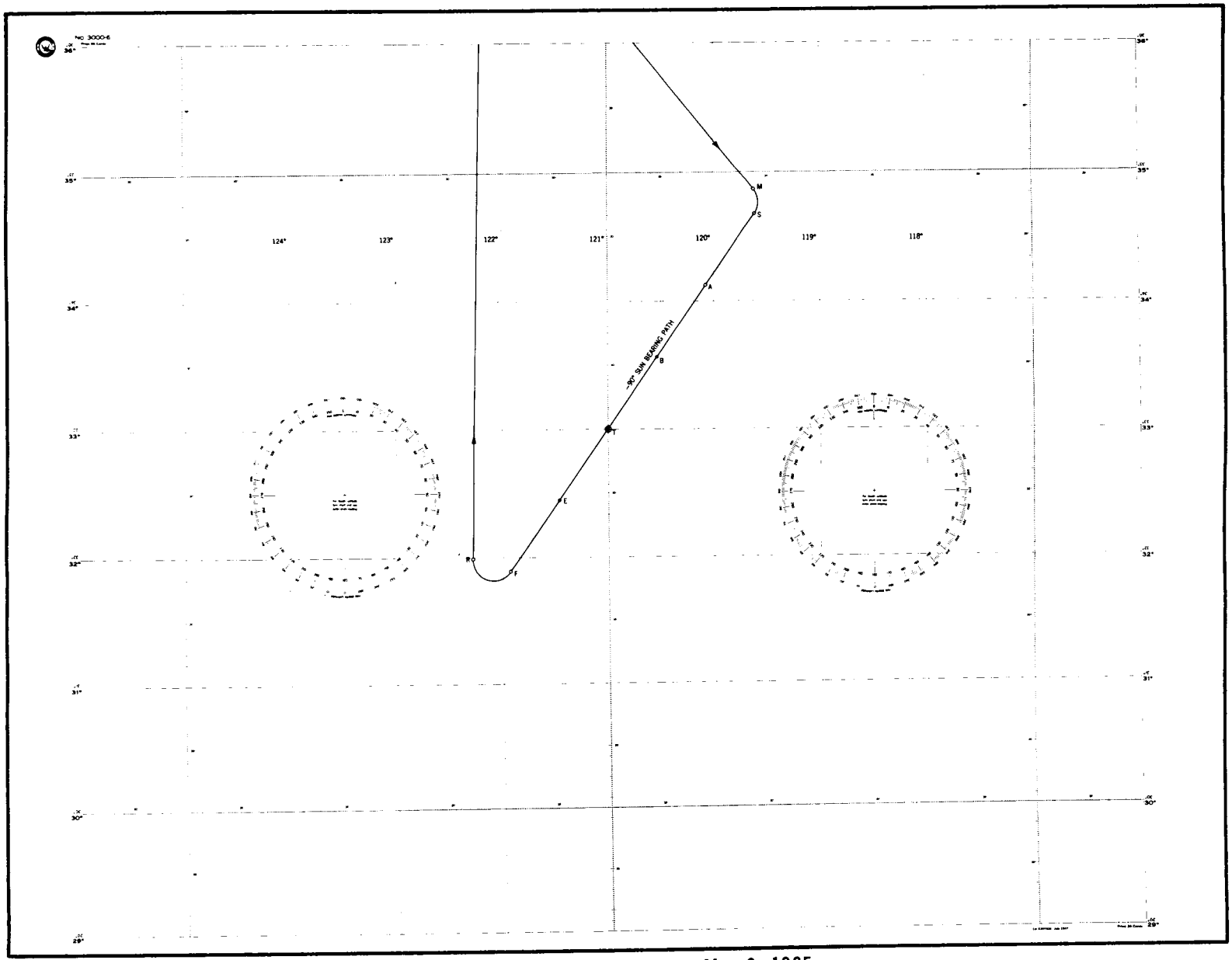

Figure E-1. Dockside Flight, May 6, 1965

TABLE E-1

FLIGHT PLAN FOR DOCK-SIDE FLIGHT FROM MOFFETT FIELD
May 6, 1965

Point	Station	Longitude	Latitude	Universal time	Maneuver	Duration	Distance n. mi.
N	Moffett field	$122^{\circ}10'$	$37^{\circ}26'$				
M	Maneuver begins	$119^{\circ}37'$	$34^{\circ}51'.5$	$18^{h}17^{m}56^{s}$	Outbound Great Circle course		200
S	Straight leg begins	$119^{\circ}36'$	$34^{\circ}41'$	$18^{h}19^{m}24^{s}$	Right turn 20° bank	$1^{m}28^{s}$	11.9
A	Arc path begins	$120^{\circ}04$	$34^{\circ}07'$	$18^{h}24^{m}24^{s}$	Straight leg	$5^{m}00^{s}$	41.0
B	Begin observation	$120^{\circ}32'$	$33^{\circ}34'$	$18^{h}29^{m}24^{s}$	Right turn $1/30^{\circ}$ bank	$5^{m}00^{s}$	41.0
T	Middle of observation	$121^{\circ}00'$	$33^{\circ}00'$	$18^{h}34^{m}24^{s}$	Continue	$5^{m}00^{s}$	41.0
E	End observation	$121^{\circ}28'$	$32^{\circ}27'$	$18^{h}39^{m}24^{s}$	Continue	$5^{m}00^{s}$	41.0
F	Finish intercept run	$121^{\circ}56'$	$31^{\circ}53'$	$18^{h}44^{m}24^{s}$	Continue	$5^{m}00^{s}$	41.0
R	Return leg begins	$122^{\circ}17'$	$31^{\circ}59'.5$	$18^{h}47^{m}25^{s}$	Right turn 20° bank	$3^{m}01^{s}$	24.6
N	Moffett field	$122^{\circ}10'$	$37^{\circ}26'$		Return trip Great Circle course		327
						Total	768.5

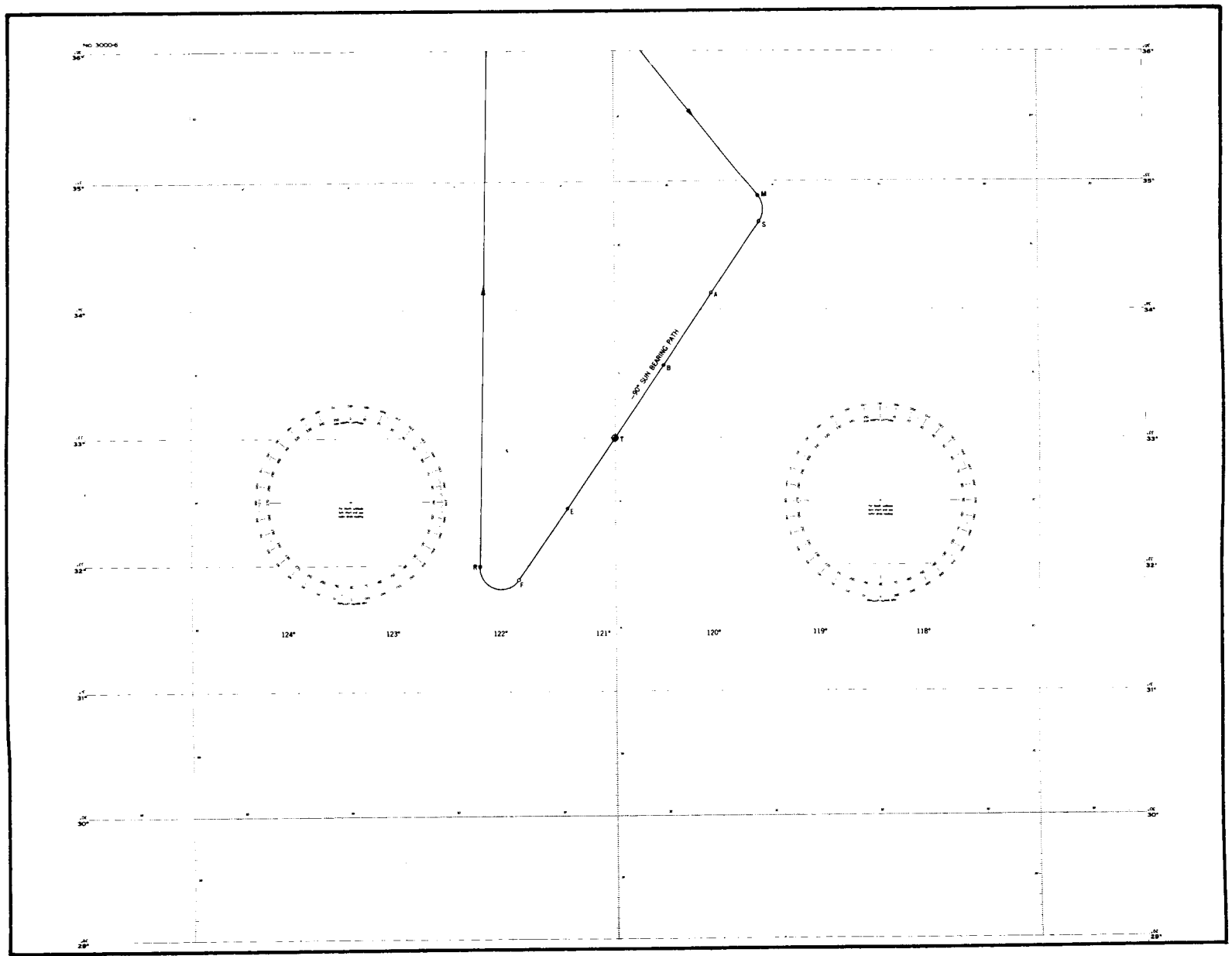

Figure E-2. Flight Plan for Dockside Flight, May 12, 1965

TABLE E-2

GHT PLAN FOR DOCK-SIDE FLIGHT FROM MOFFETT FIELD

May 7, 1965

nt	Station	Longitude	Latitude	Universal time	Maneuver	Duration	Distance n. mi.
	Moffett field	$122^{\circ}10'$	$+37^{\circ}26'$				
[	Maneuver begins	$119^{\circ}39'$	$34^{\circ}53'$	$18^{h}25^{m}53^{s}$	Outbound Great Circle course		196
	Straight leg begins	$119^{\circ}38'$	$34^{\circ}41'$	$18^{h}27^{m}25^{s}$	Right turn 20° bank	$1^{m}32^{s}$	12.5
	Arc path begins	$120^{\circ}05'$	$34^{\circ}08'$	$18^{h}32^{m}25^{s}$	Straight leg	$5^{m}00^{s}$	41.0
	Begin observation	$120^{\circ}32'.5$	$33^{\circ}34'$	$18^{h}37^{m}25^{s}$	Right turn $1/30^{\circ}$ bank	$5^{m}00^{s}$	41.0
	Middle of observation	$121^{\circ}00'$	$33^{\circ}00'$	$18^{h}42^{m}25^{s}$	Continue	$5^{m}00^{s}$	41.0
	End observation	$121^{\circ}27'$	$32^{\circ}26'$	$18^{h}47^{m}25^{s}$	Continue	$5^{m}00^{s}$	41.0
	Finish intercept run	$121^{\circ}55'$	$31^{\circ}53'$	$18^{h}52^{m}25^{s}$	Continue	$5^{m}00^{s}$	41.0
	Return leg begins	$122^{\circ}17'$	$31^{\circ}59'$	$18^{h}55^{m}26^{s}$	Right turn 20° bank	$3^{m}01^{s}$	24.6
	Moffett field	$122^{\circ}10'$	$37^{\circ}26'$		Return trip Great Circle course		328
						Total	766.1

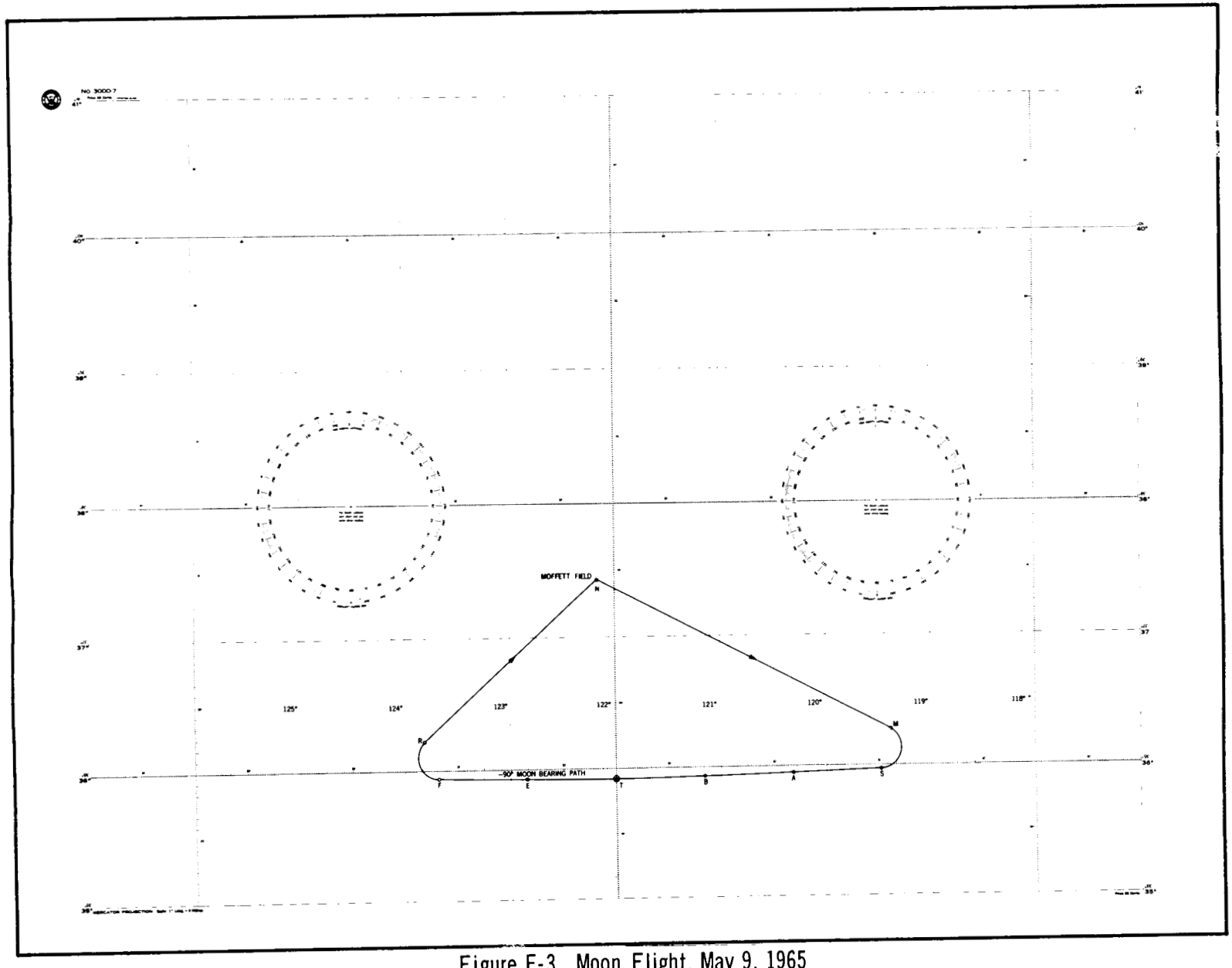

Figure E-3. Moon Flight, May 9, 1965

TABLE E-3

FLIGHT PLAN FOR MOON FLIGHT FROM MOFFETT FIELD
May 9, 1965

Point	Station	Longitude	Latitude	Universal time	Maneuver	Duration	Distance n. mi.
N	Moffett field	$122^{\circ}10'$	$+37^{\circ}26'$				
M	Maneuver begins	$119^{\circ}23'$	$36^{\circ}17'$	$03^{h}47^{m}58^{s}$	Outbound Great Circle course		152
S	Straight leg begins	$119^{\circ}29'$	$35^{\circ}58^{\circ}$	$03^{h}51^{m}00^{s}$	Right turn 20° bank	$3^{m}02^{s}$	24.8
A	Arc path begins	$120^{\circ}19'$	$35^{\circ}57'$	$03^{h}56^{m}00^{s}$	Straight leg	$5^{m}00^{s}$	41.0
B	Begin observation	$121^{\circ}10'$	$35^{\circ}56'$	$04^{h}01^{m}00^{s}$	Right turn $1/12^{\circ}$ bank	$5^{m}00^{s}$	41.0
T	Middle of observation	$122^{\circ}00'$	$35^{\circ}55'$	$04^{h}06^{m}00^{s}$	Continue	$5^{m}00^{s}$	41.0
E	End observation	$122^{\circ}50'$	$35^{\circ}55'$	$04^{h}11^{m}00^{s}$	Continue	$5^{m}00^{s}$	41.0
F	Finnish intercept run	$123^{\circ}41'$	$35^{\circ}56'$	$04^{h}16^{m}00^{s}$	Continue	$5^{m}00^{s}$	41.0
R	Return leg begins	$123^{\circ}49'$	$36^{\circ}13'$	$04^{h}18^{m}43^{s}$	Right turn 20° bank	$2^{m}43^{s}$	22.2
N	Moffett field	$122^{\circ}10'$	$37^{\circ}26'$		Return trip Great Circle course		106.0
						Total	510.0

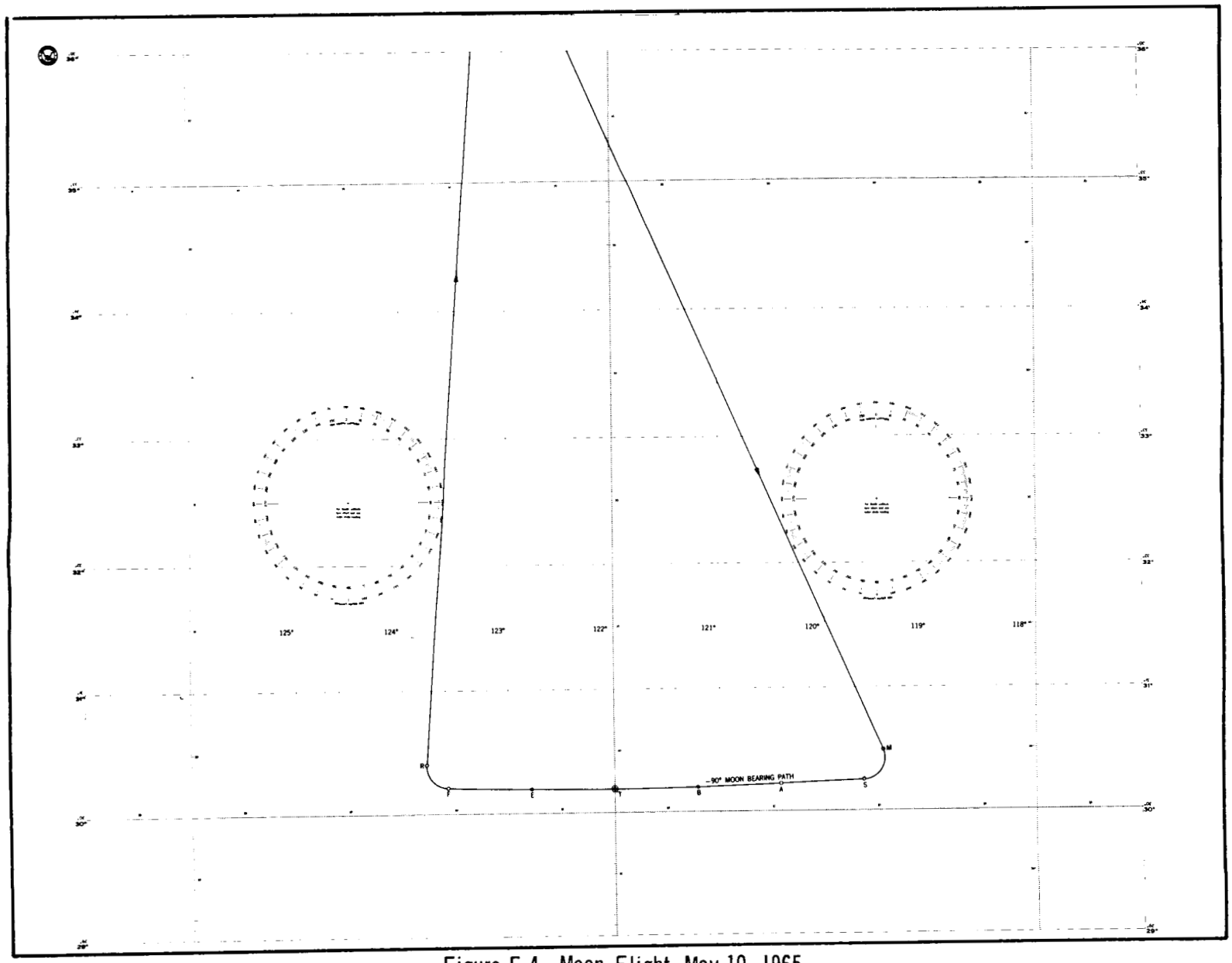

Figure E-4. Moon Flight, May 10, 1965

TABLE E-4

FLIGHT PLAN FOR MOON FLIGHT FROM MOFFETT FIELD
May 10, 1965

Point	Station	Longitude	Latitude	Universal time	Maneuver	Duration	Distance n. mi.
N	Moffett field	122°10'	+37°26'				
M	Maneuver begins	119°27'	30°30'	$04^h37^m45^s$	Outbound Great Circle course		437
S	Straight leg begins	119°38'	30°15'	$04^h39^m00^s$	Right turn 20° bank	2^m15^s	18.3
A	Arc path begins	120°25'.5	30°13'	$04^h44^m00^s$	Straight leg	5^m00^s	41.0
B	Begin observation	121°13'	30°12'	$04^h49^m00^s$	Right turn 1/10° bank	5^m00^s	41.0
T	Middle of observation	122°00'	30°11'	$04^h54^m00^s$	Continue	5^m00^s	41.0
E	End observation	122°47'	30°12'	$04^h59^m00^s$	Continue	5^m00^s	41.0
F	Finish intercept run	123°34'.5	30°12'.5	$05^h04^m00^s$	Continue	5^m00^s	41.0
R	Return leg begins	123°46'	30°24'	$05^h05^m54^s$	Right turn 20° bank	1^m54^s	15.5
N	Moffett field	122°10'	37°26'		Return trip Great Circle course		430
						Total	1,105.8

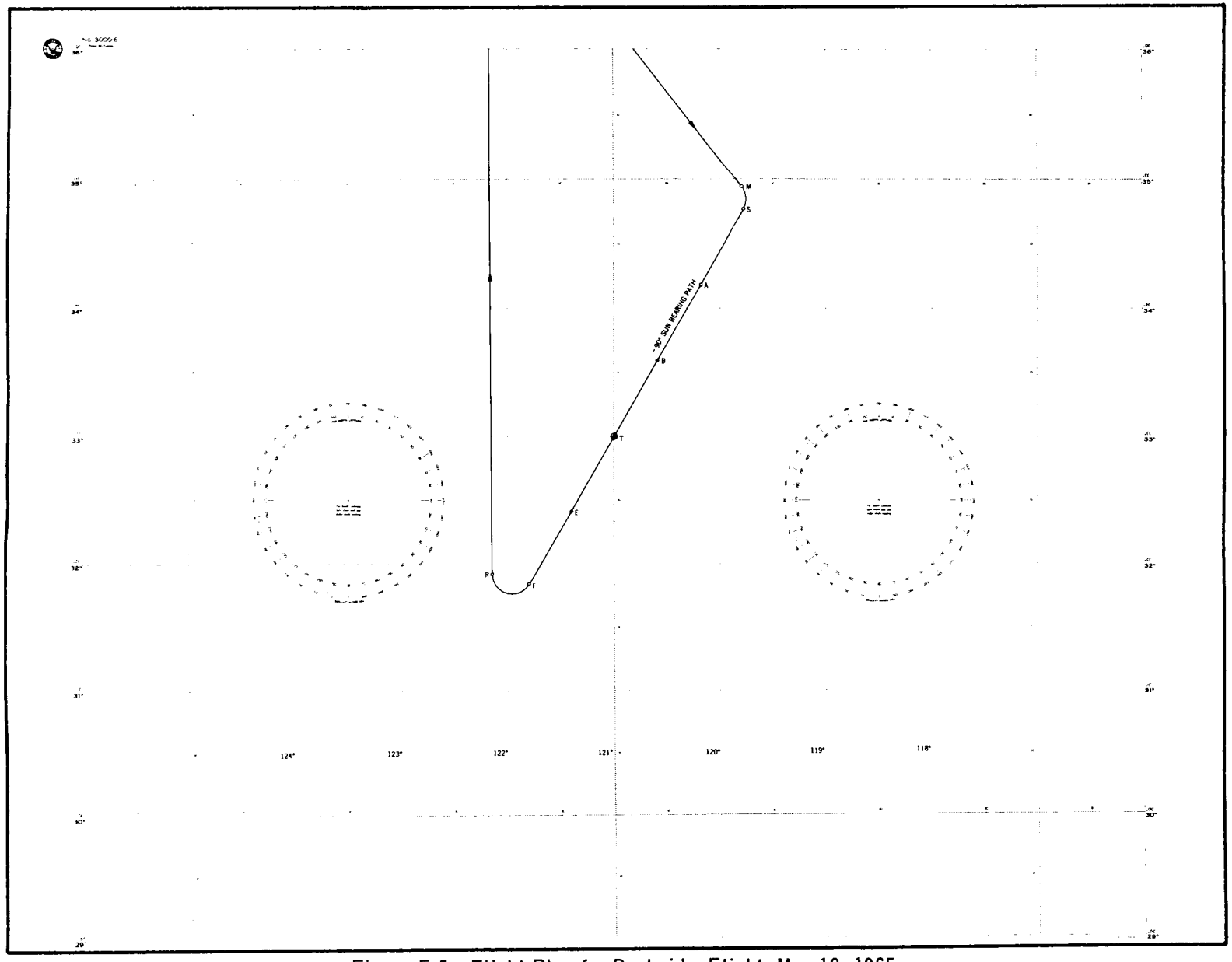

Figure E-5. Flight Plan for Dockside Flight, May 12, 1965

TABLE E-5

FLIGHT PLAN FOR DOCK-SIDE FLIGHT FROM MOFFETT FIELD
May 12, 1965

Point	Station	Longitude	Latitude	Universal time	Maneuver	Duration	Distance n. mi.
N	Moffett field	$122^{\circ}10'$	$37^{\circ}26'$				
M	Maneuver begins	$119^{\circ}47.5$	$34^{\circ}56.5$	$18^{h}12^{m}38^{s}$	Outbound Great Circle course		189.0
S	Straight leg begins	$119^{\circ}46.5$	$34^{\circ}46'$	$18^{h}14^{m}00^{s}$	Right turn 20° bank	$1^{m}22^{s}$	11.3
A	Arc path begins	$120^{\circ}10.8$	$34^{\circ}10.7$	$18^{h}19^{m}00^{s}$	Straight leg	$5^{m}00^{s}$	41.0
B	Begin observation	$120^{\circ}35.5$	$33^{\circ}35.3$	$18^{h}24^{m}00^{s}$	Level flight 0° bank	$5^{m}00^{s}$	41.0
T	Middle of observation	$121^{\circ}00'$	$33^{\circ}00'$	$18^{h}29^{m}00^{s}$	Continue	$5^{m}00^{s}$	41.0
E	End observation	$121^{\circ}24.4$	$32^{\circ}24.8$	$18^{h}34^{m}00^{s}$	Continue	$5^{m}00^{s}$	41.0
F	Finish intercept run	$121^{\circ}48'$	$31^{\circ}50.5$	$18^{h}39^{m}00^{s}$	Continue	$5^{m}00^{s}$	41.0
R	Return leg begins	$122^{\circ}09'$	$31^{\circ}55.3$	$18^{h}42^{m}04^{s}$	Right turn 20° bank	$3^{m}04^{s}$	25.3
N	Moffett field	$122^{\circ}10'$	$37^{\circ}26'$		Return trip Great Circle course		330.7
						Total	761.3

TABLE E-6

HEADING ANGLES FOR FLIGHT PATH OF MAY 12, 1965

Point	Heading Angle
S	$209^{\circ}.954$
A	$209^{\circ}.954$
B	$210^{\circ}.100$
T	$210^{\circ}.238$
E	$210^{\circ}.370$
F	$210^{\circ}.497$

TABLE E-7

SUN ELEVATION HISTORY FOR MAY 12 PRACTICE FLIGHT

Point	Elevation Angle to Sun
S	$62^{\circ}.07$
A	$62^{\circ}.97$
B	$63^{\circ}.87$
T	$64^{\circ}.77$
E	$65^{\circ}.68$
F	$66^{\circ}.56$

TABLE E-8

FLIGHT PLAN FOR DOCK-SIDE FLIGHT FROM MOFFETT FIELD

May 13, 1965

Point	Station	Longitude	Latitude	Universal time	Maneuver	Duration	Distance n. mi.
N	Moffett field	$122^{\circ}10'$	$37^{\circ}26'$				
M	Maneuver begins	$120^{\circ}55'$	$33^{\circ}56'$	$18^{h}13^{m}09^{s}$	Outbound Great Circle course		218.7
S	Straight leg begins	$120^{\circ}55!5$	$33^{\circ}49!2$	$18^{h}14^{m}00^{s}$	Right turn 20° bank	$0^{m}51^{s}$	7.0
A	Arc path begins	$121^{\circ}16!8$	$33^{\circ}13!1$	$18^{h}19^{m}00^{s}$	Straight leg	$5^{m}00^{s}$	41.0
B	Begin observation	$121^{\circ}38!4$	$32^{\circ}36!5$	$18^{h}24^{m}00^{s}$	Level flight 0° bank	$5^{m}00^{s}$	41.0
T	Middle of observation	$122^{\circ}00'$	$32^{\circ}00'$	$18^{h}29^{m}00^{s}$	Continue	$5^{m}00^{s}$	41.0
E	End observation	$122^{\circ}21!4$	$31^{\circ}23!5$	$18^{h}34^{m}00^{s}$	Continue	$5^{m}00^{s}$	41.0
F	Finish intercept run	$122^{\circ}42!7$	$30^{\circ}47'$	$18^{h}39^{m}00^{s}$	Continue	$5^{m}00^{s}$	41.0
R	Return leg begins	$123^{\circ}04'$	$30^{\circ}52'$	$18^{h}43^{m}38^{s}$	Right turn 20° bank	$4^{m}38^{s}$	37.8
N	Moffett field	$122^{\circ}10'$	$37^{\circ}26'$		Return trip Great Circle course		396.6
						Total	865.1

APPENDIX E

TABLE E-9

HEADING ANGLES FOR FLIGHT PATH OF MAY 13, 1965

Point	Heading
S	$206.^{\circ}429$
A	$206.^{\circ}429$
B	$206.^{\circ}490$
T	$206.^{\circ}534$
E	$206.^{\circ}561$
F	$206.^{\circ}568$

TABLE E-10

SUN ELEVATION HISTORY FOR MAY 13, 1965 PRACTICE FLIGHT

Point	Elevation Angle To Sun
S	$61.^{\circ}838$
A	$62.^{\circ}772$
B	$63.^{\circ}711$
T	$64.^{\circ}656$
E	$65.^{\circ}608$
F	$66.^{\circ}566$

TABLE E-11

FLIGHT PLAN FOR PRACTICE FLIGHT FROM MOFFETT FIELD
MAY 14, 1965

Point	Station	Longitude	Latitude	Universal time
S	Straight leg begins	$120^{\circ}56'$	$+33^{\circ}50'$	$18^{h}13^{m}30^{s}$
A	Arc path begins	$121^{\circ}17'$	$+33^{\circ}13'$	$18^{h}18^{m}30^{s}$
B	Begin observation	$121^{\circ}39'$	$+32^{\circ}37'$	$18^{h}23^{m}30^{s}$
T	Middle of observation	$122^{\circ}00'$	$+32^{\circ}00'$	$18^{h}28^{m}30^{s}$
E	End of observation	$122^{\circ}21'$	$+31^{\circ}23'$	$18^{h}33^{m}30^{s}$
F	Finish intercept run	$122^{\circ}42'$	$+30^{\circ}47$	$18^{h}38^{m}30^{s}$

APPENDIX E

TABLE E-12

HEADING ANGLES AND SUN ELEVATION HISTORY FOR PRACTICE FLIGHT OF MAY 14, 1965

Point	Heading angle	Elevation angle to sun
S	205°.78	61°.88
A	205°.84	62°.82
B	205.88	63.76
T	205.91	64.71
E	205.92	65.67
F	205.90	66.63

TABLE E-13

HEADING ANGLES AND SUN ELEVATION HISTORY FOR PRACTICE FLIGHT OF MAY 15, 1965

Point	Heading angle	Elevation angle to sun
S	328°.24	67°.36
A	328.39	66.46
B	328.54	65.57
T	328.70	64.68
E	328.86	63.80
F	329.02	62.92

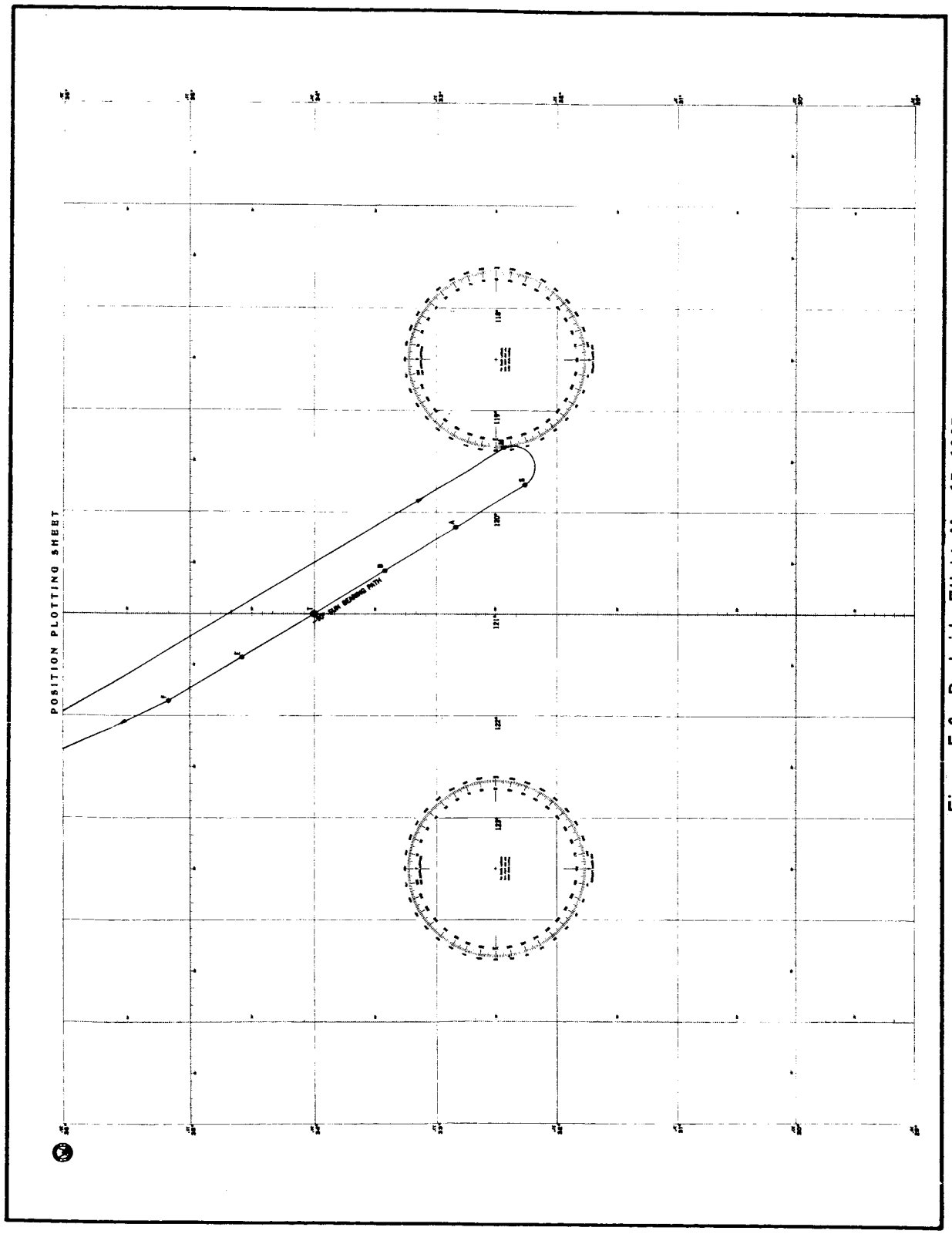

Figure E-6. Dockside Flight, May 15, 1965

TABLE E-14

FLIGHT PLAN FOR PRACTICE FLIGHT FROM MOFFETT FIELD
MAY 15, 1965

Point	Station	Longitude	Latitude	Universal time
S	Straight leg begins	$119^{o}43'$	$+32^{o}16'$	$21^{h}12^{m}00^{s}$
A	Arc path begins	$120^{o}09'$	$+32^{o}50'$	$21^{h}17^{m}00^{s}$
B	Begin observation	$120^{o}34'$	$+33^{o}25'$	$21^{h}22^{m}00^{s}$
T	Middle of observation	$121^{o}05'$	$+34^{o}00'$	$21^{h}27^{m}00^{s}$
E	End of observation	$121^{o}26'$	$+34^{o}35'$	$21^{h}32^{m}00^{s}$
F	Finish intercept run	$121^{o}51'$	$+35^{o}10'$	$21^{h}37^{m}00^{s}$

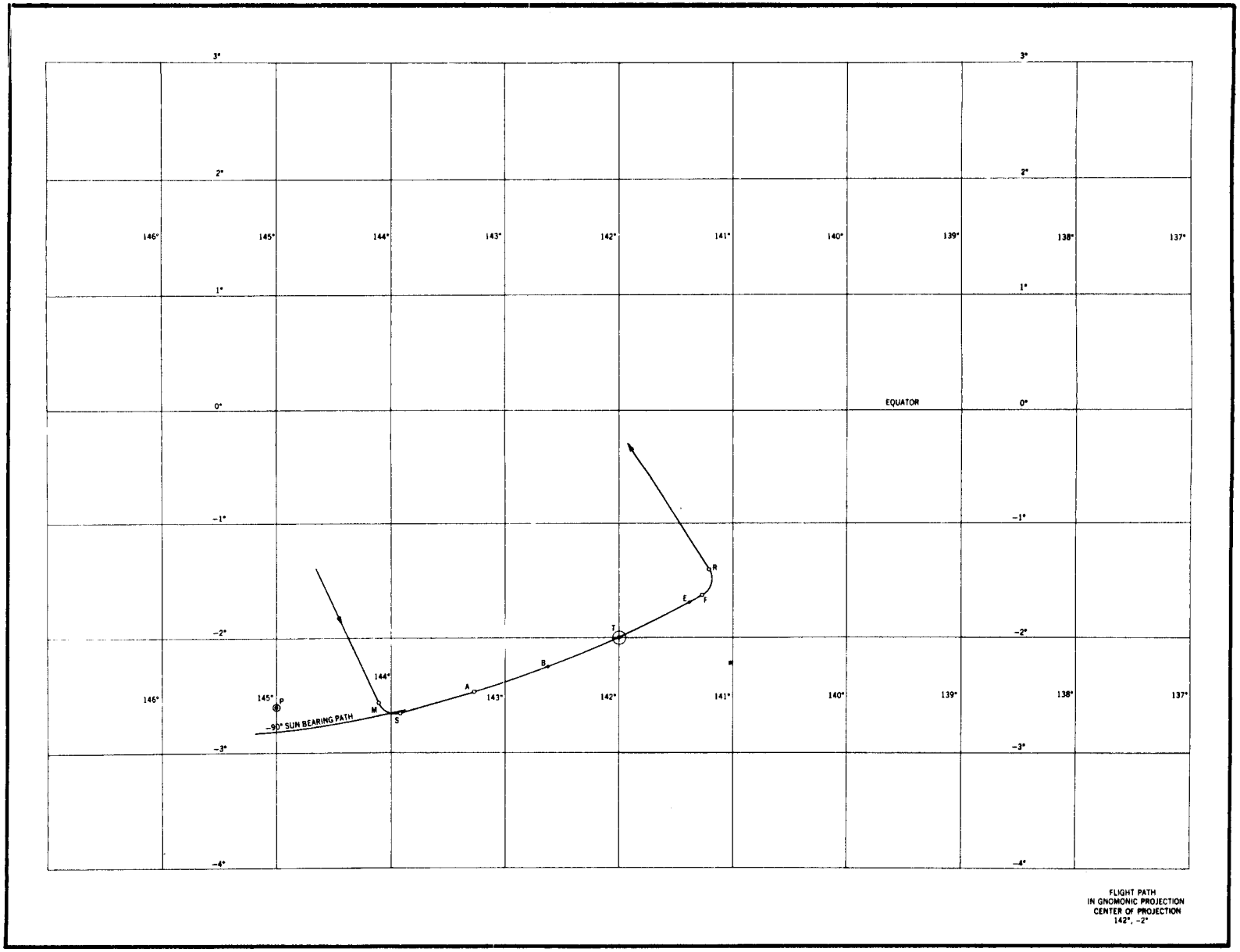

Figure E-7. Flight Plan for Hilo Practice Flight, May 24, 1965

TABLE E-15

FLIGHT PLAN FOR PRACTICE FLIGHT FROM HILO
May 24, 1965

Point	Station	Longitude	Latitude	Universal time	Maneuver	Duration	Distance n. mi.
H	Hilo airport	$155^{\circ}10'$	$+19^{\circ}45'$				
M	Maneuver begins	$144^{\circ}07'$	$-2^{\circ}34'$	$21^{h}50^{m}46^{s}$	Outbound Great Circle course		1,490
S	Straight leg begins	$143^{\circ}55'$	$-2^{\circ}39'$	$21^{h}52^{m}30^{s}$	Left turn 20° bank	$1^{m}44^{s}$	14.2
A	Arc path begins	$143^{\circ}16'$	$-2^{\circ}28'$	$21^{h}57^{m}30^{s}$	Straight leg	$5^{m}00^{s}$	41.0
B	Begin observation	$142^{\circ}38'$	$-2^{\circ}15'$	$22^{h}02^{m}30^{s}$	Left turn $1/3^{\circ}$ bank	$5^{m}00^{s}$	41.0
T	Middle of observation	$142^{\circ}00'$	$-2^{\circ}00'$	$22^{h}07^{m}30^{s}$	Continue	$5^{m}00^{s}$	41.0
E	End observation	$141^{\circ}23'$	$-1^{\circ}42'$	$22^{h}12^{m}30^{s}$	Continue	$5^{m}00^{s}$	41.0
F	Finish intercept run	$141^{\circ}17'$	$-1^{\circ}38'$	$22^{h}13^{m}30^{s}$	Continue	$1^{m}00^{s}$	8.2
R	Return leg begins	$141^{\circ}13'$	$-1^{\circ}24'$	$22^{h}15^{m}22^{s}$	Left turn 20° bank	$1^{m}52^{s}$	15.3
H	Hilo airport	$155^{\circ}10'$	$+19^{\circ}45'$		Return trip Great Circle course		1,512
						Total	3,203.7

APPENDIX E

TABLE E-16

HEADING ANGLES FOR FLIGHT PATH OF MAY 24, 1965

Point	Heading Angle
S	$78^{\circ}.452$
A	$74^{\circ}.142$
B	$69^{\circ}.960$
T	$65^{\circ}.931$
E	$62^{\circ}.075$
F	$61^{\circ}.326$

TABLE E-17

SUN ELEVATION HISTORY FOR MAY 24, 1965 PRACTICE FLIGHT

Point	Elevation Angle to Sun
S	$65^{\circ}.99$
A	$65^{\circ}.80$
B	$65^{\circ}.41$
T	$64^{\circ}.87$
E	$64^{\circ}.32$
F	$64^{\circ}.21$

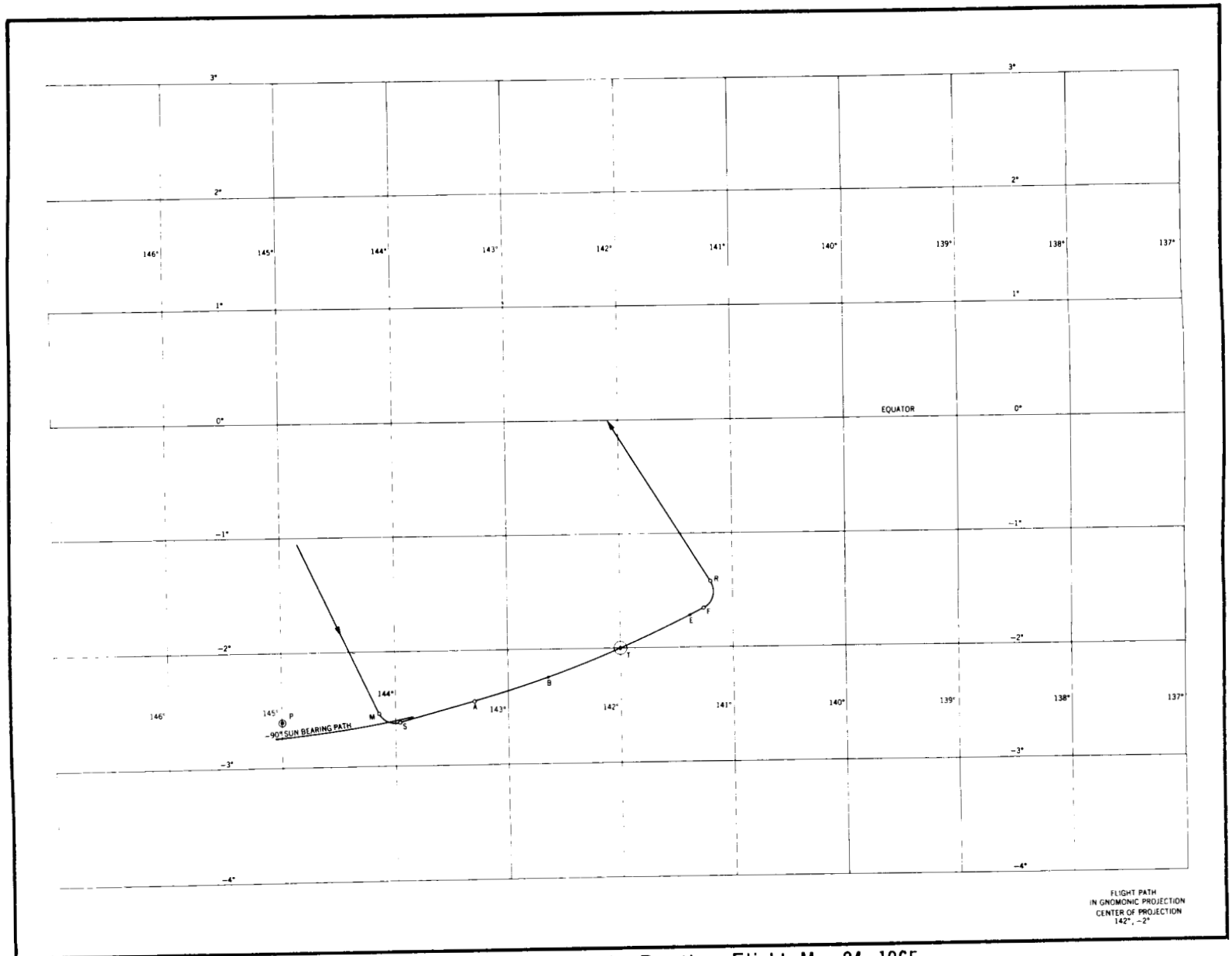

Figure E-8. Flight Plan for Hilo Practice Flight, May 24, 1965

TABLE E-18

FLIGHT PLAN FOR PRACTICE FLIGHT FROM HILO
May 26, 1965

Point	Station	Longitude	Latitude	Universal time	Maneuver	Duration	Distance n. mi.
H	Hilo airport	$155^{\circ}10'$	$+19^{\circ}45'$				
M	Maneuver begins	$144^{\circ}08'$	$-2^{\circ}32'$	$21^{h}48^{m}24^{s}$	Outbound Great Circle course		1,487
S	Straight leg begins	$144^{\circ}03'$	$-2^{\circ}37'$	$21^{h}50^{m}00^{s}$	Left turn 20° bank	$1^{m}36^{s}$	13.1
A	Arc path begins	$143^{\circ}18'$	$-2^{\circ}27'$	$21^{h}55^{m}00^{s}$	Straight leg	$5^{m}00^{s}$	41.0
B	Begin observation	$142^{\circ}38'$	$-2^{\circ}15'$	$21^{h}00^{m}00^{s}$	Left turn $1/3^{\circ}$ bank	$5^{m}00^{s}$	41.0
T	Middle of observation	$142^{\circ}00'$	$-2^{\circ}00'$	$22^{h}05^{m}00^{s}$	Continue	$5^{m}00^{s}$	41.0
E	End observation	$141^{\circ}23'$	$-1^{\circ}43'$	$22^{h}10^{m}00^{s}$	Continue	$5^{m}00^{s}$	41.0
F	Finish intercept run	$141^{\circ}16'$	$-1^{\circ}39'$	$22^{h}11^{m}00^{s}$	Continue	$1^{m}00^{s}$	8.2
R	Return leg begins	$141^{\circ}12'$	$-1^{\circ}25'$	$22^{h}12^{m}59^{s}$	Left turn 20° bank	$1^{m}59^{s}$	16.2
H	Hilo airport	$155^{\circ}10'$	$+19^{\circ}45'$		Return trip Great Circle course		1,513
						Total	3,201.5

APPENDIX E

TABLE E-19

HEADING ANGLES FOR FLIGHT PATH OF MAY 26, 1965

Point	Heading angle
S	$79^{\circ}.787$
A	$75^{\circ}.500$
B	$71^{\circ}.330$
T	$67^{\circ}.301$
E	$63^{\circ}.435$
F	$62^{\circ}.683$

TABLE E-20

SUN ELEVATION HISTORY FOR MAY 26 PRACTICE FLIGHT

Point	Elevation angle to sun
S	$65^{\circ}.82$
A	$65^{\circ}.60$
B	$65^{\circ}.27$
T	$64^{\circ}.80$
E	$64^{\circ}.28$
F	$64^{\circ}.19$

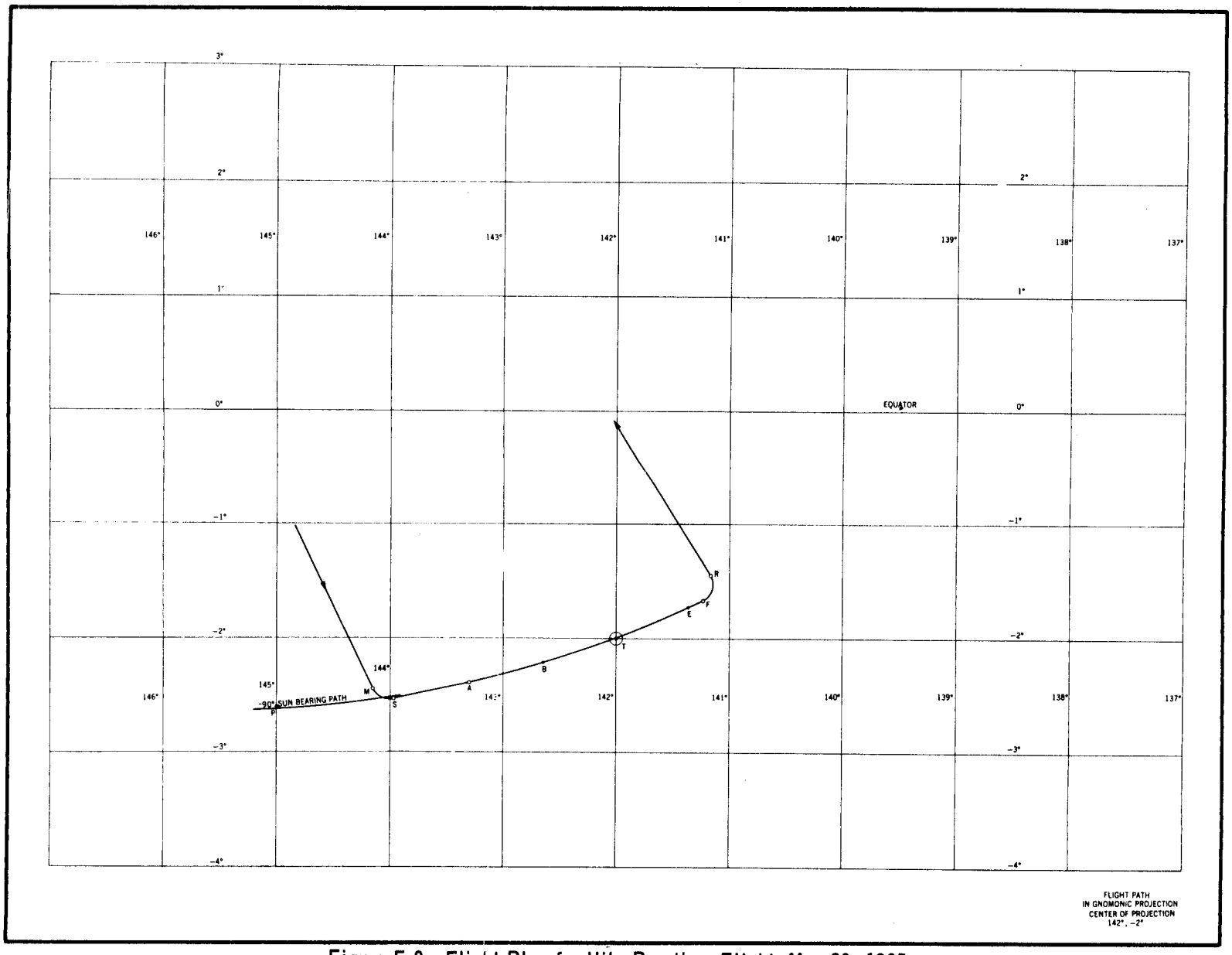

Figure E-9. Flight Plan for Hilo Practice Flight, May 28, 1965

TABLE E-21

FLIGHT PLAN FOR PRACTICE FLIGHT FROM HILO
May 28, 1965

Point	Station	Longitude	Latitude	Universal time	Maneuver	Duration	Distance n. mi.
H	Hilo airport	155°10'	+19°45'				
M	Maneuver begins	144°09'	-2°27'	$21^h45^m54^s$	Outbound Great Circle course		1,482
S	Straight leg begins	143°58'	-2°32'	$21^h47^m30^s$	Left turn 20° bank	1^m36^s	13.0
A	Arc path begins	143°18'	-2°23'	$21^h52^m30^s$	Straight leg	5^m00^s	41.0
B	Begin observation	142°39'	-2°13'	$21^h57^m30^s$	Left turn 1/3° bank	5^m00^s	41.0
T	Middle of observation	142°00'	-2°00'	$22^h02^m30^s$	Continue	5^m00^s	41.0
E	End observation	141°22'	-1°44'	$22^h07^m30^s$	Continue	5^m00^s	41.0
F	Finish intercept run	141°15'	-1°41'	$22^h08^m30^s$	Continue	1^m00^s	8.2
R	Return leg begins	141°10'	-1°27	$22^h10^m26^s$	Left turn 20° bank	1^m58^s	15.8
H	Hilo airport	155°10'	+19°45'		Return trip Great Circle Course		1,516
						Total	3,199.0

APPENDIX E

TABLE E-22

HEADING ANGLES FOR FLIGHT PATH OF MAY 28, 1965

Point	Heading angle
S	81.°826
A	77.°541
B	73.°355
T	69.°297
E	65.°390
F	64.°628

TABLE E-23

SUN ELEVATION HISTORY FOR MAY 28 PRACTICE FLIGHT

Point	Elevation angle to sun
S	65.°67
A	65.°52
B	65.°23
T	64.°75
E	64.°25
F	64.°16

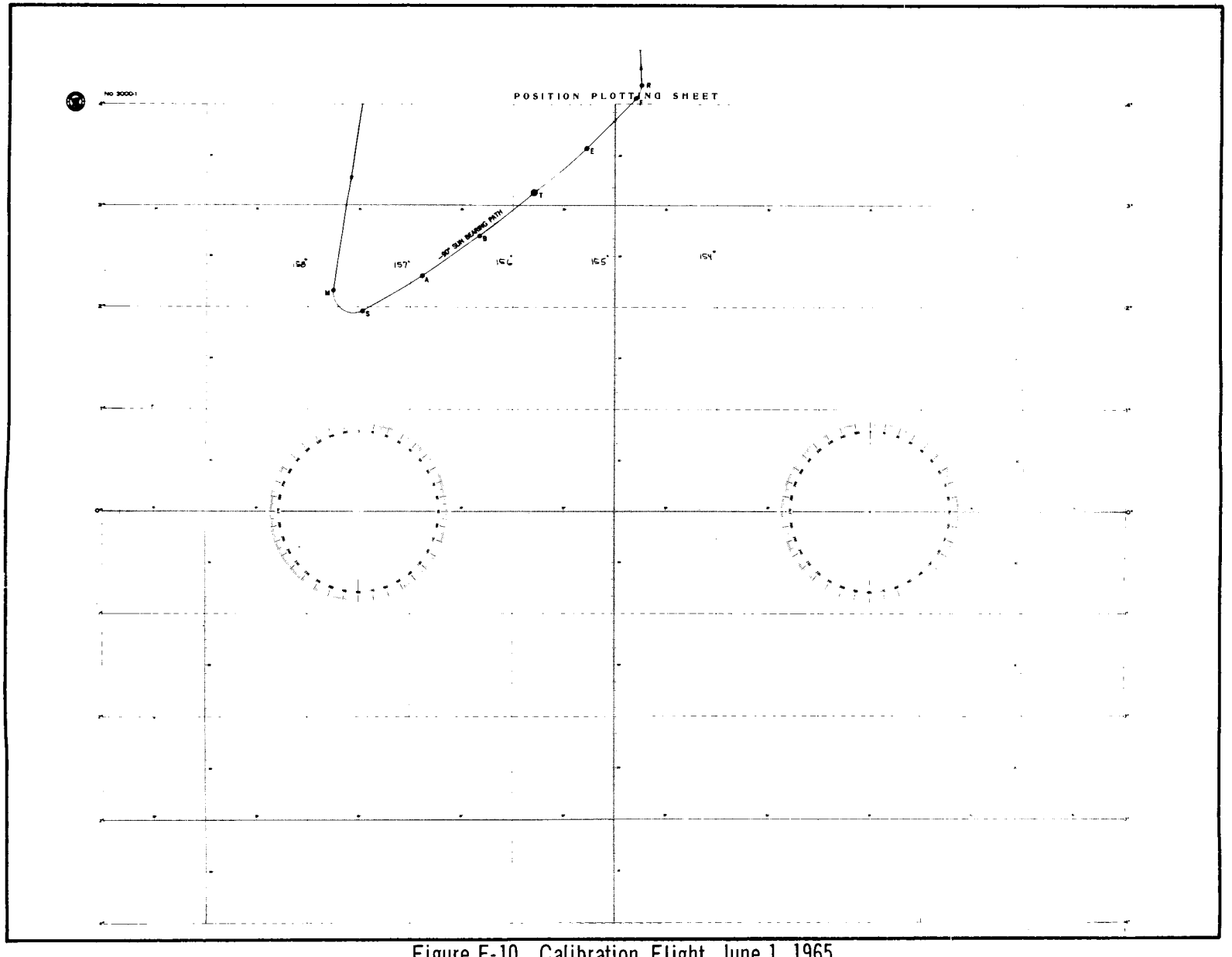

Figure E-10. Calibration Flight, June 1, 1965

TABLE E-24

FLIGHT PLAN FOR CALIBRATION FLIGHT FROM HILO
June 1, 1965

Point	Station	Longitude	Latitude	Universal time
S	Christmas Island - straight leg begins	$157^{\circ}28.2'$	$1^{\circ}57.8'$	$23^{h}15^{m}00^{s}$
A	Arc path begins	$156^{\circ}53.1'$	$2^{\circ}18.7'$	$23^{h}20^{m}00^{s}$
B	Begin observation	$156^{\circ}19.5'$	$2^{\circ}41.9'$	$23^{h}25^{m}00^{s}$
T	Middle of observation	$155^{\circ}47.4'$	$3^{\circ}07.2'$	$23^{h}30^{m}00^{s}$
E	End of observation	$155^{\circ}16.8'$	$3^{\circ}34.3'$	$23^{h}35^{m}00^{s}$
F	Finish intercept run	$154^{\circ}47.8'$	$4^{\circ}03.1'$	$23^{h}40^{m}00^{s}$

APPENDIX F

INSTRUMENT ORIENTATION IN THE AIRCRAFT

Since the slueing range of the astronomical instruments was greatly restricted, it was important for the instruments to be properly aligned with the floor of the aircraft so the sun, when 90° abeam, would appear in the center of the field of view of the instrument. The nonlevel flight attitude required that the instrumental pointing direction differ from perpendicular to the aircraft longitudinal axis at an elevation angle of 64 .7 from the floor plane. To maintain 37,000 ft altitude at about 490 knots ground speed, the angle of attack (or pitch angle) of the CV990 aircraft is about +2° (i.e., nose up).

Figure F-1 illustrates the instrument orientation problem, in which the aircraft is flying in the negative Y-direction. Z represents the direction of the local vertical (or zenith) and the XY plane is parallel to the local horizon plane. In this system, the sun appears in space at coordinates (X_O, Y_O, Z_O) lying at unit distance from the origin, where the observer's instrument is located. Since the aircraft flies at an angle of attack, i, its floor plane, $\overline{X}\overline{Y}$, and vertical axis, $\overline{Z}$, are not coincident with the true horizontal plane and vertical, respectively. Neglecting the coupling effects of roll resulting from the coordinated turn required for the observation run, the correct instrument orientation may be determined by considering the effect on target bearing and elevation angle of a single rotation, i.e., about the X-axis. Therefore

$$\overline{X} = X$$

$$\overline{Y} = Y \cos i - Z \sin i$$

$$\overline{Z} = Y \sin i + Z \cos i$$

In particular, since the sun appears 90° abeam in the XYZ system, $Y_O = O$; hence

$$\overline{X}_O = X_O$$

$$\overline{Y}_O = -Z_O \sin i$$

$$\overline{Z}_O = Z_O \cos i$$

Note that $Z_O/X_O = \tan \epsilon$, where ϵ is the solar elevation angle in the XYZ system; then

$$\tan \psi = \frac{\overline{Y}_O}{\overline{X}_O} = \frac{-Z_O \sin i}{X_O} = -\tan \epsilon \sin i$$

so that ψ = ARCTAN (-tan ϵ sin i) is the angular shift in the sun's bearing, measured from the port direction. A positive angle of attack yields a negative azimuth shift, i.e., clockwise toward the nose of the aircraft. With $\epsilon = 65°$ and $i = +2°$, $\psi = -4.0$. The rigidly mounted astronomical telescopes

and cameras carried by the CV 990 aircraft were preslued by this latter amount upon installation.

The elevation angle ϵ of the sun in the $\bar{X}\bar{Y}\bar{Z}$ system is not equal to ϵ, but is given by

$$\epsilon' = \text{ARCTAN}\left[\frac{\bar{Z}_O}{\sqrt{\bar{X}_O^2 + \bar{Y}_O^2}}\right]$$

$$= \text{ARCTAN}\left[\frac{\tan \epsilon \cos i}{\sqrt{1 + \tan^2 \epsilon \sin^2 i}}\right]$$

This formula shows that for small pitch angles, ϵ' differs very little from ϵ. Inserting E = 65°.0 and i = +2°.0, ϵ' = 64° .9 is obtained; the difference from ϵ is negligible.

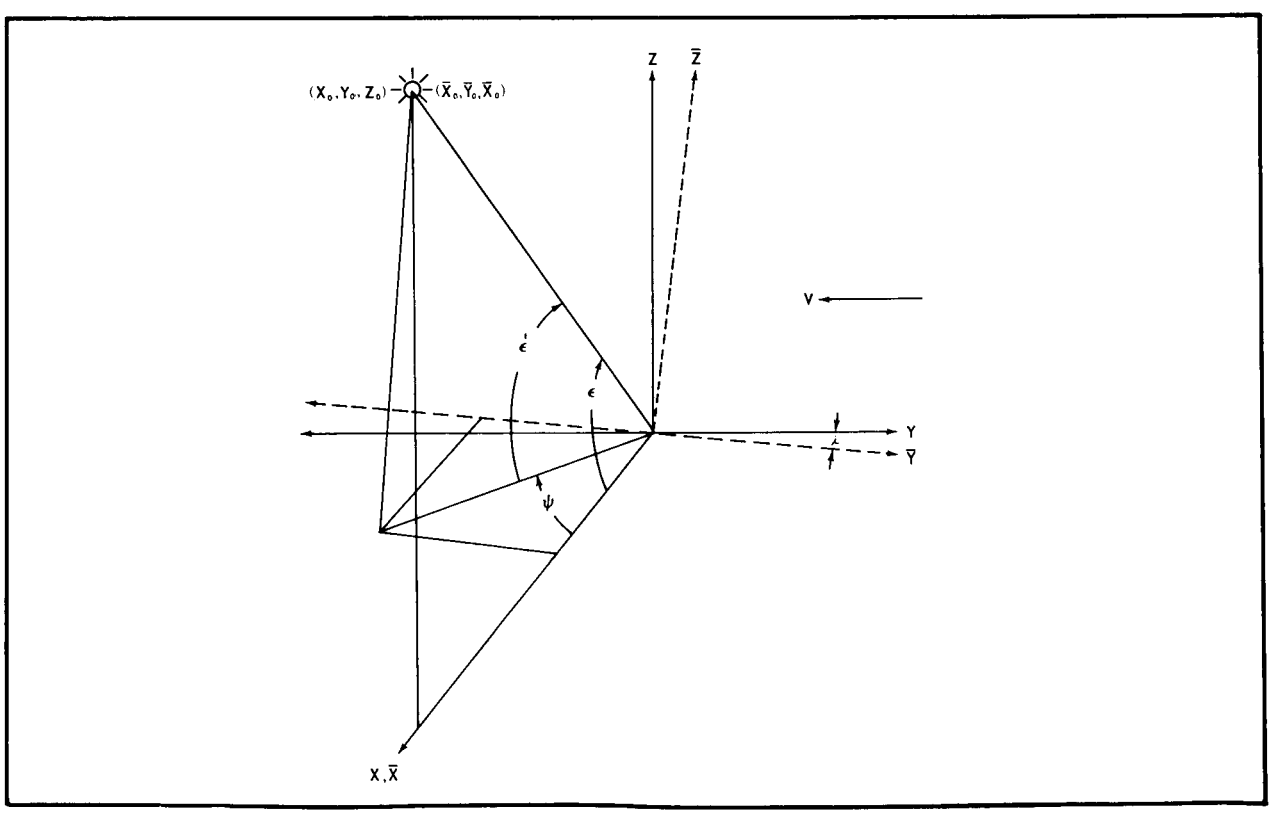

Figure F-1. Sun Elevation and Azimuth Change with Aircraft Pitch

APPENDIX G

DEFINITION OF TERMINOLOGY

Gimbal

A gimbal has been defined (ref. 15) as a mechanical frame containing two mutually perpendicular intersecting axes of rotation. It should be added that rotating the frame about one axis, called the outer axis, changes the position or direction of the other axis of rotation, called the inner axis.

Gyro

The term gyro is synonymous with gyroscope. For the purpose of this report, a gyroscope is a device which utilizes the angular momentum of a spinning rotor to sense angular motion of its case about one or more axes orthogonal to the spin axis. These gyros may be defined as devices, which, when rotated about a specified axis, provide an electrical signal whose amplitude is proportional to the angle through which they are rotated (rate-integrating gyro).

Gyro-Sensing

Gyro-sensing is defined as detecting motion through use of gyroscopes.

Heliostat

A heliostat has been defined (ref. 16) as an arrangement of mirrors driven automatically and used to reflect a beam of sunlight on a fixed direction as the sun appears to move across the sky. The heliostat described in this report is defined as a mirror mounted on a gimbal which can be driven automatically and used to reflect a beam of sunlight in a given direction with reference to a specified coordinate system (that of the aircraft) as the sun appears to move about in the sky. The overall system, including the mirror mounted on the gimbal, the servomotors which rotate the mirror about the gimbal axes, the gyros which sense motion about the gimbal axes, the electronics and controls which make possible the automatic or normal mode of operation, is called a heliostatic system.

APPENDIX G

Platform

A reference surface of table mounted on a gimbal or set of gimbals, which, through the use of gyros and servos, may be made to maintain an orientation in space.

Servo

Servo is an abbreviation for servomechanism. A servomechanism is an automatic control system employing feedback to cause an output to follow an input. Input and outputs may be such as shaft positions or rates, voltages or currents, temperatures, energy levels, etc.

Compensation

The process of introducing additional equipment into a system to improve the system performance.

Bode Plot

A graph of decibel gain and phase shift as a function of frequency. This plot graphically represents the particular equation of the servoloop-transfer junction.

Autostabilization

The physical characteristic, implied by Newton's Laws, is that a mass has the quality of inertia and, therefore, tends to remain fixed in inertial space, independent of other considerations.

Servoloop Type

A classification of servoloops is inferred from the loop equation. The type number indicates the number of integrators in the open loop-transfer function and implies the accuracy of the system that the equation defines.

APPENDIX H

HELIOSTATIC SYSTEM BLOCK DIAGRAMS

This appendix contains a brief explanation of the analog block diagrams of the heliostatic system. As stated previously in the text, a Type III servoloop was utilized for the heliostatic system; as is implied by the term Type III, there are three integration terms in the open loop-transfer function. Physically, this means that for a linearized system the output follows the input with zero steady-state error for a constant position, velocity, or acceleration input.

Figure H-1 diagrams the entire outer axis control system. Although the motor-back EMF was reduced to a negligible value in the actual system, the characteristic was retained in the block diagrams to illustrate the importance of its reduction. The electromechanical system, neglecting all velocity feedback, is represented in the loop containing the gyro, which senses the error from the reference; the electronics, which amplifies and shapes the error signal; and the motor, which provides the torque to move the gyro to null output. This loop is only disturbed by friction torque and motor-back EMF torque, which are generated by the relative motion of the motor stator and rector, $\Delta\dot{\theta}$. These torques are algebraically summed with the motor output torque, which results in an error producing torque, T_e. This torque causes the outer axis to accelerate. This acceleration, $\ddot{\theta}_M$, is operated on by two integraters to move the gyro. The motor rate, $\dot{\theta}_M$, is summed with the aircraft rate, $\dot{\theta}_{Aircraft}$, to yield $\Delta\dot{\theta}$, the relative rate between motor rotor and stator. It can be seen that if the friction and back EMF torques were reduced to zero, the outer axis would remain fixed in space as a result of autostabilization.

Figure H-2, the inner axis block diagram, illustrates the similarities of the inner and outer axis systems. The mirror must rotate half as much about its inner axis as the airplane moves in that axis. To accomplish this, the mirror is driven through half the angle necessary to maintain the gyro output of null. Because the mirror is then required to move in inertial space, its motions are directly dependent on the aircraft motions, as shown on the diagram. The additional loop containing the gyro and amount inertia, I_{GP}, may be combined with the inner axis inertia, I_{IA}, to form an equivalent inertia equal to $I_{IA} + 4\,I_{GP}$. Calculations show that $4\,I_{GP}$ was less than 4% of I_{IA} and can, for most purposes, be neglected. For stability studies, therefore, the inner and outer axis loops can be considered identical if the difference in loop gain, caused by different values of inertial loads and gearing mechanical gain, are taken into account. In the physical design, this difference in gain was equalized in the shaping network. Stability studies for inner and outer axis loops, as well as response studies for the inner axis loop, were conducted using analog computing equipment.

Details of these studies are presented in Douglas Report SM-48335 (ref. 2).

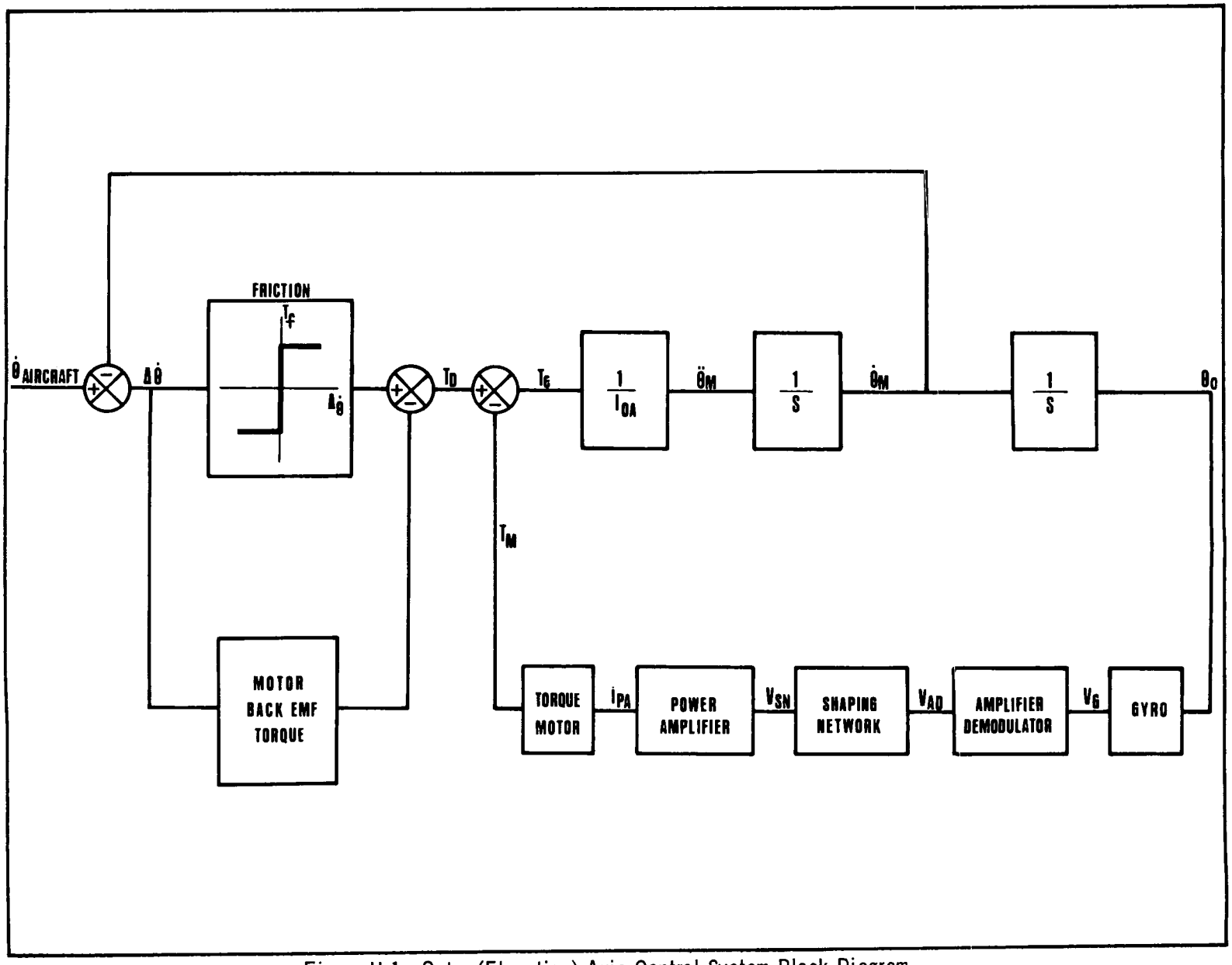

Figure H-1. Outer (Elevation) Axis Control System Block Diagram

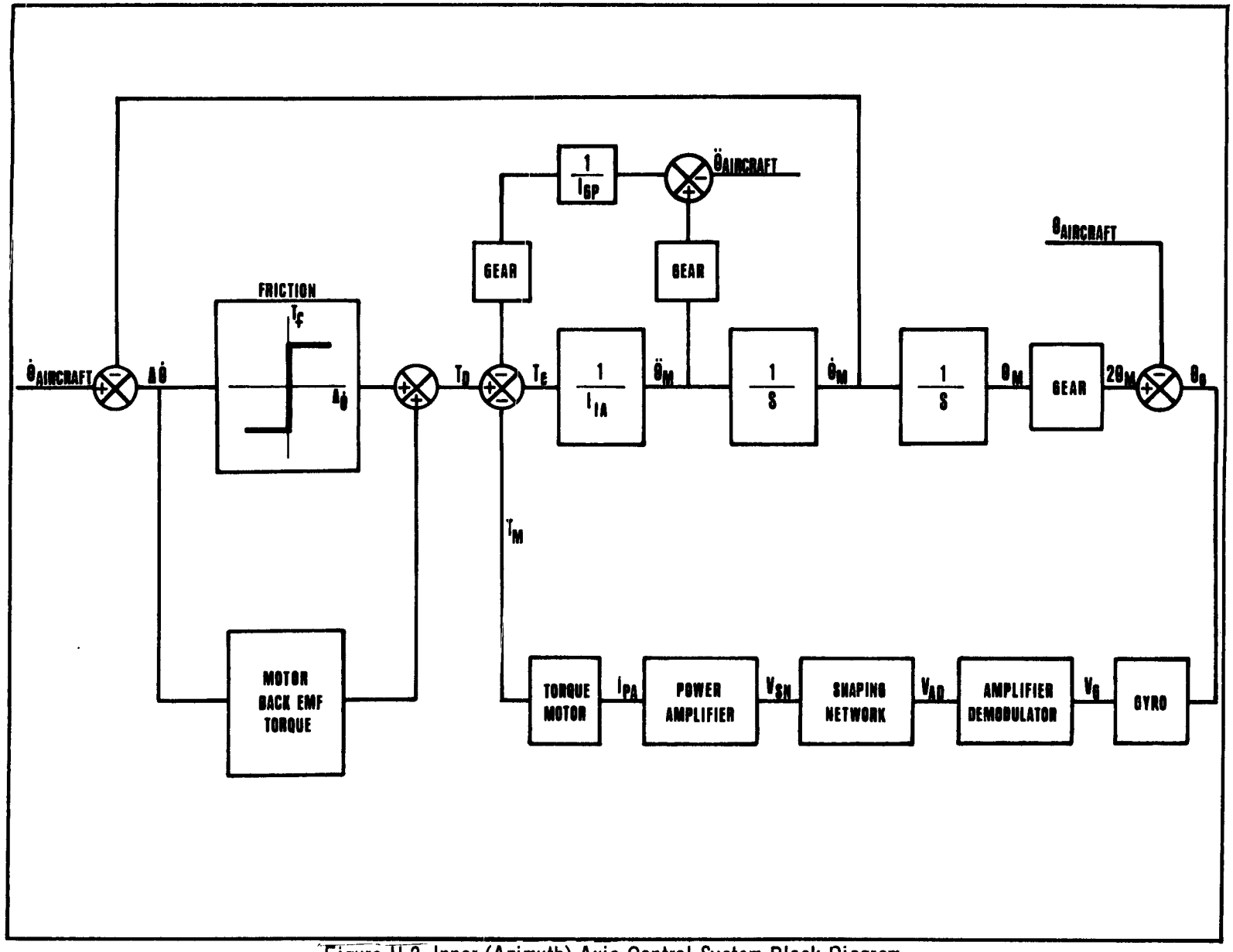

Figure H-2. Inner (Azimuth) Axis Control System Block Diagram

APPENDIX I

ASSEMBLY AND OPERATIONAL PROCEDURES

Mechanical Assembly

The gimbal was assembled in a clean-room environment; special care was taken in the assembly of the torque motors. Further information on torque motor handling and installation is treated in Appendix K.

The torque on the main nuts fixing the motor rotors to their shafts should be 50 to 60 lb-ft. The small nut on the shaft in the outer axis housing should be adjusted to remove all end play from the shaft, but should not preload the two bearings. This adjusts both bearings for proper angular contact of the balls and race. With this nut in place, the small locknut may be torqued to from 10 to 20 lb-ft.

The steel band used on the inner axis mirror to gyro drive is spliced by cementing the ends together with PM1000 (DPM 2999 Specification 1P20033) or AF32 (DPM 2132 Specification 9020211).

The band is positioned so that in normal operation the splice remains on the large pulley to maintain constant tension over a wide angle. Tension in the band is adjusted by holding the six mounting bolts in the gyro mount housing snug and then tightening the adjusting bolt. When the band is first taut, the relative position of the gyro mount housing to the flat mounting surface can be marked. The adjusting belt should then be adjusted to move the gyro mount housing 0.020 to 0.030 in. from the other pulley shaft. The six lock bolts can be tightened.

The heliostat assembly may be transported in any attitude, but preferably with its outer axis vertical because this position reduces the cantilever loads on the outer axis bearings. The carrying rack must be shock mounted for transportation to reduce shocks which may cause brinelling of the bearing races.

Equipment Operation (Electrical)

Connect the equipment cables. Determine that all switches on the power chassis (fig. I-1) are in the off position and that the control unit cage-uncage switch is in the cage position.

Apply 115 V rms, 400 cycle, single phase sinusoidal power with a capacity of 600 W to TP1 on the power chassis. Turn ac power and heaters switches on. The red indicator lights above these switches should go on, as should the azimuth heat and elevation heat amber lights on the control chassis.

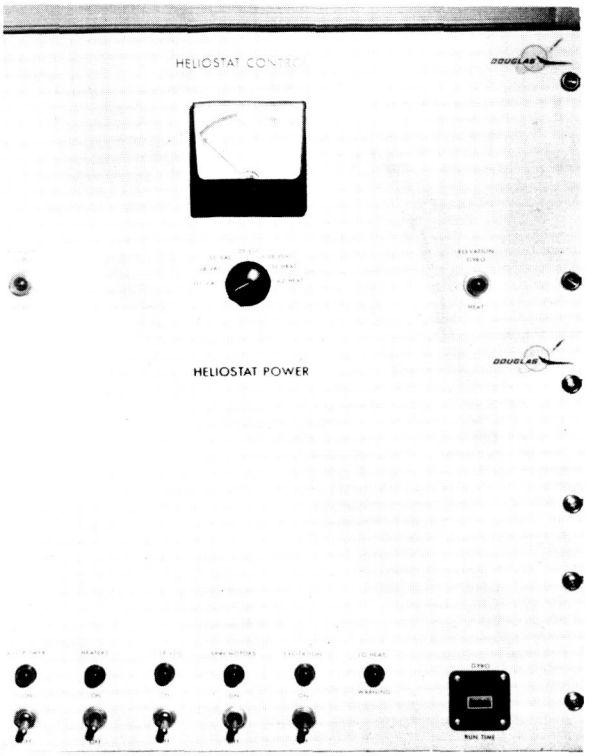

Figure I-1. Heliostat Electronics Panel

APPENDIX I

The meter on the control chassis should indicate in the small black region for the 115 Vac, elevation heat and azimuth heat positions of the meter switch. For other switch positions, the meter should indicate nothing.

The heater switch activates a 180-sec time delay that prevents the accidental starting of the gyro spin motors while they are cold. A warning is given by the lo heat warning light, which, under proper operating procedures, should not be on. Turn off all switches if the lo heat light is on.

For ambient temperature 70°F, the gyros normally attain operating temperature in 10 min. This condition is verified when the meter indicates a reading in the large black region for the azimuth heat and elevation heat switch positions.

When this condition is reached, the 28 Vdc switch and the spin motors switch may be turned on. Their associated indicator lights should go on, and the 26 Vac position of the meter switch should cause a meter indication in the small black region.

The gyro spin motors will normally reach full speed in 30 sec. Switch excitation on. The meter should read in the small black region for the 115, 26, 10, +28, and -28 Vdc switch positions and in the large black region for the elevation heat and azimuth heat switch positions.

Remove the mechanical locks from the gimbal axes of the heliostat and set the gimbal free of the mechanical stops. Move the cage-uncage switch on the control unit to uncage. Both system loops are now closed, and light finger torque applied to either axis should indicate the fixity of the axis. If too much torque is applied, the system loop tends to command full power and will drive the heliostat into the mechanical stop. This may necessitate caging the gyros momentarily to move the heliostat from the stop and then uncaging the gyros.

Each axis may be controlled by slueing its associated gyro. Three rate modes are available: (1) fixed fast, (2) variable medium, and (3) variable slow. These modes are selected by the heat-slow switch on the control unit. The slue rates may vary from 2.4 deg/sec to 3.3 deg/sec. The axes are slued by the manipulation of the control unit lever switches.

To correct for drift, each gyro may be trimmed by adjusting the trim potentiometers on the control unit. Trim rates are variable from 0 to 40 deg/hr in either direction.

APPENDIX I

Caution: When turning the heliostat system off, cage must be switched to first; then turn off the excitation, the spin motors, the 28 Vdc, the heaters, and the ac power switches, in that order.

Secure the gimbal axes with the mechanical locks.

The gyro run-time indicator shows the cummulative time that the spin motor power is on; this time must be applied to the individual gyros mounted on the assembly. A run-time chart is included in Appendix K.

APPENDIX J

ELECTRONIC/ELECTRICAL COMPONENT SELECTION

This appendix contains a brief description of the components that were selected or designed to match the requirements specified in the analytical study of the servoloop.

Servo Power Amplifier

The power amplifier is a complementary-symmetry, direct coupled, solid-state amplifier designed and built by Douglas. The amplifier is applied as a current source to the torque motor and capable of 75W maximum continuous output power. The input impedance is 9,000 ohms and the output impedance is 8,000 ohms.

Operational Amplifier

The operational amplifier is a Zeltex-supplied component of air solid-state design and utilized as the shaping amplifier in each of the servoloops of the system. Further information is available in Appendix K.

Amplifier Demodulator

The amplifier demodulator amplifies and converts the modulated ac carrier signal from the gyro to a dc signal which is then connected to the shaping amplifier for electronic signal conditioning. Specifications on components supplied by Natel Engineering are available in Appendix K.

DC to AC Inverter

An inverter provides ac power of the proper frequency and amplitude from a dc power source. Two Natel Engineering inverters are utilized in the heliostat system: one to provide excitation to the gyros and demodulators and one to provide gyro spin motor power.

APPENDIX J

DC Power Supply

Two dc power supplies built by Deltron, Inc. are used in the system. The power supplies are connected to provide positive and negative dc voltage and to provide power for the inverters, motors, and amplifiers in the system.

Torque Motor

The motors used to drive the two axes of the system are Inland direct drive dc torque motors. The motor is a high-torque, low-speed servo actuator integrated into the assembly housing. Specifications on the motors are in Appendix K.

Gyroscope

A Minneapolis Honeywell miniature-rate integrating gyro provides the inertial reference for each axis of the heliostat system. The device is a precision, high-performance, inertial grade gyro with single degree of freedom, floated gimbal construction.

Gyro Heater Control Amplifier

Each gyro is maintained at a constant temperature by a circuit consisting of a temperature sensitive bridge, a power amplifier, and heater coil built into the gyro. The amplifier, built by Magnetic Controls Company, contains two legs of the bridge and the power amplifier. Further explanation of the temperature control is given in Appendix K.

APPENDIX K

VENDOR LITERATURE

APPENDIX K

DIRECT DRIVE DC TORQUE MOTORS
INLAND MOTOR CORPORATION

Precautions in Motor Handling

Because a torque motor is designed to be applied as an integral part of other equipment, the manner in which it is assembled and shipped requires special handling other than that normally given conventional motors. Such precautions are necessary, because if the handling recommendations are not followed, motor performance can be substantially degraded.

Receiving Inspection. — Torque motors are, in most cases, frameless or semiframeless assemblies, and as such, should be handled carefully. They should be unpacked with great care, especially the brush-ring and commutator surface. Mechanical inspection of the parts for critical dimensions is performed at the factory before shipment. Should the customer require such inspection for any reason, precautions must be taken to avoid bending any of the brush springs, scratching the commutator surfaces, or scoring the mounting diameters. Also, DO NOT LOOSEN OR MOVE THE FLUX KEEPERS until installation, which is described later. If performance checkout is required, it should be restricted only to those tests described on the Inland test results form which accompanies each unit.

Torque motor parts are tested, assigned serial numbers, and are guaranteed only as matched sets. Performance guarantees are void if the parts are interchanged between motors. The motor parts should be transported in the original shipping package to protect them against shock and vibration.

Storage. — Containers and racks used for storage should be of nonmagnetic materials. Motor parts should be protected against exposure to, or contact with, small magnetic particles such as iron filings, chips, or dust. Such precautions are necessary because once the particles are attracted to the magnetic areas of the motor, the particles are very difficult to remove. In addition, if some of this material accidentally becomes lodged in or across the motor airgap, performance may be seriously degraded.

Storing motor parts exposed to normal factory ambient-temperature variations is acceptable. For extended storage, care must be taken to prevent corrosion. It is recommended that the parts be stored in a sealed plastic bag together with a bag of desiccant, suitable for protecting the motor against excessive humidity.

APPENDIX K

Installation

For frameless motors, such as those used on the heliostat, only one acceptable installation technique, described in the following steps, exists:

(1) Insert the PM field part into the housing cavity allocated for it DO NOT LOOSEN OR REMOVE THE KEEPER RING

(2) Install the motor within the field in its final position

(3) Remove the keeper ring, using the jack screw

(4) Install the field mounting bolts

(5) Install the brush-ring, using its mounting bolts. While slipping the brushes over the commutater, do not bend the springs or scratch the commutator surface.

CHARACTERISTICS OF TORQUE MOTOR INLAND MOTOR CORPORATION TYPE T-2950A

The T-2950 motor is a frameless dc permanent magnet torque motor. It is shipped as three unmounted components--rotor, brush ring, and permanent magnet field. When installed, the structure with which the circumferentially oriented field is in direct contact must be nonmagnetic. The rotor-to-field eccentricity should not exceed 0.004 in. (See installation section for detailed installation instructions and specific precautions.) Brush life will normally exceed 10^7 rev. Rotor hubs and field adapters are supplied to customer specifications.

Peak Torque	1.2 lb-ft
Damping coefficient (zero impedance source)	25×10^{-3} lb-ft/rad/sec
Damping coefficient (infinite impedance source)	0.8×10^{-3} lb-ft/rad/sec
Motor friction torque	17×10^{-3} lb-ft
Ripple torque, average to peak	5%
Ripple cycles/revolution	41 cycles/rev.
Ultimate temperature rise/rms watt	2.5° C
Maximum permissible winding temperature	105° C
Rotor moment of inertia	0.32×10^{-3} lb-ft-sec^2
Max. theoretical acceleration	3.8×10^3 rad/sec^2
Max. no-load speed	48 rad/sec
Motor weight	2.0 lb
DC resistance (25° C)	7.5 ohms
Volts at peak torque (35° C)	24.4 V

Amperes at peak torque	3.25 A
Torque sensitivity	0.37 lb-ft/A
Back EMF	0.50 V/rad/sec
Inductance	16×10^{-3} H

PROPORTIONAL AMPLIFIER
MAGNETIC CONTROLS COMPANY
MODEL PA48B-1

The PA48B-1 Proportional Amplifier is designed to provide temperature control. The amplifier senses small changes in temperature by a resistance-type sensing element within a bridge circuit and supplies heater power in an amount proportional to the deviation from the desired control temperature.

The amplifier utilizes an unbalance signal from a resistance bridge, two legs which are contained within the amplifier case. The third leg, or control point adjusts resistance, and determines the sensing element resistance (fourth leg) at which the bridge will balance. The fourth leg is the high-temperature coefficient sensing element resistance. When the system is initially energized, the low temperature results in a low resistance of the sensing element causing a large unbalance of the bridge. The unbalance signal is sufficient to saturate the amplifier, resulting in delivery of maximum output power. Maximum output power delivery is maximum output power. Maximum output power delivery is maintained until the device being controlled approaches its operating temperature (balance-bridge condition). Once in this temperature range, the amplifier becomes a high-gain device and supplies power in an amount proportional to the deviation from the control temperature. The output is continually modified by the control point reset function, thereby providing optimum system performance.

The amplifier is designed to control temperature within 0.1°C under worst-on-worst combinations of input and environment.

The device contains two legs of a wheatstone bridge circuit. These legs are 780 ohms each. An internal Zener regulated bridge supply of 16 ± 10% V dc is provided for bridge excitation. This will result in a nominal sensing element current of 10.3 ma through a 780 ohm sensing element. The device will operate with sensing elements in the range of 300 to 3,000 ohms whose resistance is beyond this range. This resistance of the reference resistor is equal to the resistance of the sensing element at the control temperature. For sensing element resistances greater than the reference resistance, the output power is less than 1 W.

Under nominal conditions of voltage, frequency, and temperature the PA48B-1 Proportional Amplifier is capable of providing 85 W to a 13 ohm resistive load. The device will provide at least 105 V rms to a resistive load in the range of 100 to 500 ohms at 115 V rms line voltage.

APPENDIX K

The unit operates from 115 V ±10%, 400 cps 5%, single-phase ac power source.

Pin Assignment

Pin 1	115 V, 400 cps (Lo) and Heater	Pin 4	Heater
Pin 2	115 V, 400 cps (Hi)	Pin 5	Sensing element and reference resistor
Pin 3	Sensing element	Pin 6	Reference resistor

OPERATIONAL AMPLIFIER
ZELTEX INCORPORATED
MODEL 140-M20

Description

The Zeltex Model 140 Amplifier is a general purpose amplifier employing a solid-state chopper with internal chopper drive. It features low-drift and fast-output voltage response with a selection of output current capabilities. The amplifier may be used in production checkout systems with predictable performance because it was designed to withstand heavy capacitive loading.

The amplifier is supplied in open loop form on a small glass epoxy-etched circuit card with mating connector. A multiturn balance potentiometer is located on the amplifier card. All units are short-circuit proof.

Voltage gain	10^6 at dc
Frequency response	100 kc at unity gain. Gain bandwith product is 100 kc with feedback impedance of 100 k ohm or less. Gain roll off is 6 db/octave
Input impedance	500 K ohm at dc
Output voltage range	±20 V
Output current	4 ma at ±20 V 20 ma at ±10 V
Voltage stability	Offset adjustable to zero with potentiometer. Input drift is 5 μV/°C and 50 μV/8 hrs at constant temperature

Current stability	Offset less than 2×10^{-10} A with temperature coefficient of less than 10^{-11} A/°C
Noise	5 mv peak at input, 2 cps to 50 kc
Slewing rate	12 V/ sec max. rate of output voltage
Temperature range	0°C to +50°C, operating -55°C to +85°C, storage
Power requirements	28 Vdc
Size	3 in. wide by 4.5 in. long by 0.6 in. deep

AMPLIFIER DEMODULATOR
NATEL ENGINEERING COMPANY
MODEL D6156

Gain	200 ± 6 db adj.
Input impedance	500 k ohms
Output voltage	±40 Vdc
Load impedance	25 K ohm min.
Reference voltage	10 Vrms, 7,200 cps

INVERTER
NATAL ENGINEERING COMPANY
MODEL V10

Input voltage	28 Vdc ±10%
Output voltage	10 Vrms, 7,200 cps
Output power	10 W

APPENDIX K

INVERTER
NATAL ENGINEERING COMPANY
MODEL V30

Input voltage	28 Vdc ±10%
Output voltage	26 Vrms, 400 cps
Output power	30 W

DC POWER SUPPLY
DELTRON INCORPORATED
MODEL A 8-11

Output voltage	28 ± 2 Vdc adj.
Output current	11 A
Input voltage	105-125 Vrms
Input frequency	50-400 cps
Line regulation	0.01% or 1 mV
Load regulation	0.01% or 1 mV
Ripple and noise	500 μV max.
Recovery time	50 μ sec max.
Stability	0.01% or 5 mV
Operating temperature	71° C max.
Overload and short circuit	Precision linear shutdown circuit reduces voltage and current simultaneously for overload or short circuit with automatic recovery after overload is removed

APPENDIX K

TYPICAL CHARACTERISTICS OF HONEYWELL GG8001B7 MINIATURE INTEGRATING GYROS

Angular momentum	1×10^5 gm-cm^2/sec
Output axis damping coefficient	11,600 dyne cm sec
Output axis moment of inertia	95 gm-cm^2
Characteristics time	0.0088 sec
Gimbal freedom	±1.3
Input angular freedom	±0.15
Gyro transfer function*	182 V/rad
Gyro operating temperature	185° F
Pickoff sensitivity*	21.7 V/rad
Torquer sensitivity	85°/hr/ma
Maximum torquing rate	12,750°/hr
Heater voltage	115 V (ac or dc)
Heater power	40 W
Spin-motor voltage	26 V (Line-to-Line)
Spin-motor frequency	400 cps
Spin-motor phase	3
Heat-sensing resistance	1140 ± 1 ohm at 185°F
Heater resistance	330 ohm

*10.5 Vrms, 7,200 cps sig. gen. primary excitation.

APPENDIX K

SPIN MOTOR OPERATING TIME RECORD
HONEYWELL GYROSCOPE
GG8001B7

Serial No. G-2		Serial No. G-3	
Date	Operating Time (Hrs)	Date	Operating Time (Hrs)
1-25-63	135	2-4-63	130
3-11-63	4.9	4-22-63	16
3-12-63	8.0		
3-12-63	1.7		

APPENDIX L

SCHEMATICS

This appendix contains schematics of the electronic circuitry of the heliostatic system.

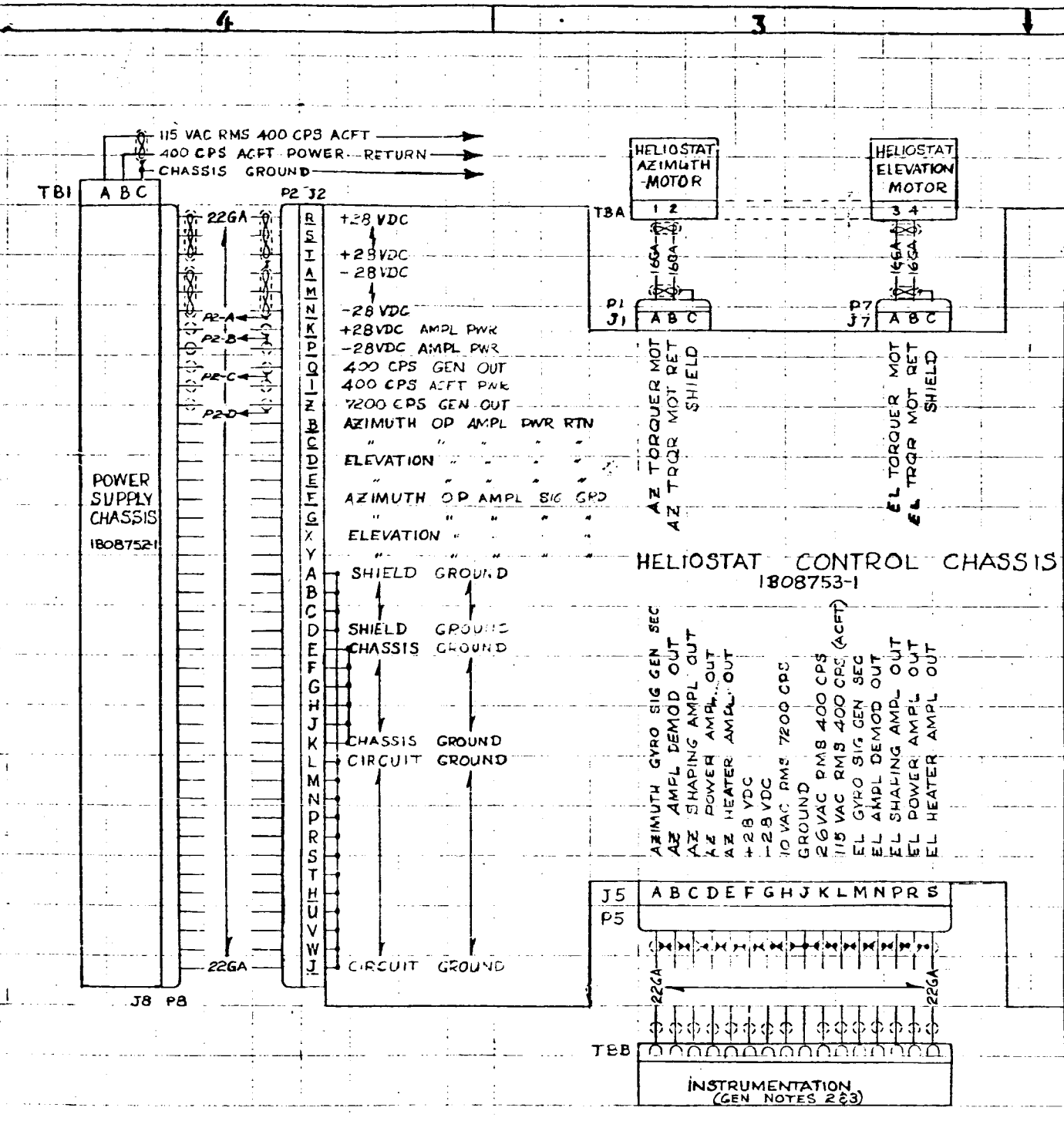

MATING CONNECTOR		INTERCONNECTING CABLE					MATING CONNECTOR	
JACK REF	JACK TYPE	PLUG REF	PLUG TYPE	CABLE FEET	PLUG TYPE	PLUG REF	JACK TYPE	JACK REF
J1	PT02SE-12-3S	P1	PT06SE-12-3P(SR)	60	N/A		N/A	TB1
J2	PT02SE-20-41P	P2	PT06SE-20-41S(SR)	1/2	PT06SE-20-41 PW(SR)	P8	PT06SE-20-41 SW	J8
J3	PT02SE-12-10P	P3	PT06SE-12-10P(SR)	25	PT06SE-12-10S(SR)	P3A	PT02SE-12-10P	J3A
J4	PT02SE-16-26PY	P4	PT06SE-16-26P(SR)	25	PT01SE-16-26SW(SR)	P4A	PT06SE-16-26PW	J4A
J5	PT02SE-4-19SX	P5	PT06SE-14-19P(SR)	3	N/A		N/A	TB6
J6	PT02SE-16-26SZ	P6	PT06SE-16-26P(SR)	20	PT01SE-16-26SW(SR)	P6A	PT06SE-16-26PW	J6A
J7	PT02SE-12-3SW	P7	PT06SE-12-3PW(SR)	30	N/A		N/A (SEE P1)	TB5

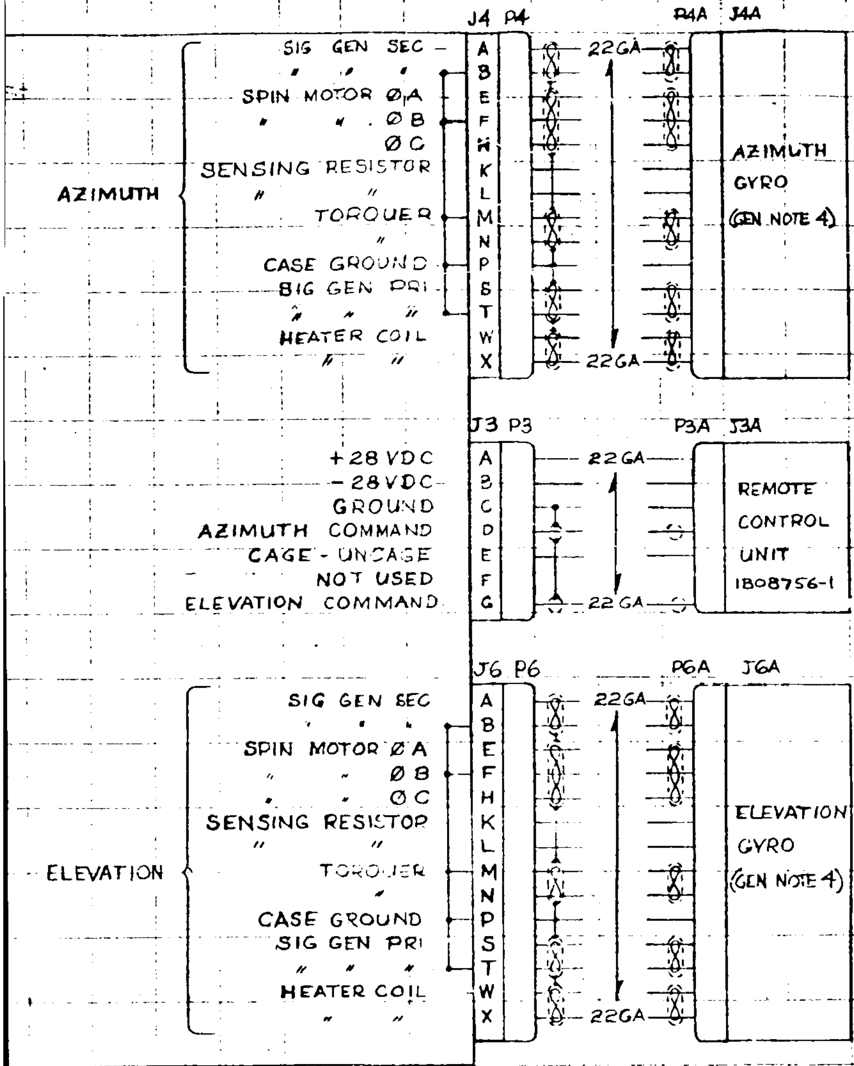

GENERAL NOTES:

1. FOR SCHEMATICS OF INDIVIDUAL CHASSIS SEE DWG AS FOLLOWS:
   1808752-1 POWER SUPPLY
   1808753-1 CONTROL CHASSIS
   1808754-1 SERVO MOTOR AMPL (PART OF 1808753-1)
   1808756-1 REMOTE CONTROL
2. ALL CABLING RUNS ARE PIN TO PIN EXCEPT AS OTHERWISE SPECIFIED.
3. SCHEMATIC OF INSTRUMENTATION AND ASSIGNMENT OF TERMINALS FOR TBB ARE DEPENDENT ON SYSTEM USE AND SHALL BE SPECIFIED IN APPROPRIATE SYSTEM OPERATION DOCUMENT.
4. GYROSCOPE AND MOTOR ASSEMBLIES SHALL BE DETERMINED BY SYSTEM USE. REFERENCE APPROPRIATE VENDOR SCHEMATICS & DWGS.

1808755

PART OR IDENTIFYING NO.	1808755
MATERIAL	FINISH
SEE ENGINEERING RECORDS FOR USAGE DATA	
UNLESS OTHERWISE SPECIFIED DIMENSIONS ARE IN INCHES. TOLERANCES FRACTIONS ± DECIMALS ± ANGLES ±	
DOUGLAS AIRCRAFT COMPANY, INC	SANTA MONICA, CALIFORNIA
TITLE	WIRING DIAGRAM, HELIOSTATIC SYSTEM
CODE IDENT NO	18355
SIZE	H
DWG NO	1808755
SCALE	
SHEET 1 OF	

154-2

DOUGLAS J808125

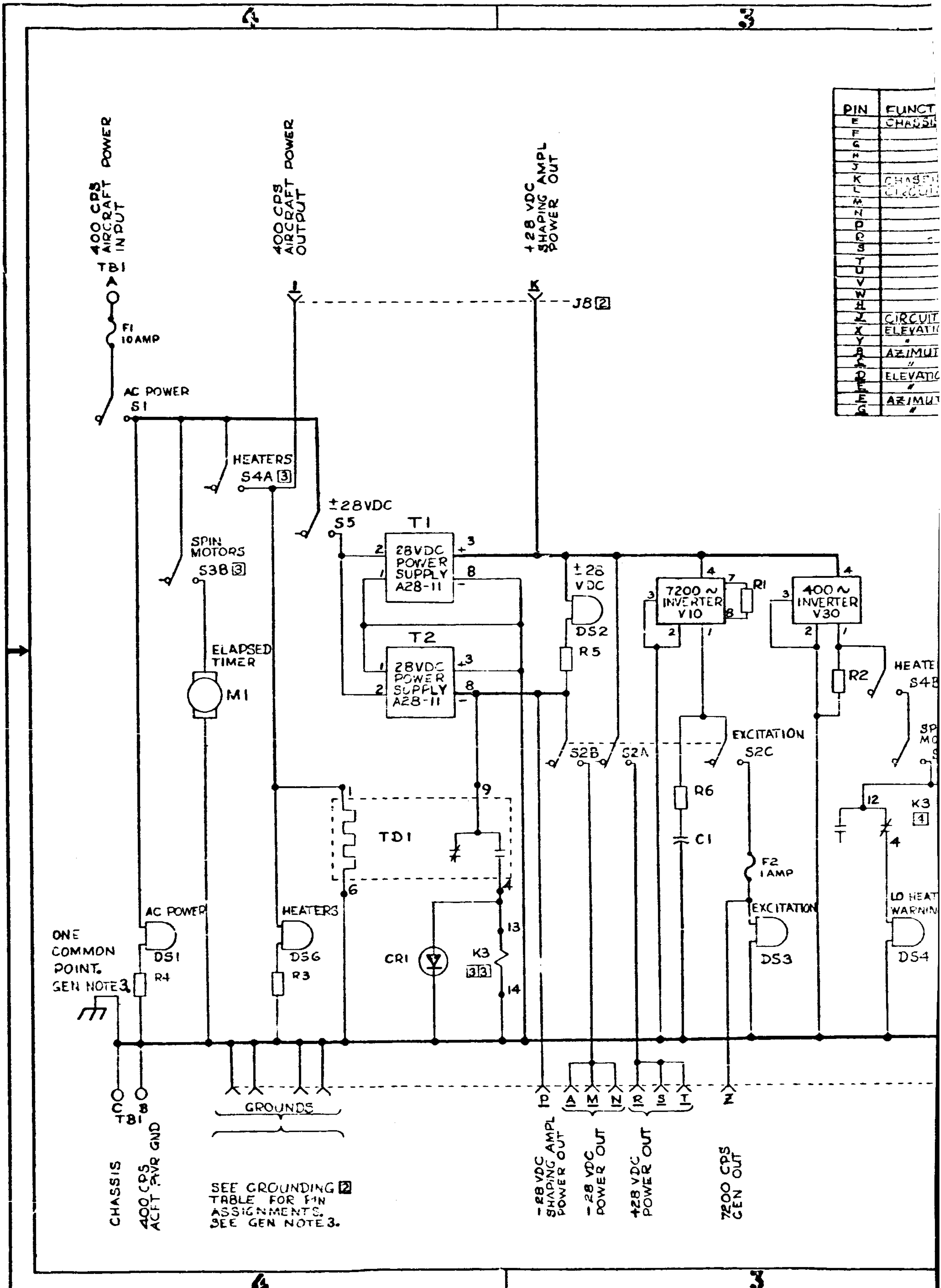

155-2

GROUNDING

...ION	WIRED COMMON
...S	
...S GROUND	
GROUND	
...N SHAPING AMPL SIGNAL GROUND	
...H SHAPING AMPL POWER GROUND	
...N SHAPING AMPL POWER GROUND	
...H SHAPING AMPL SIGNAL GROUND	

GENERAL NOTES
UNLESS OTHERWISE SPECIFIED:

1. ALL LEADS APPROX 6 INCHES OR LONGER HAVE SHIELDS WHICH ARE CONNECTED TO PINS A THRU D OF CONNECTOR J8.
2. NO SHIELD SHALL HAVE CONTINUITY TO CHASSIS WITH J8 DISCONNECTED.
3. CHASSIS GROUND SHALL BE MADE ONLY AT POINTS SPECIFIED.
4. FOR INTERCONNECTIONS AND SYSTEM FUNCTIONS SEE WIRING DIAGRAM 1B08755-1.

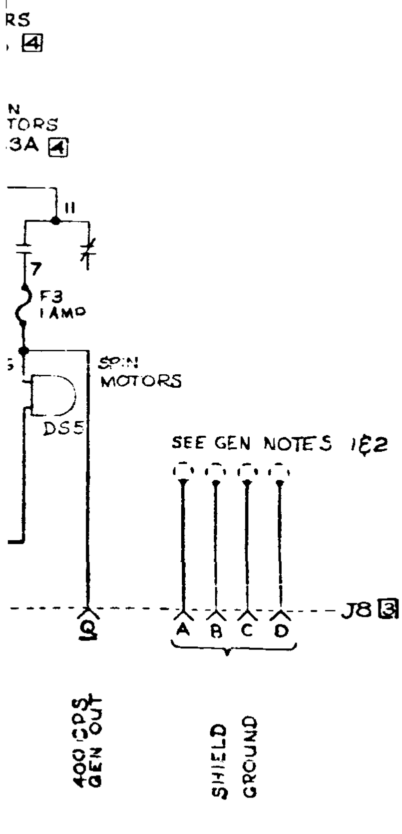

	REF DES	MFR PART	NOM / DESCRIPTION	MFR NAME
	T1, T2	A28-11	POWER SUPPLY, 28VDC	DELTRON
	M1	K25207	METER, ELAPSED TIME	A.W. HAYDON
	V30	V30	INVERTER, 400 CPS	NATEL
	V10	V10	INVERTER, 200 CPS	NATEL
	TD1	115 N0 120	RELAY, TIME DELAY	AMPERITE
	F2, F3	3AG-1	FUSE	LITTLE FUSE
	F1	3AB-10	FUSE	LITTLE FUSE
	K3	KHS 17D11-24DC	RELAY 4PDT	POTTER & BRUMFIELD
	K1, K2	NOT ON THIS SCHEMATIC		
	DS3	GE 344	LAMP	GENERAL ELECTRIC
	DS1,2,4,5,6	GE 327	LAMP	GENERAL ELECTRIC
	CR1	IN2071	SEMI COND, DIODE	
	C1		CAPACITOR, .05 MF, 200V	
	R6		RES, [illegible]	
	R5		RES, [illegible], 2W, 5%	
	R3, R4		RES, 2550Ω, [illegible]	
	R2		RES, [illegible], 50W, [illegible]	
	R1		RES, 3.3[illegible]	
DASH NUMBERS OF THIS DRAWING ODD DASH NUMBERS SHOWN EVEN DASH NUMBERS OPPOSITE	1B08752-1			

REVISIONS

SYM	DESCRIPTION	DATE	APPROVED

FINISH

UNLESS OTHERWISE SPECIFIED
DIMENSIONS ARE IN INCHES.
TOLERANCES
FRACTIONS ±
DECIMALS ±
ANGLES ±

MATL / WT CHK / STR CHK / CHECK / PR ENGR / DES ENGR / GR ENGR / DRAWN BY

SEE ENGINEERING RECORDS FOR USAGE DATA

DESIGN ACTIVITY APPROVAL

CUSTOMER APPROVAL

DOUGLAS AIRCRAFT COMPANY, INC — SANTA MONICA, CALIFORNIA

SCHEMATIC, POWER SUPPLY, HELIOSTATIC SYSTEM

CODE IDENT NO 18355 | SIZE H | 1B08752

SCALE | SHEET 1 OF

1B08752

155

3

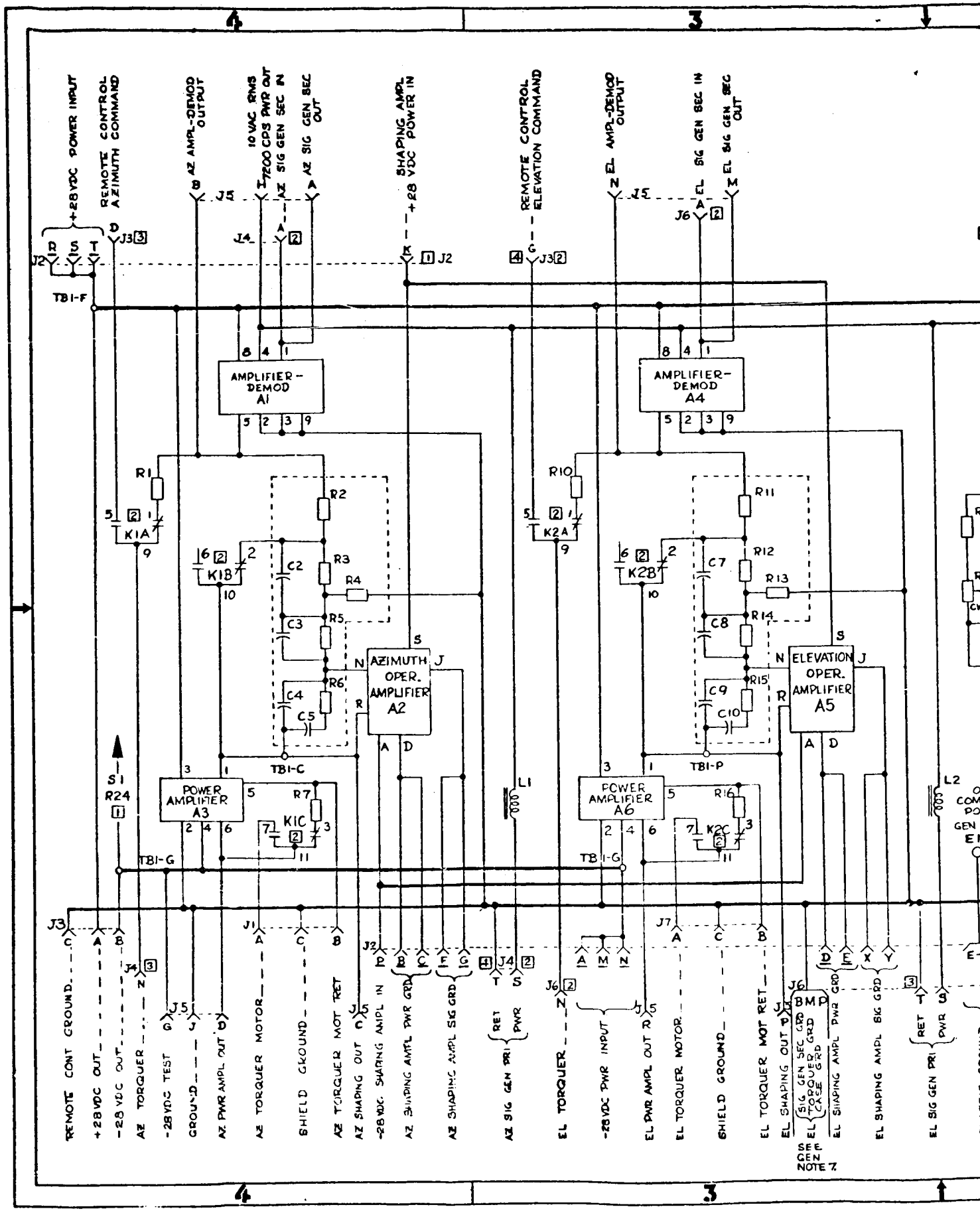
+28VDC POWER INPUT
REMOTE CONTROL AZIMUTH COMMAND
AZ AMPL-DEMOD OUTPUT
10VAC RMS 7200 CPS PWR OUT
AZ SIG GEN SEC IN
AZ SIG GEN SEC OUT
SHAPING AMPL +28 VDC POWER IN
REMOTE CONTROL ELEVATION COMMAND
EL AMPL-DEMOD OUTPUT
EL SIG GEN SEC IN
EL SIG GEN SEC OUT
AMPLIFIER-DEMOD A1
AMPLIFIER-DEMOD A4
AZIMUTH OPER. AMPLIFIER A2
ELEVATION OPER. AMPLIFIER A5
POWER AMPLIFIER A3
POWER AMPLIFIER A6
TB1-F
TB1-C
TB1-P
TB1-G
K1A
K1B
K1C
K2A
K2B
K2C
R1
R2
R3
R4
R5
R6
R7
R10
R11
R12
R13
R14
R15
R16
C2
C3
C4
C5
C7
C8
C9
C10
L1
L2
S1
R24
REMOTE CONT GROUND
+28 VDC OUT
-28 VDC OUT
AZ TORQUER
-28VDC TEST
GROUND
AZ PWR AMPL OUT
AZ TORQUER MOTOR
SHIELD GROUND
AZ TORQUER MOT RET
AZ SHAPING OUT
-28VDC SHAPING AMPL IN
AZ SHAPING AMPL PWR GRD
AZ SHAPING AMPL SIG GRD
AZ SIG GEN PRI
EL TORQUER
-28VDC PWR INPUT
EL PWR AMPL OUT
EL TORQUER MOTOR
SHIELD GROUND
EL TORQUER MOT RET
EL SHAPING OUT
SIG GEN SEC GRD
EL TORQUER CASE GRD
SEE GEN NOTE 7
EL SHAPING AMPL PWR GRD
EL SHAPING AMPL SIG GRD
EL SIG GEN PRI
RET
PWR

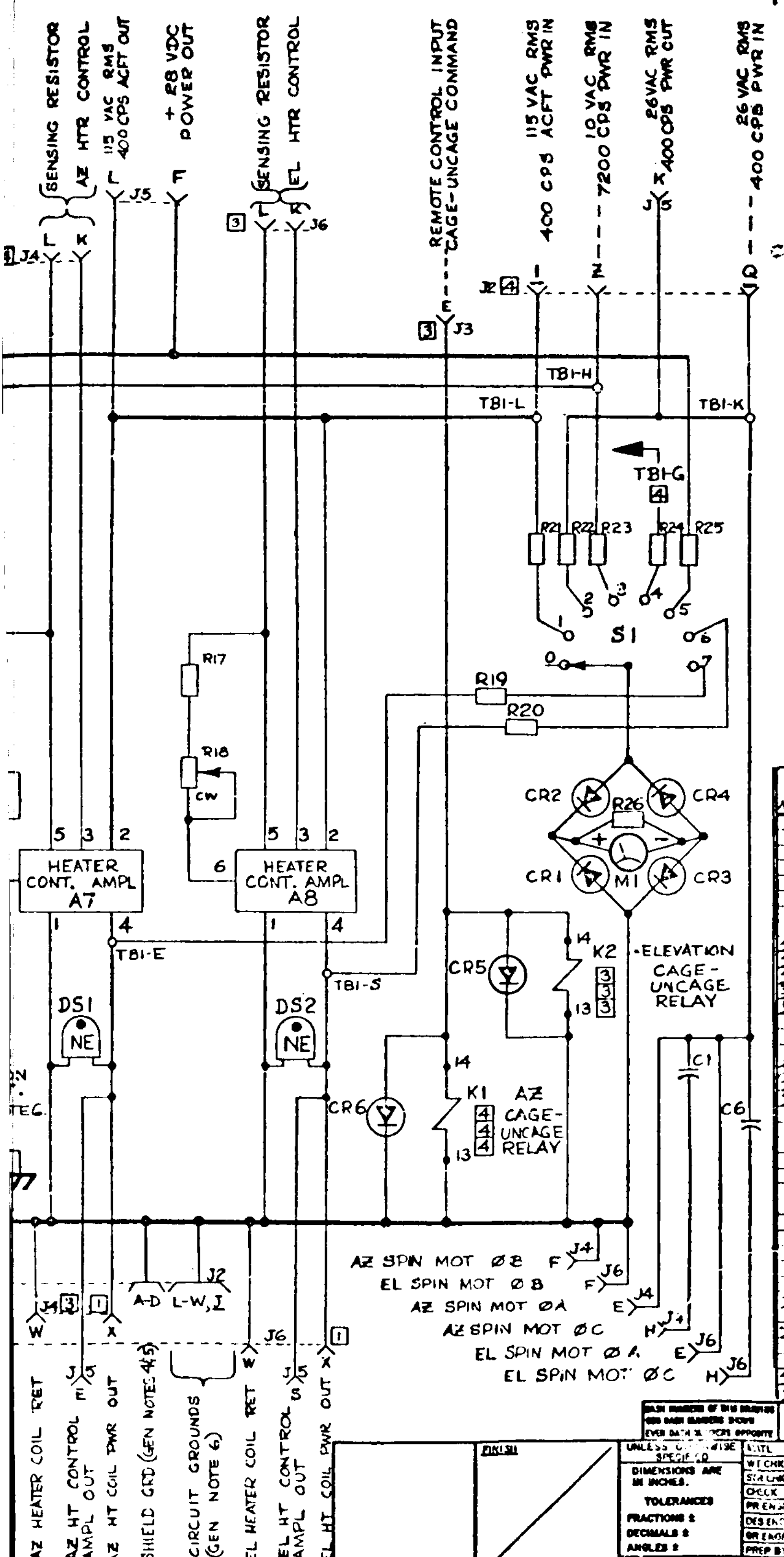

REVISIONS			
SYM	DESCRIPTION	DATE	APPROVED

GENERAL NOTES:

1. FOR EXTERNAL CONNECTIONS & SYSTEM FUNCTIONS SEE WIRING DIAG 1B08755-1.
2. FOR SCHEMATIC OF DACo AMPLIFIERS A3 & A6 SEE DWG 1B08754-1.
3. RELAYS K1 & K2 SHOWN IN "CAGE" CONDITION (NOT ACTUATED).
4. ALL LEADS APPROX 6 INCH OR LONGER ARE SHIELDED. SHIELDS TERMINATE ON CONNECTOR PINS J2 A THRU D.
5. NO SHIELD SHALL HAVE CONTINUITY TO CHASSIS GROUND WITH CONNECTOR J2 DISCONNECTED.
6. CONNECTIONS TO CHASSIS GROUND WILL NOT BE MADE EXCEPT AS SPECIFIED.
7. GROUNDS TO AZIMUTH GYRO IDENTICAL EXCEPT USE PINS B, M & P OF CONNECTOR J4.
8. FUNCTIONS LISTED FOR CONNECTOR J5 ARE INSTRUMENTATION OUTPUTS.

REFERENCE DESIGNATION LIST

ZONE	ITEM	REF DES	NOMENCLATURE /DESCRIPTION	MANUFACTURER
1	31	M1	MET, 1327, 100 MKAMP	SIMPSON
1	30	S1	SW, PA 205, 2P 12 POS	CENTRALAB
2	29	A7, 8	AMPL, CONT, PA44B1	MAGNETIC CONTROLS
4/3	28	A3, 6	PWR AMPL, 1B08754	DAC.
4/3	27	A2, 5	OP AMPL, 140-M20	ZELTEX
4/3	26	A1, 4	AMPL, DEM, D-156	NATEL
3/2	25	L1, 2	CHOKE 10MH, ECO10A	TRIAD
1/2	24	CR1-6	SEMICOND, 1N2071	GENERAL ELECTRIC
2	23	DS1, 2	LAMP, NE 51	GENERAL ELECTRIC
3	22	C9	CAP, 0.0015 MFD 200V	AEROVOX V146XR-17
4	21	C5	CAP, .0068 MFD, 200V	AEROVOX V146XR-6
4/3	20	C4, 10	CAP, 0.01 MFD, 200V	AEROVOX V146XR-1
4/3	19	C3, 8	CAP, 0.47 MFD, 200V	AEROVOX V146XR-11
4/2	18	C2, 7	CAP, 0.1 MFD, 200V	AEROVOX V146XR-7
1	17	C1, 6	CAP, 1.5 MFD, 200V	AEROVOX V146XR-14
1	16	R26	RES, 3.9K, ½W, 5%	OHMITE
1	15	R25	RES, 267K, ½W, 1%	DALE
1	14	R24	RES, 249K, ½W, 1%	DALE
1	13	R23	RES, 51K, ½W, 5%	OHMITE
1	12	R22	RES, 221K, ½W, 1%	DALE
1	11	R21	RES, 976K, ½W, 1%	DALE
1	10	R19, 20	RES, [illegible], ½W, 1%	DALE
2	9	R15	RES, 3.3 MEG, ½W, 1%	DALE
2	8	R9, 18	RES, 100Ω TRIMPOT	224S BOURNS
2	7	R8, 17	RES, 100Ω, 1W, 1%	DALE RS2A OR RS-A
4/3	6	R7, 16	RES, 100Ω, 10W, 10%	OHMITE
4	5	R6	RES, 487K, ½W, 1%	DALE
4/3	4	R4, 13	RES, 1.91K, ½W, 1%	DALE
4		R2, 14	RES, 453K, ½W, 1%	DALE
3	3	R3, 5		
4/3	2	R7, R11	RES, 14.7K, ½W, 1%	DALE
4/3	1	R1, R10	RES, 1K, ½W, 5%	OHMITE

1B08753-1

UNLESS OTHERWISE SPECIFIED
DIMENSIONS ARE IN INCHES.
TOLERANCES
FRACTIONS ±
DECIMALS ±
ANGLES ±

FINISH

SEE ENGINEERING RECORDS FOR USAGE DATA

FIRST RELEASE JUL 26 1965
ORIGINAL DATE OF DRAWING JUL 1 '65

MATL
WT CHK
STR CHK
CHECK
PREP BY D. I. MAL...

DESIGN ACTIVITY APPROVAL
CUSTOMER APPROVAL

DOUGLAS AIRCRAFT COMPANY, INC. SANTA MONICA, CALIFORNIA

SCHEMATIC, CONTROL CHASSIS, HELIOSTATIC SYSTEM

CODE IDENT NO 18355 | SIZE H | 1B08753

SCALE | SHEET 1 OF

1B08753

#156-2

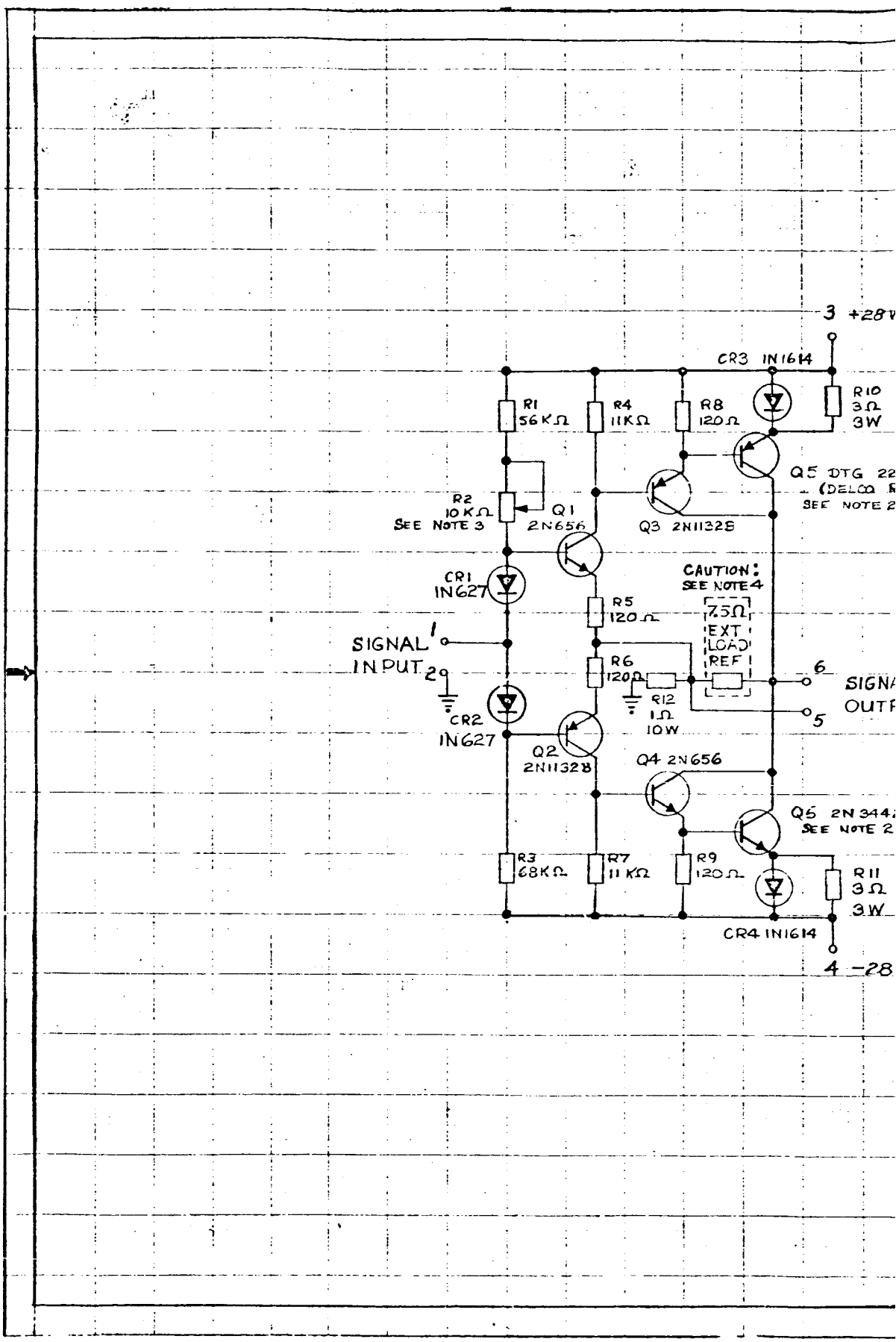
3 +28V
CR3 IN1614
R1 56KΩ
R4 11KΩ
R8 120Ω
R10 3Ω 3W
Q5 DTG 22
(DELCO
SEE NOTE 2
R2 10KΩ SEE NOTE 3
Q1 2N656
Q3 2N1132B
CR1 IN627
CAUTION: SEE NOTE 4
R5 120Ω
7.5Ω EXT LOAD REF
SIGNAL INPUT
1
2
R6 120Ω
R12 1Ω 10W
6
5
SIGNA
OUTP
CR2 IN627
Q2 2N1132B
Q4 2N656
Q5 2N344
SEE NOTE 2
R3 68KΩ
R7 11KΩ
R9 120Ω
R11 3Ω 3W
CR4 IN1614
4 -28

157-1

1B08754

DC

00
ADIO PART NO.)

GENERAL NOTES:

UNLESS OTHERWISE SPECIFIED, REQUIREMENTS ON FIELD OF DWG ARE FOR REFERENCE ONLY.

1. ALL RESISTORS ½ WATT UNLESS NOTED.
2. HEAT SINKS ARE REQUIRED FOR SAFE OPERATION AS FOLLOWS:
   Q3 & Q4 REQ INSULATED, MEDIUM POWER, CLAMP-ON TYPE HEAT RADIATORS.
   Q5 & Q6 REQ INSULATED, HEAVY DUTY, FULLY MOUNTED HEAT SINKS.
3. ADJUST R2 TRIMMER FOR NO CHANGE IN OUTPUT OFFSET VOLTAGE WITH INPUT OPEN OR SHORTED.
4. ALWAYS PROVIDE OUTPUT LOAD BEFORE CONNECTING POWER. 7.5 Ω 100 WATT MIN RESISTOR MAY BE SUBSTITUTED FOR NORMAL SYSTEM LOAD.
5. FOR EXTERNAL CONNECTIONS SEE NEXT HIGHER SCHEMATIC 1B08753-1.

IL
PUT

VDC

D 1B08754

DESIGN NUMBERS OF THIS DRAWING OR DASH NUMBERS SYSTEM	PART OR IDENTIFYING NO. 1B08754-1		
MATERIAL	FINISH	UNLESS OTHERWISE SPECIFIED	DRAWN / TRACED / CHECKED
		DIMENSIONS ARE IN INCHES. TOLERANCES FRACTIONS ± DECIMALS ± ANGLES ±	BOEING AIRCRAFT COMPANY, INC SANTA MONICA, CALIFORNIA
			SCHEMATIC, POWER AMPLIFIER, SERVO MOTOR
SEE ENGINEERING RECORDS FOR USAGE DATA		DESIGN ACTIVITY APPROVAL / CUSTOMER APPROVAL	CAGE IDENT NO 18355 / SIZE D / 1B08754 / SCALE / SHEET 1 OF

157-2

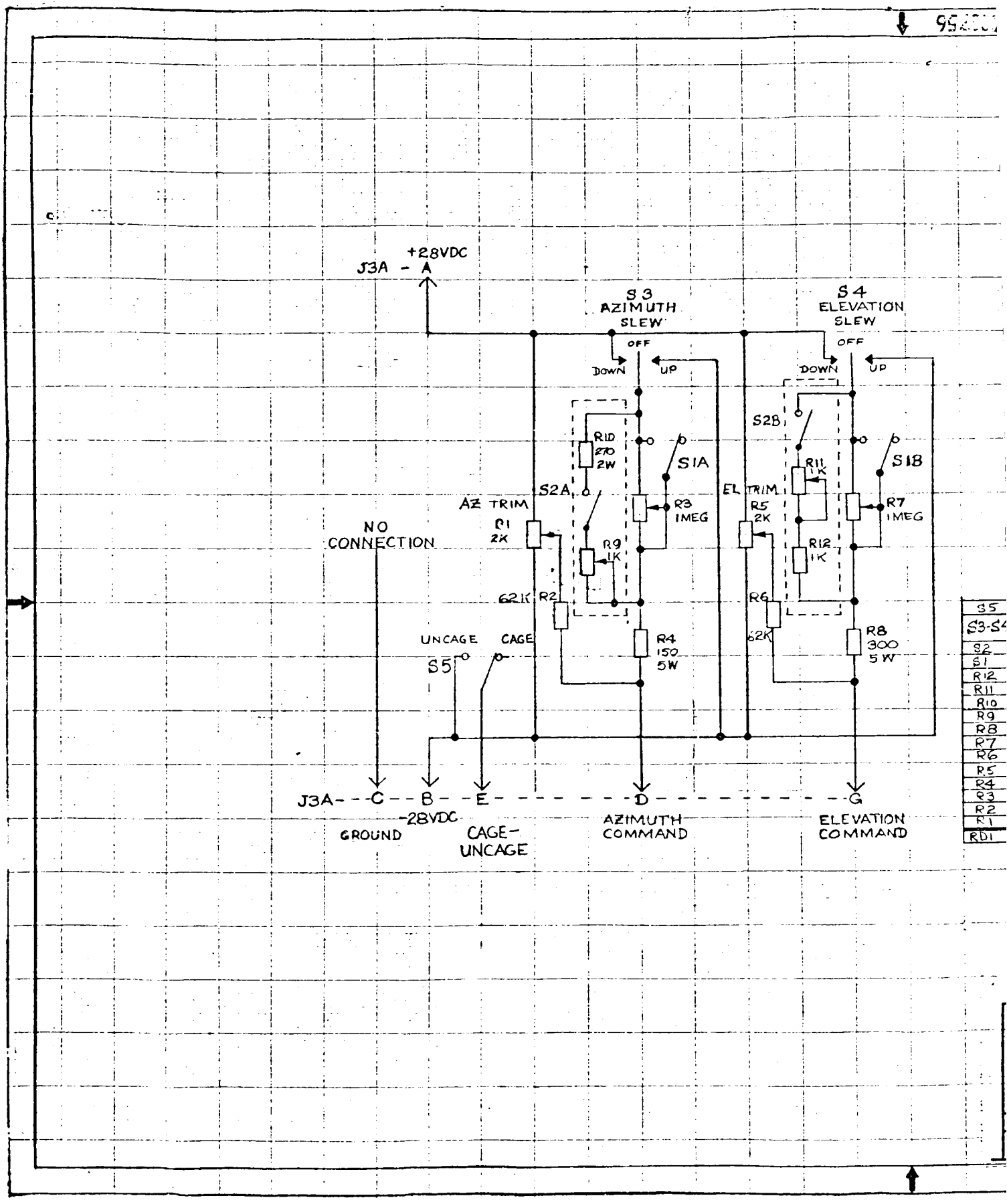
+28VDC
J3A - A
S3
AZIMUTH
SLEW
OFF
DOWN
UP
S4
ELEVATION
SLEW
OFF
DOWN
UP
R10
270
2W
S1A
S2A
AZ TRIM
R1
2K
R3
1MEG
R9
1K
62K R2
NO
CONNECTION
UNCAGE
CAGE
S5
R4
150
5W
S2B
R11
1K
S1B
EL TRIM
R5
2K
R7
1MEG
R12
1K
R6
62K
R8
300
5W
J3A - - C - - B - - E - - - - - - - - D - - - - - - - - G
-28VDC
GROUND
CAGE-
UNCAGE
AZIMUTH
COMMAND
ELEVATION
COMMAND
S5
S3-S4
S2
S1
R12
R11
R10
R9
R8
R7
R6
R5
R4
R3
R2
R1
RD1

GENERAL NOTES:
UNLESS OTHERWISE SPECIFIED
REQUIREMENTS ON FIELD OF DWG ARE
FOR REFERENCE ONLY.

1. ALL RESISTORS RATED ½ WATT UNLESS OTHERWISE SPECIFIED.
2. COMPONENTS INSIDE DASHED LINES (S2A & B, R9 THRU 12) ON NACA UNIT ONLY. SHOWN HERE FOR REF.
3. ALL RESISTOR VALUES IN OHMS.
4. FOR EXTERNAL CONNECTIONS SEE SYSTEM INTERCONNECTING DIAGRAM 1808755-1.

	SWITCH, DPDT	
160312	SW DP3T MOM-OFF-MOM	SWITCHCRAFT
83054	SWITCH, DPDT	ARROW, HART & HEGEMAN
8824-K8	SWITCH, DPDT	CUTLER HAMMER
	RES. 1K 2W	OHMITE
CLU1052	POT, 1MEG, 2W	OHMITE
	RES, 270Ω 2W	OHMITE
CLU1021	POT 1K, 2W	OHMITE
RH-5	RES. 390Ω, 5W	OHMITE
CLU1052	POT, 1MEG, 2W	OHMITE
	RES, 62K 2W	OHMITE
207-L	POT 2K, 2W	BOURNS TRIMPOT
RH-5	RES 150Ω 5W	OHMITE
CLU1052	POT 1MEG 2W	OHMITE
	RES 62K 2W	OHMITE
207-L	POT 2K, 2W	BOURNS TRIMPOT
PART NO	DESCRIPTION	MFR

D 1C03756

DASH NUMBERS OF THIS DRAWING: COD DASH NUMBERS SHOWN [illegible] OPPOSITE
PART OR IDENTIFYING NO. 1808756-1

MATERIAL | FINISH

UNLESS OTHERWISE SPECIFIED
DIMENSIONS ARE IN INCHES.
TOLERANCES
FRACTIONS ±
DECIMALS ±
ANGLES ±

DRAWN		
TRACED		
STRESS		
CHECKED		
PROJ ENGR		7-22-5
DES ENGR		7-22-5
CG ENGR		7-22-5
PREP BY	[illegible]	7-22-5

DESIGN ACTIVITY APPROVAL
CUSTOMER APPROVAL

SEE ENGINEERING RECORDS FOR USAGE DATA

[illegible] SANTA MONICA, CALIFORNIA

SCHEMATIC, REMOTE CONTROL, HELIOSTATIC SYSTEM

CODE IDENT NO. 18355 | SIZE D | 1C03756

SCALE | SHEET 1 OF

158-2

REFERENCES

1. Proposal to Assist NASA in the Solar Eclipse Expedition of May, 1965. Douglas Rept. SM-48088, Nov., 1964.

2. Burdin, C.; Clarke, J. D.; and Whittaker, J. L.: A Gyro - Referenced Heliostat - 1965 ASEE. Douglas Rept. SM-48335, Aug., 1965.

3. Roark, R. J.: Formulas for Stress and Strain. McGraw-Hill Book Company, Inc., 1954.

4. Loef, P. T.: Window Tests - Solar Eclipse Flight Expedition of May 30, 1965. Douglas Rept. TM-Gen-ME-R5073, May, 1965.

5. Gehris, J. D.: Verification of Flight Safety Specifications for Equipment Installed in the Project ASEE Airplane. Douglas Rept. SM-48330, May, 1965.

6. Convair Rept. ZS-30-307 Stress Analysis - Model 30 Aircraft. Vols. I, II, III, and IV, Nov., 1962.

7. Convair Rept. ZS 30-307 Stress Analysis - Model 30 Aircraft. Vol. III, Feb.-March, 1960.

8. Air/Aeronautics Regulation - Model 30 Aircraft. Civil Aeronautics Board, Sept., 1962.

9. Duncombe, J. S. and Morrison, B. L.: Total Solar Eclipse of May 30, 1965. U.S. Naval Observatory Circular 102, 1964.

10. Duncombe, R. L.: Private Communication, Nov. 5, 1964.

11. Smart, W. M.: Textbook on Spherical Astronomy, Cambridge University Press, Cambridge, England, 1960.

12. Taylor, A. E.: Advanced Calculus (Girrard Publishing Company), 1955.

13. American Ephemeris and Nautical Almanac 1965. U. S. Government Printing Office, Washington, D. C.

14. Martin, J. T. and Eckstein, M. C.: Solar Eclipse Navigation by Observations of the Partially Eclipsed Sun. Douglas Rept. SM-47808, Feb. 3, 1965.

15. Von Nostrand, D.: Dictionary of Missile & Space Flight.

16. Encyclopedia Dictionary of Physics. Pergamon Press.

NAS 2-2703
Douglas Aircraft Company, Inc.,
Missile and Space Systems Division.
DOUGLAS TASKS FOR AIRBORNE SOLAR ECLIPSE EXPEDITION OF MAY 30, 1965

Four tasks associated with the NASA airborne solar eclipse expedition (Project ASEE) of May 30, 1965 are discussed. These tasks include (1) pressure and environment testing of the optical windows installed in the NASA CV-990 aircraft, (2) certification of safe installation of participants' observational equipment in the aircraft, (3) preparation of navigational strategy for intercepting the eclipsed sun on May 30, 1965 and preparation of flight plans for practice flights, and (4) the design, operation, and performance of a gyroscopically controlled heliostat system used during the expedition by the Aerospace Research Center of Wright-Patterson AFB, Ohio.

I. Cameron, R. M.
II. NAS 2-2703

NAS